Poly 3-Hexylthiophene as a Photocathode for Solar Water Splitting

by

Graeme Suppes

M.Sc., University of Manitoba, 2010
B.Sc., University of Winnipeg, 2006

Thesis Submitted in Partial Fulfillment of the
Requirements for the Degree of
Doctor of Philosophy

in the
Department of Chemistry
Faculty of Science

SIMON FRASER UNIVERSITY

Fall 2015

Approval

Name: **Graeme Suppes**

Degree: **Doctor of Philosophy**

Title: ***Poly 3-Hexylthiophene as a Photocathode for Solar Water Splitting.***

Examining Committee: **Chair:** David Volcadlo
Professor

Steven Holdcroft
Senior Supervisor
Professor

Michael Eikerling
Supervisor
Professor

Vance Williams
Supervisor
Associate Professor

Jeffery J. Warren
Internal Examiner
Assistant Professor

Curtis Berlinguette
External Examiner
Associate Professor
Department of Chemistry
University of British Columbia

Date Defended/Approved: October 22 2015

Abstract

The focus of this research is to determine the extent to which poly 3-hexylthiophene (P3HT) can be used as a photoelectrode for solar water splitting. Research in the area of solar water splitting mostly focuses on inorganic materials but conjugated polymers, such as P3HT, offer several advantages. Most metal oxides used as photoelectrodes are only able to carry out water oxidation, require thick films to absorb significant amounts of light, and absorb light mainly in the ultraviolet part of the sun's spectrum. Conjugated polymers are able (thermodynamically) to reduce protons, require thinner films, and absorb mostly in the visible region of the electromagnetic spectrum. Additionally, conjugated polymers are processed from solution at room temperature and pressure, and can be cast onto many different types of substrates (rigid or flexible).

The ability of P3HT, on its own, to produce hydrogen gas (H_2) from acidic aqueous solution is first examined. Figures of merit such as photocurrent and incident photon to current efficiency as a function of thickness are determined through photoelectrolysis in a homemade cell. In addition, the oxidation state of the polymer film in contact with aqueous acid area investigated using spectroelectrochemistry. Platinum was also employed as a hydrogen evolution reaction (HER) catalyst, either by photoelectrochemical deposition of nanoparticles directly on the polymer or as a colloidal dispersion.

Thermodynamically, P3HT should reduce protons following light absorption. However, no H_2 was detected in the absence of a HER catalyst. Hydrogen was produced when platinum was photoelectrochemically deposited. This deposition technique resulted in the formation of Pt nanoparticles on the polymer film. Also, this demonstrates that a single layer conjugated polymer device is capable of performing H_2 evolution under illumination.

Keywords: Conjugated polymer; solar water splitting; photoelectrochemistry; poly 3-hexylthiophene

Acknowledgements

I would like to thank:

My senior supervisor, Dr. Steven Holdcroft, for the opportunity to work and study in his lab.

My supervisory committee, Dr. Michael Eikerling and Dr. Vance Williams, for their suggestions to improve my research and different ideas I should consider pursuing.

My examination committee for reading my thesis

Dr. Tim Peckham, Mr. Patrick Fortin, Dr. Bob Gholamkhass, and Mr. Edward Ballard for help with my research and great, technical discussion

Mr. Bruce Harwood for fabricating several photoelectrochemistry cells.

Mr. Howard Proulx and Mr. Bob Zubic for help designing and fabricating the lamp enclosure and accessories for the photoelectrochemistry cell.

Mr. Ray Holland and Mr. Ken Van Wieren for assistance with the thermal evaporator.

Merrill Isenor for her support throughout my time at SFU and for reading my thesis.

Table of Contents

List of Tables

List of Figures

List of Acronyms

Ag/AgCl	Silver/Silver Chloride electrode
BHJ	Bulk heterojunction
C_{60}	Spherical fullerene molecule
C_{Gouy}	Gouy layer capacitance
C_H	Helmholtz layer capacitance
C_{sc}	Space charge layer capacitance
C_{tot}	Total capacitance in an electrochemical system
CV	Cyclic voltammetry
E_{cb}	Conduction band energy
EDTA	Ethylenediaminetetraacetic acid
E_F	Fermi level
E_{fb}	Flat band potential
E_g	Band gap energy
E_{vb}	Valence band energy
EIS	Electrochemical impedance spectroscopy
Fc	Ferrocene
FF	Fill factor
GC	Gas chromatography
GPC	Gel permeation chromatography
HER	Hydrogen evolution reaction
IPCE	Incident photon to converted electron
I_{sc}	Short circuit current
ITO	Indium tin oxide
J	Current density
J_{op}	Operating current
J_{ph}	Photocurrent density (difference between current measured under illumination and the dark)
k_B	Boltzmann`s constant
λ	Wavelength
LSV	Linear sweep voltammetry
MeCN	Acetonitrile

MPc	Phthalocyanine where M = Co, Zn, or H_2
MV^{2+}	Methyl viologen
N	Charge carrier density
NHE	Normal hydrogen electrode
NIR	Near infrared
NMR	Nuclear magnetic resonance
OER	Oxygen evolution reaction
P3HT	Poly (3-hexylthiophene)
PCBM	Phenyl-C61-butyric acid methyl ester
PCE	Power conversion efficiency
PEC	Photoelectrochemistry or photoelectrochemical or photoelectrolysis
PEDOT	Poly(3,4-ethylenedioxythiophene)
P_{in}	Incident light power density
PL	Photoluminescence
PPV	Poly(para-phenylene vinylene)
PPy	Polypyrrole
PSS	Polystyrene sulfonate
PTCBI	3,4,9,10-perylenetetracarboxylic acid bisbenzimidazole
PTh	Polythiophene
PV	Photovoltaic
q	Charge of an electron
RR	Regioregular
RRa	Regiorandom
$Ru(bipy)_3$	Tri(bipyridene)ruthenium
SCE	Saturated calomel electrode
SEC	Spectroelectrochemistry
STH	Solar-to-hydrogen efficiency
T	Temperature
TBAP	Tetrabutyl ammonium perchlorate
TCD	Thermal conductivity detector
TEOA	Triethanolamine
UV	Ultraviolet

V_{oc}	Open circuit potential
α	Absorption coefficient
δ_p	Penetration depth
ε	Dielectric constant
ε_0	Permittivity of free space

Chapter 1.

Introduction

1.1.1. Introduction to Conjugated Polymers

Conjugated polymers are a unique class of materials that, unlike their electrically insulating cousins, have many properties that make them useful for a number of modern applications. The conjugation of the polymer backbone results in semiconducting behaviour (see Section 1.1.1), which makes these materials useful in light-emitting diodes (LEDs)[1–3] and photovoltaics (PVs).[4,5] The ability of conjugated polymers to be reversibly oxidized and reduced results in near metallic conductivity and gives these materials charge storage properties that have been made use of in batteries[6–8] and in capacitors.[9-11] The discovery of metallic conductivity was first made using polyacetylene, the conjugated polymer with the smallest monomer unit (C_2H_2), in the 1970's. When the polymer (*trans*-polyacetylene) was oxidized by exposure to chlorine, bromine, and iodine vapours, its conductivity increased to 10^5 S cm^{-1} from a neutral value of 3.2×10^{-6} S cm^{-1}.[12,13] The increase in conductivity due to oxidation was likened to addition of electron donating or accepting species in an inorganic semiconductor, known as doping, which results in the same effect. This discovery led to the Nobel Prize in Chemistry being awarded to Alan J. Heeger, Alan G. MacDiarmid, and Hideki Shirakawa in 2000.

Conjugated polymers are organic materials, and as such, a wide array of synthetic techniques can be applied to tailor properties such as solubility and electronic structure. Polymers such as polypyrrole (PPy) and polythiophene (PTh) (Figure 1.1) are insoluble in water and organic solvents limiting their processability. Electrochemical oxidation of the monomer can produce films of various thickness but this technique limits the substrates to conductive materials that are usually rigid (glassy carbon, indium:tin oxide, Pt, Au) and typically results in porous films.[14,15] Judicious choice of solvent and

oxidant can result in meta-stable solutions where the polymerization occurs slowly at first then speeds up as the solvent evaporates and the monomer and oxidant concentration increases[16,17] The meta-stable solution can be used to coat non-conducting substrates such as glass or porous conducting material such as carbon paper.[11]

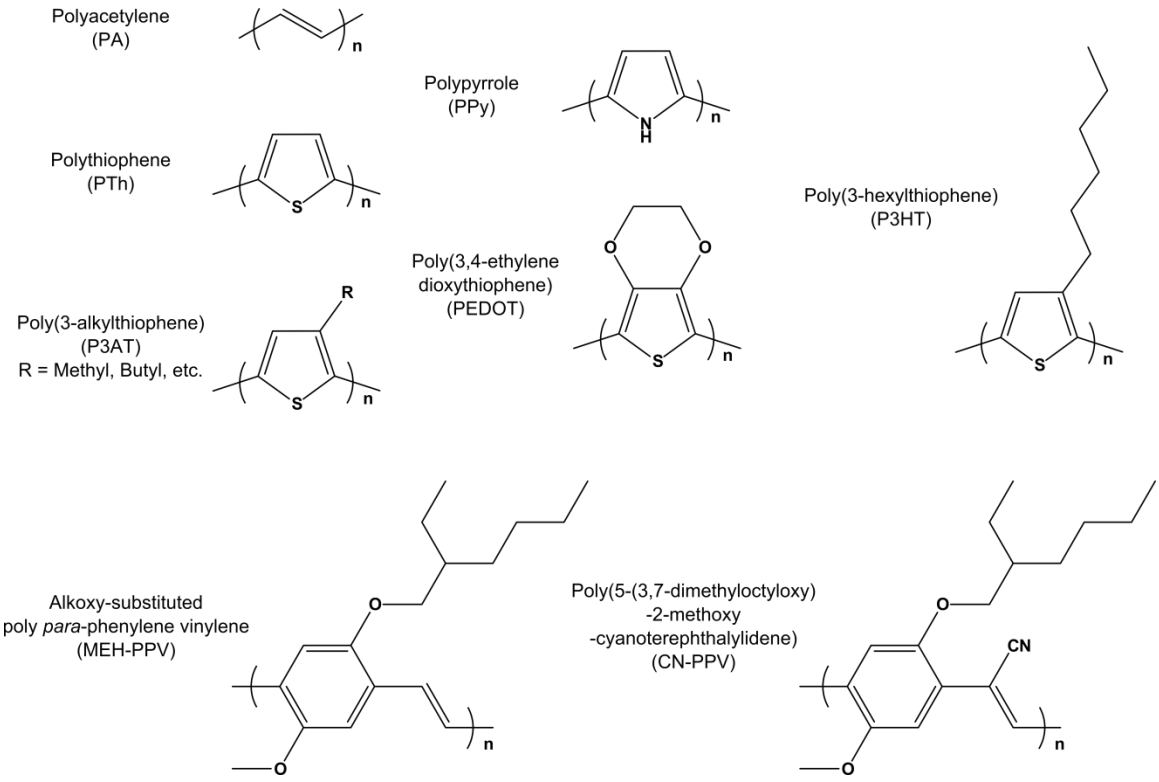

Figure 1.1 Example of conjugated polymers

A major advancement in solubility for conjugated polymers was achieved by the addition of long, flexible alkyl[18–20] or alkoxy[21,22] side chains. Long side chains allowed polymers of high molecular weight to be dissolved in organic solvents (most chlorinated solvents, toluene, THF). The alkyl chains prevent the strong aggregation polymer chains. Aggregation leads to interchain conductivity, so if the alkyl chains are too long the conductivity of the film will be negatively affected. For example, hexyl chains used in poly(3-hexylthiophene) (P3HT) give a good compromise between solubility and conductivity.[23]

The electronic structure of polymers can be manipulated by the incorporation of electron donating or withdrawing groups along the polymer backbone. For example, cyano-substituted poly *para*-phenylene vinylene (CN-PPV) has a higher electron affinity than the unsubstituted polymer and can more easily accept an electron.[24,25] Poly(3,4-ethylenedioxythiophene) (PEDOT) is a derivative of PTh where the 3- and 4- positions of thiophene have been replaced by a cyclic dioxy substituent. The oxygen atoms donate electron density to the conjugated backbone resulting in a lower oxidation potential.[26,27] Electron rich and electron deficient units can even be incorporated in same polymer as alternating donors and acceptors, respectively. Alternating donor-acceptor structures lead to more red-shifted absorbance and greater charge carrier mobility.[28,29]

Conjugated polymers also benefit from a large absorption coefficient (α). Poly-[2-(3,7-dimethyloctyloxy)-5-methyloxy]-para-phenylene-vinylene (MDMO-PPV) has $\alpha = 2.0 \times 10^5$ cm^{-1} at wavelength (λ) = 500 nm.[30] This corresponds to a penetration depth ($\delta_p = \alpha^{-1}$) of 50 nm which is the distance light will travel through a material before its intensity is reduced by 1/e (~37 %). Inorganic materials have smaller absorption coefficients, for example: Fe_2O_3 δ_p = 125 nm at λ = 550 nm,[31,32] Si δ_p = 684 at 516 nm,[33] and TiO_2 δ_p = 250 nm at 308 nm.[34] To absorb >90 % of the incident light, a material`s thickness should be about 2.3 times it's δ_p.[35]

1.2. Organic Semiconductor Properties

1.2.1. Electronic Band Gap

The semiconducting properties of conjugated polymers are due the formation of an energy gap (band gap) between the π (bonding) and π* (antibonding) orbitals of the highest occupied molecular orbital (HOMO) and lowest unoccupied molecular orbital (LUMO), respectively. In monomers the energy gap is between discrete energy levels. In a conjugated polymer the energy level of each monomer's π and π* level remains discrete but close in energy to its neighbor monomer. The HOMO and LUMO of the polymer appears as a band of continuous energy levels made up of the closely spaced monomer energy levels (Figure 1.2). The continuous energy bands of the HOMO and LUMO of conjugated polymers are analogous with the conduction band (CB) and

valence band (VB) of inorganic semiconductors and are sometimes referred to as such (HOMO / valence band and LUMO / conduction band).

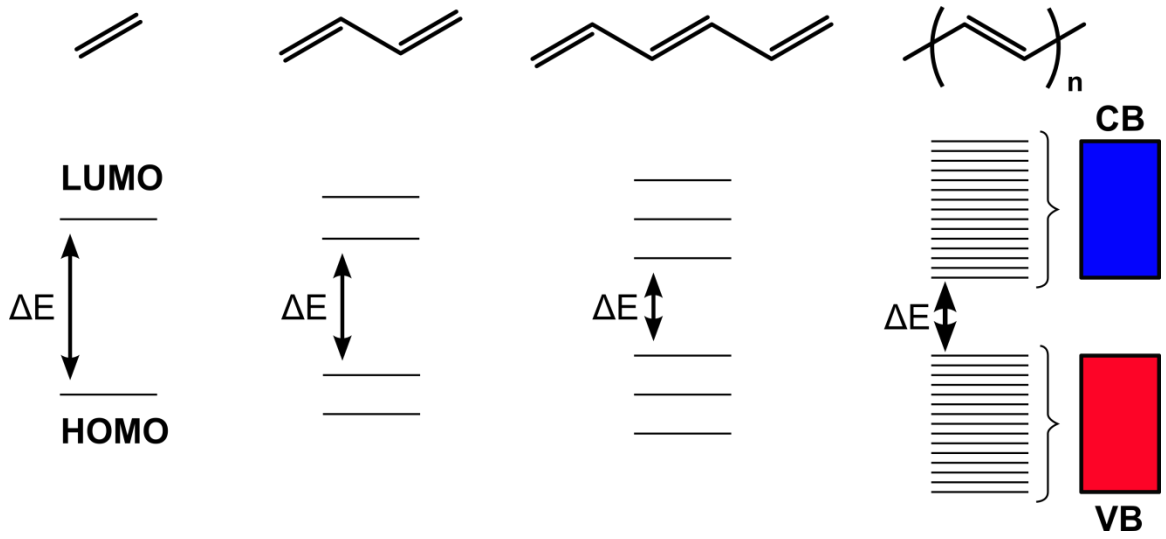

Figure 1.2 **An illustration of the changes that happen to the energy levels as acetylene goes from a molecule to a polymer. The energy difference ΔE = HOMO-LUMO. In a polymer chain the LUMO and HOMO are approximated by bands, the conduction band (CB) and valence band (VB), respectively.**

The magnitude of the energy gap, or band gap, (E_g) is also relevant to the classification of conjugated polymers as semiconductors. Figure 1.3 shows examples of simple band diagrams for materials based on the size of E_g. Conductive metals have a band gap of zero. The conduction band is only partially full and electrons are able to move freely with only thermal energy input. Insulators, on the other hand, have such a large band gap that the energy required to promote an electron from the VB to the CB would result in chemical or physical breakdown of the material. Conjugated polymer semiconductors have a band gap on the order of 1-3 eV.[36–38] This makes excitation possible by photons in the UV-visible-NIR portion of the electromagnetic spectrum, making conjugated polymers useful for electrochromic, PV, and LED applications.

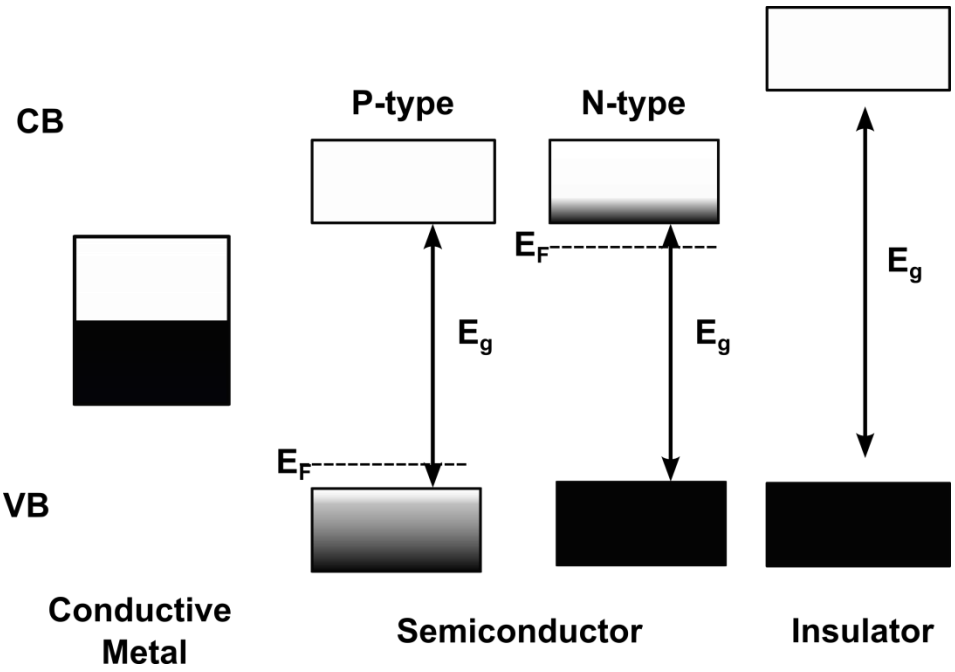

Figure 1.3 Simple band diagrams for conductive metals, semiconductors (p- and n-type), and insulators showing the energy gap (E_g) between the conduction band (CB) and valence band (VB). The diagram also indicates the relative position of the Fermi level (E_F) for p-type vs. n-type semiconductors.

Semiconductors can be further classified into n- and p-type based on their majority charge carrier and the Fermi level (E_F) position. Semiconductors with a nearly full valence band/HOMO are called “p-type” and holes are the majority charge carriers. If the valence band/HOMO is completely full and the conduction band/LUMO is partially full the semiconductor is called “n-type” and electrons are the majority charge carriers. The non-majority charge carrier is simple called the minority charge carrier. The Fermi level represents the electrochemical potential $\bar{\mu}$ of the electrons in the solid. It also represents a hypothetical energy level with a 50 % probability of being occupied by an electron. Therefore, in p-type semiconductors, E_F lies closer to the valence band/HOMO whereas in n-type semiconductors, it is closer to the conduction band/LUMO.

The band gap can also be referred to as a zone of forbidden states meaning that no accessible energy levels exist between the top of the valence band to the bottom of the conduction band. Oxidation or reduction, however, introduces states in the band gap and allow electrons to move about freely, which results in a huge increase in

conductivity. Iodine-doped polyacetylene can achieve conductivities up to 10^5 S cm^{-1}, comparable to the conductivity of copper.[13] Conductivities of 100-1000 S cm^{-1} have been reported for electrochemically grown PPy[39] and PEDOT films prepared using iron(III) tosylate as a chemical oxidant for polymerization.[40] The types of charge carriers produced by electrochemical oxidation are described in more detail in Section 1.5.4.

1.2.2. Photophysics

Charge generation due to absorption of light in organic semiconductors does not follow the same process as in inorganic semiconductors.[41–44] In conventional semiconductor solar cells (CSC), such as Si solar cells, light absorption results in generation of electron-hole pairs that are immediately separated into free charge carriers by an internal electric field. In organic semiconducting devices, charge carriers (electrons and holes) must undergo several transitions before current is generated by a PV device or reactions can be performed at the surface of a photoelectrode. Initially, a photon with energy equal to or greater than the band gap of the chosen semiconducting material (S) is absorbed and an electron is promoted to the LUMO, leaving a hole in the HOMO and placing the material in an electronically excited state (S*). These two charge carriers form a bound pair, known as an exciton, which is delocalized over several repeat units along a conjugated polymer chain. To be useful, the exciton must dissociate into a separate hole and electron before they can recombine. For this reason, organic semiconductor PV devices are referred to as excitonic solar cells.[43] Exciton dissociation occurs at the interface with an electron acceptor, A (or donor, D):

$$\boldsymbol{S \overset{h\nu}{\rightarrow} S^*} \qquad (1.1)$$

$$\boldsymbol{S^* + A \rightarrow S^+ + A^-} \qquad (1.2)$$

$$\boldsymbol{S^* + D \rightarrow S^- + D^+} \qquad (1.3)$$

Where A accepts an electron from S* and D donates an electron to S* to fill a hole. Reaction equations (1.2) and (1.3) are reversible so either the back reaction should be

slow or the products, A^- and D^+, should be removed quickly. In the equations above only photoexcitation of S is considered and S* would be considered the donor and acceptor in reaction (1.2) and (1.3), respectively. In polymer solar cells, the conjugated polymer donor is layered or mixed with an electron accepting material. Several reviews of the history, physics, and construction of devices include those produced by Heeger,[45,46] Wudl *et al*.,[28] and Brabec *et al*.[47]

The inability of organic semiconductors to separate excitons is due to the small dielectric constant, ε, and small electron-hole pair radius (analogues to the Bohr radius of a hydrogen atom), r_B, when compared to inorganic material.[41,46] The dielectric constant determines the ability of a material or solvent to overcome the electrostatic charge binding an electron-hole pair or electrolyte salt, respectively. Organic semiconductors have a dielectric constant ε = 3-4[48,49] compared to an inorganic semiconductor, such as Si where ε = 11.9.[50] In inorganic semiconductors, all atoms are covalently bound to their nearest neighbors in three dimensions resulting in delocalization of electron wave functions and a large r_B. In polymer semiconductors, electrons are delocalized along a chain resulting in strong intrachain interactions but interchain interactions are weak, giving a small value for r_B. Figure 1.4 shows the effect of dielectric constant on the binding energy of an exction when ε = 4 and ε = 15. With a much narrower potential energy well (due to large ε) and larger r_B, thermal energy (T ~ 300 K, k_BT = 26 meV where k_B is Boltzmann`s constant, 1.38×10^{-23} J K^{-1}) is strong enough to dissociate electron-hole pairs in inorganic semiconductors (ε = 15). As mentioned above, excitons in polymer semiconductors must reach an interface with an electron accepting or donating material in order to dissociate into free charge carriers. Photo generated excitons reach the interface by diffusion where one diffusion length is typically <10 nm.[51] Additionally, it is common for the LUMO of the acceptor to be about 0.3 eV more negative than the donor LUMO to overcome the excitons binding energy and prevent back reactions.[52]

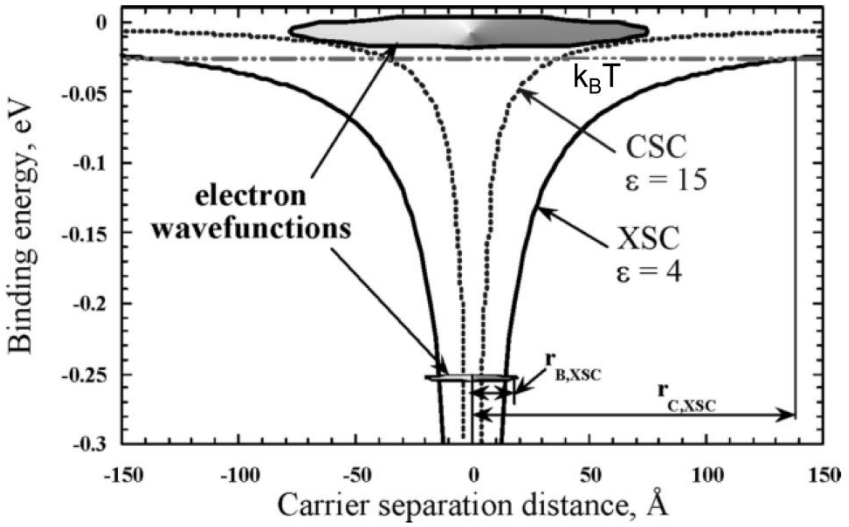

Figure 1.4 **Schematic representation of the fundamental difference between conventional semiconductors (CSC) and excitonic semiconductors (XSC). When the size of the electron-hole pair radius (r_B) sits inside the Coulomb potential well (r_C) excitonic behavior is observed. T ~ 300 K for the thermal energy line (k_BT). Reprinted figure with permission from ref. [42]. Copyright 2011 by Cambridge University Press.**

1.2.3. Poly(3-Hexylthiophene)

Poly(3-hexylthiophene) is the highly soluble (in organic solvents) derivative of polythiophene and is a benchmark material in solar cell research. Previously, solar cell research focused on poly *para*-phenylene vinylene (PPV) derivatives mixed with a fullerene derivative, phenyl-C61-butyric acid methyl ester (PCBM), as an acceptor but efficiencies in devices were limited to 3 %.[53–55] Efficiency was increased to over 4 % when P3HT was used as the donor material and the films were annealed following deposition.[56,57] Thermal annealing allowed the P3HT:PCBM mixture to phase separate into crystalline domains.[58] Lack of crystallinity in the solid state reduces charge carrier mobility.[59–61] Polymer chains of P3HT, on the other hand, stack perpendicular to the π-conjugated backbone which improves interchain charge transport.[62,63]

Another important factor is the regioregularity of the polymer backbone. P3HT is considered regioregular if the coupling between monomer units is >90 % head-to-tail (HT).[64] Other couplings that are possible are head-to-head (HH) and tail-to-tail (TT) and

can result in regioisomers. The possible couplings are illustrated in Figure 1.5 using poly(3-alkylthiophene) as an example. If the HT content of a polymer is <90 % planarization of the backbone is more difficult, interrupting π-stacking, lowering the crystallinity, and decreasing conjugation of the polymer chains.[65,66] Advances in synthesis by Rieke[67] and McCullough[68,69] make it possible to prepare P3HT with very high HT ratios (>98 %).

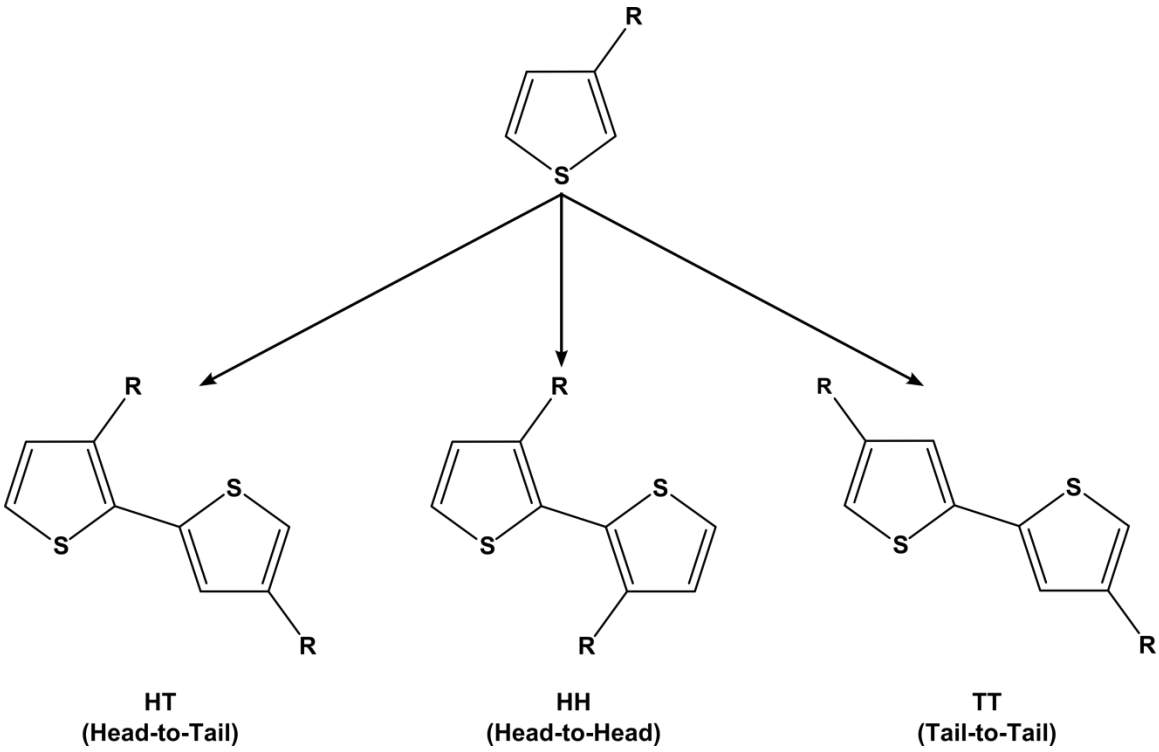

Figure 1.5 A monomer of 3-alkylthiophene and an illustration of the possible HT, TT, and HH coupling for poly(3-alkylthiophene).

The performance of P3HT, however, degrades when exposed to air and oxygen. A low ionization potential (defined as the top of the HOMO band) leads to oxidation of the material when the film is exposed to ambient conditions.[70] The air oxidation threshold is approximately 5.27 eV[71] compared to the HOMO level of P3HT which is approximately 5.0 eV.[72–74] This leads to photobleaching of the film in the presence of light and oxygen.[59-61] Chain scission and oxidation destroys the conjugation of the polymer chains and leaves the polymer transparent to visible light.

1.3. Photoelectrochemistry

1.3.1. Introduction

Photoelectrochemistry (PEC) studies the redox reactions at semiconductor electrodes under illumination.[78,79] These systems are similar in operation to a photovoltaic cells, but a portion of the solid state device is replaced with a semiconductor-electrolyte junction. For an organic PV device to usefully produce energy, the photogenerated electron-hole pair must be separated. Equations (1.1), (1.2), and (1.3) can be applied to PEC as well except that the acceptor (A) and donor (D) can be redox species in solution. One important difference between solid state photovoltaic cells and PEC is the lack of a true chemical reaction in the solid state device. Electrons generated in solar cells travel through an external circuit to generate current but in a PEC system the electrons and holes are shuttled through the electrolyte by redox couples (these charge carriers are not independently stable in solution).[80] The type of reaction (oxidation vs. reduction) and energy level of the species in solution dictates which semiconducting material should be used.

Figure 1.6A shows the band structure of a n-type semiconductor before immersion in an electrolyte solution containing a redox couple (A/A^-). When a semiconductor electrode is placed in solution containing a redox species, the Fermi levels, $\bar{\mu}$, of both equilibrate (Figure 1.6B). Equilibration is achieved by charge transfer across the interface. An electric field forms due to the energy difference between the surface and the bulk of the material. This electric field drives the mobile majority carriers into the bulk of the material. A zone starting at the semiconductor/electrolyte interface and extending into the material is called the “depletion layer” because it has been depleted of majority carriers. It is also referred to as a space charge layer because the immobile minority charge carriers are spread out to a measureable depth from the electrode/electrolyte interface. Band edges bend upwards or downwards across the depletion layer depending on the initial positon of the semiconductor E_F. An electric field is generated due to the potential difference between the new positions of the bands at the surface relative to the bulk.

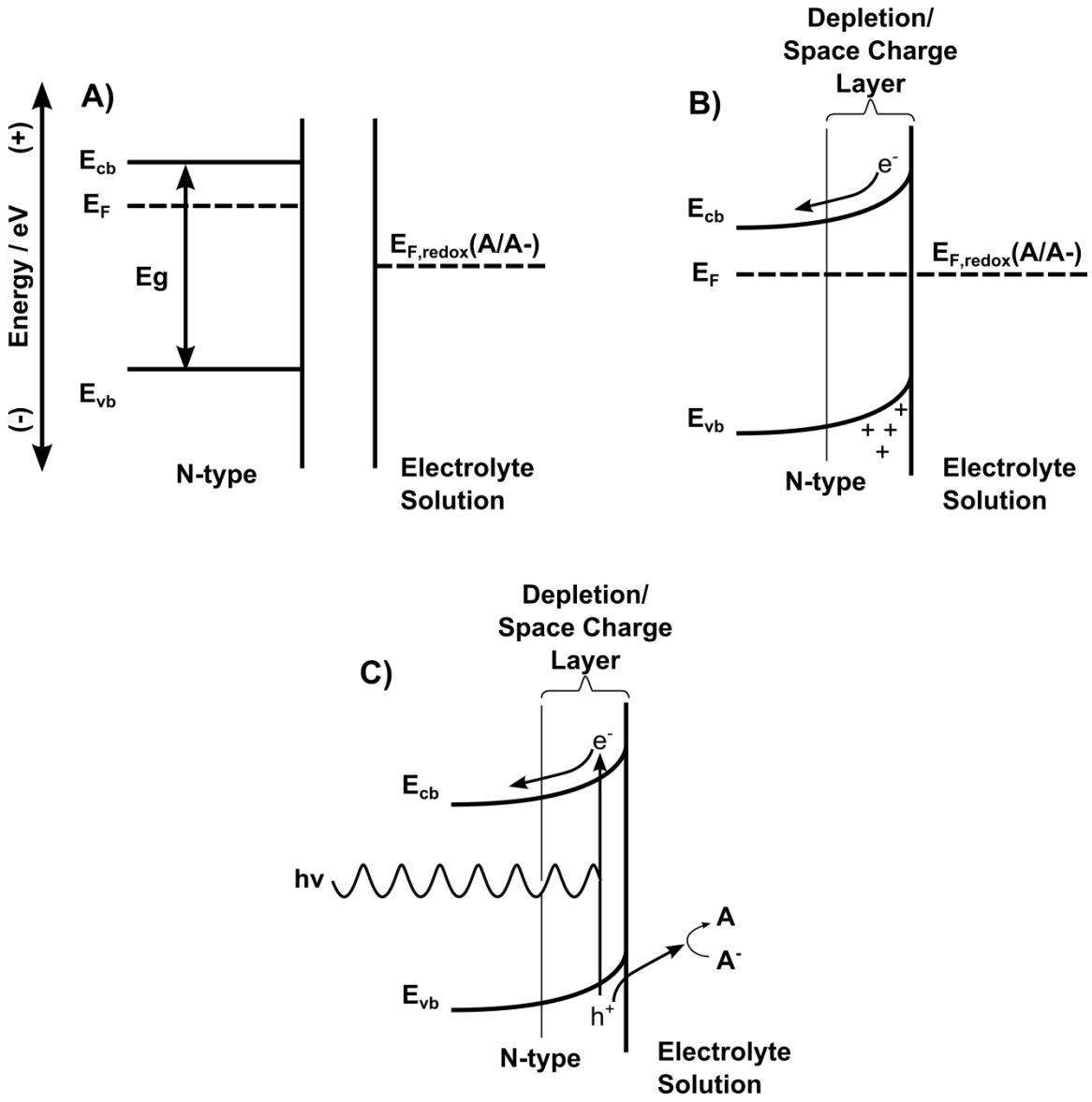

Figure 1.6 **N-type semicondutor photoelectrode before (A) and after (B) contact in the dark and in contact and under illumination, hv ≥ E_g, (C). The Fermi level of the semiconductor, E_F, equilibrates with the Fermi level of the redox couple in solution, $E_{F,redox}$,when the semicondutor and electrolyte are brought into contact. Illumination generates holes (h^+) and additional electrons. Electrons promoted to the conduction band migrate to the bulk and holes left in the valence band migrate to the surface due to the electric field in the depletion region.**

When a photon with energy $h\nu \geq E_g$ is absorbed by the active material, an electron is promoted to the conduction band/LUMO and hole is left in the valence band/HOMO (Figure 1.6C). If the photon is absorbed within the depletion layer, the internal electric field drives the photogenerated minority carriers towards the surface and majority carriers migrate into the bulk. In other words, any exction generated in the depletion region is immediately separated. Also, any exciton generated one diffusion length away from the depletion region could be separated following diffusion into the depletion zone. An illuminated p-type semiconductor electrode can carry out reductions and is referred to as a photocathode. Photogenerated electrons of a p-type semiconductor can only reduce species in solution that have a redox couple below the conduction band edge; i.e., the electrons must be thermodynamically energetic enough to carry out the reaction. Similarly, photogenerated holes produced by n-type semiconductors can only carry out oxidation if the species redox couple is above the valence band.

Figure 1.7 shows the competing pathways that exist for charge recombination.[35,81] Charge recombination negatively impacts photoelectrolysis by decreasing the steady state concentration of charge carriers. For films with thickness (d) greater than the depletion region (L_D), the electric field established at the surface due to band bending will prevent recombination in the depletion layer (J_{dr}). Recombination in the bulk (J_{br}) is a major loss mechanism for these types ($d>>L_D$) of systems. As the thickness of a material is decreased below the depletion layer thickness ($d<<L_D$), the electric field at the surface weakens or disappears altogether. When this happens, recombination near the surface becomes possible (J_{dr}). Majority carriers are no longer swept to the bulk and instead can participate in reactions at the surface (J_t and J_{et}). Surface states present in inorganic semiconductors have been shown to act as recombination centers and affect the charge transfer of minority carriers, generated by illumination, to redox couples in solution.[82]

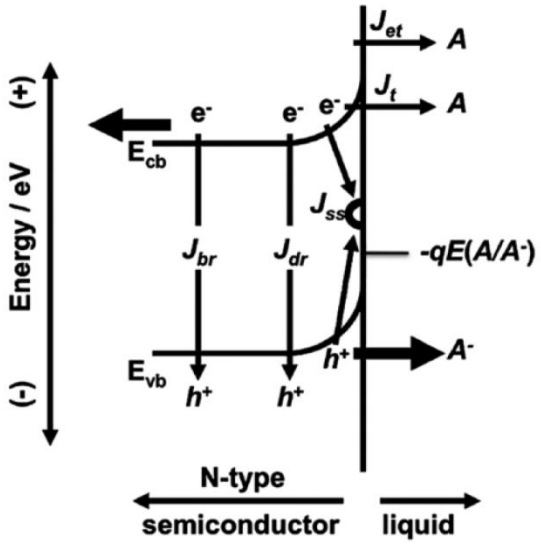

Figure 1.7 **Recombination pathways of photogenerated charge carriers in an n-type semiconductor-based photoelectrochemical cell. The electron-hole pairs can recombine through a current density in the bulk of the semiconductor J_{br}, the depletion region, J_{dr}, or at defects (trap states) at the semiconductor/electrolyte interface, J_{ss}. Charges can also tunnel through the electric potential barrier near the surface, J_t, or transfer across the interface, J_{et}. The bold arrows indicate the favorable current processes in the operationof a photoelectrochemical cell. Reprinted with permission from ref. [81]. Copyright 2005 American Chemical Society.**

1.3.2. Photoelectrolysis of Water

One of the most important PEC reactions studied is the photoelectrolysis of water by illuminated semiconductors.[83] Light from the sun can provide 4.3×10^{20} J in one hour which is comparable to amount of energy used on Earth in one year (4.1×10^{20} J).[84] Harnessing that energy would give us the ability to generate sustainable fuels as an alternative to non-renewable fossil fuels. H_2 production from solar water splitting is seen as a major goal for PEC. Currently, H_2 is produced by steam methane reforming which uses methane as a fuel and produces CO_2 as a by-product.

Under acidic conditions solar energy would have to drive the following half reactions in order to carry out solar water splitting:

$$H_2O + 2h^+ \rightarrow \frac{1}{2}O_2 + 2H^+ \quad \textbf{(OER)}$$

$$2H^+ + 2e^- \rightarrow H_2 \quad \textbf{(HER)}$$

Solar water splitting was first demonstrated by Honda and Fujishima using a TiO_2 photoanode. Here, water is the donor and protons generated by water oxidation are the acceptors under acidic conditions. The photogenerated holes of TiO_2 are energetic enough to oxidize water but the conduction band is too low to reduce protons so an additional bias is supplied by an external source (potentiostat).

There are many materials that are useful for solar water splitting and several reviews on the subject have been published.[35,85,86] Some of these materials are discussed in Section 1.4. There are several figures of merit to be considered when evaluating a materials use as a photoelectrode such as the size of the band gap, the position of the band edges, and stability of the material in contact with an electrolyte solution (in the dark and under illumination).

An ideal semiconductor must supply a voltage of 1.23 V plus any required overpotential. Another important characteristic is the position of the band edges. The valence band (or HOMO) must be more positive than the water oxidation potential so that photogenerated holes are sufficiently energetic to carry out the reaction. At pH 0 this value is E_{O_2/H_2O} = +1.23 V_{NHE}. The conduction band must be more negative than 0 V_{NHE} at pH 0 for photogenerated electrons to reduce protons. The vacuum energies of these reactions are -5.73 eV for water oxidation and -4.5 eV for proton reduction. A photoelectrode must be chemically, electrochemically, and photoelectrochemically stable in the environments it will most likely find use, which is, in water and, possibly, in low or high pH. Figure 1.8 shows the band diagram for an ideal material that possess all these characteristics.

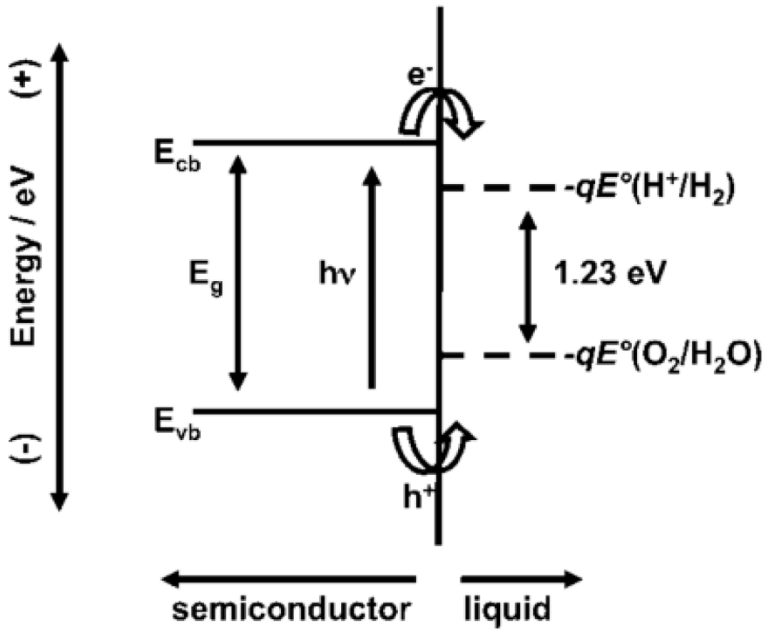

Figure 1.8 **Ideal semiconducting material for splitting water at its surface under illumination with absolute energy scale represented for E_{cb} and E_{vb} and the electrochemical potentials given by –qE°, where E° is the reduction potential for both (H^+/H_2 and O_2/H_2O) redox couples. Reprinted with permission from ref. [85]. Copyright 2010 American Chemical.**

1.3.3. Devices

There are several device structures possible for solar water splitting, some of which are shown in Figure 1.9. The most basic design is a single band gap device, while more complex structures involve multiple semiconductors (either layered or as separate electrode). Solar water splitting can also be achieved without semiconductor/liquid junctions using a standalone PV device connected to an electrolyser or without any electrodes at all in the case of photocatalysts.

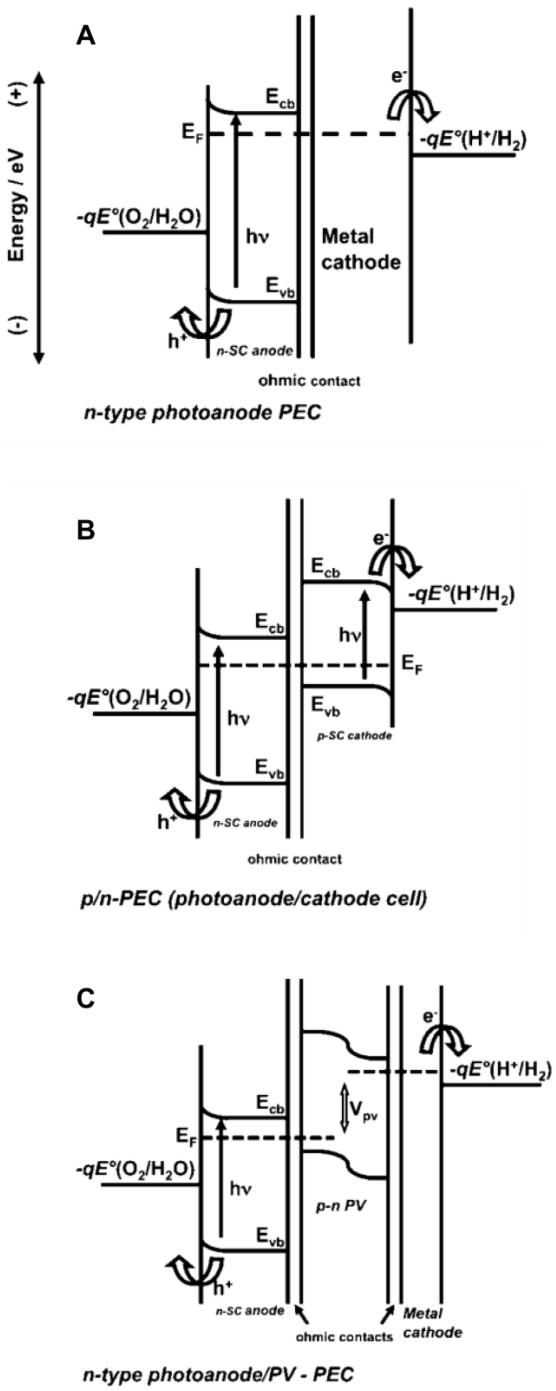

Figure 1.9 **Energy diagram for a single band gap photoanode (n-SC = n-type semiconductor) with metal cathode back contact (A); a dual band gap p-n PEC configuration with p-type and n-type photoelectrodes electronically connected in series (B); n-type photoelectrode in series with an integrated p-n PV cell to provide additional bias and connected to a metal cathode for hydrogen evolution (C). Adapted with permission from ref. [85]. Copyright 2010 American Chemical.**

Single band gap devices (Figure 1.9A) have the advantage of being the least complex. The band edges of any single band gap device would have to straddle the redox potential of water. Although the voltage difference needed to split water could be obtained by photons with energy of 1.23 eV, any real device will have to overcome additional overpotentials (catalyst and wiring for example). Single devices are impacted by the fact that the size of the band gap (and energy per photon) is inversely proportional to the number of solar photons that can be absorbed. Single band edge water splitting systems may also refer to dispersed photocatalyst where semiconductor nanoparticles are dispersed in aqueous solutions and illuminated.

Tandem devices (Figure 1.9B) use a layered architecture which provides several advantages over the single layer device. More light can be absorbed by using semiconductors with different band gaps. For example, a typical device would have a large band gap material stacked on a small band gap material. The first absorber would absorb light with $\lambda \leq \lambda_{g1}$, where λ_{g1} is the longest wavelength light that will excite an electron to the conduction band. The sun's lower energy (longer wavelength) light will be absorbed by the second layer ($\lambda_{g1} < \lambda \leq \lambda_{g2}$). Another advantage is that by having the layers connected in series, the chemical potential produced from each layer is combined and the stack can carry out higher energy reactions than each semiconductor could carry out alone. Using water splitting as an example, the top layer would have a valence band/HOMO positioned for water oxidation and the bottom layer would have a conduction band/LUMO positioned for proton reduction.

Other tandem or multijuntion devices are possible. The layered structure can be replaced by duel photoelectrodes where both band gap materials form semiconductor/liquid junctions (similar to Figure 1.9B). The advantage of this system is that the mixing of product gases is prevented because the electrodes (which are connected in series) operate in separate compartments. Another type of layered device uses a buried p-n junction PV layer (Figure 1.9C). The p-n junction layer is considered buried because it is covered with a photoelectrode material which is capable of either water oxidation or proton reduction. The PV layer is chosen so that it is able to provide

the additional voltage needed to perform the other half of the water splitting reaction at a metal electrode.

An early attempt to determine the optimal band gap under solar illumination was made by Bolton *et al*. in 1985.[87] These early researchers considered single and dual, or tandem, band gap devices for complete water splitting. A device with E_g = 1.6 eV (775 nm) gave the highest efficiency in the single absorber category with an ideal limiting solar conversion efficiency of 30.7 %. When considering a tandem device, a maximum efficiency of 42.4 % was calculated for a device with a top layer that absorbed light up to 655 nm (E_g = 1.9 eV) and a bottom layer that absorbed up to 930 nm (E_g = 1.3 eV). It should be noted that the model does not consider kinetics of the hydrogen and oxygen evolution reactions, HER and OER, respectively.

A more detailed analysis of tandem cells was conducted by Hu *et al*. which included variables such as the absorber fill factor (FF), solution resistance, and electrocatalyst (Pt, RuO_2, NiMo and $NiFeO_x$) efficiency.[88] The FF of a solar cell is the ratio between the cell's maximum power and the product of the open circuit voltage (V_{OC}) and the short circuit current (I_{SC}), the FF is also inversely related to the equivalent series resistance. Tandem devices were also compared to photoanode-photocathode and a system were a standalone PV is connected in series to an electrolyser. Solar light was simulated using 1 sun which provides 1000 W m^{-2} of irradiance over the wavelength range 0.3-4.0 µm. The spectra of the sun is recorded under AM 1.5 (air mass 1.5) conditions where the sun is at a zenith angle of 48.2° and light travels 1.5 times longer through the atmosphere than when the zenith angle is 0°.

Under 1 sun illumination (100 mW cm^{-2}, AM 1.5) an ideal system composed of a top absorber with E_g = 1.60 eV and a bottom absorber with E_g = 0.95 eV with an FF = 0.85 for all three systems produces a solar-to-hydrogen (STH) (equation (1.4)) efficiency of approximately 29 %. The tandem and photocathode + photoanode system used Pt and RuO_2 as HER and OER electrocatalyts, respectively and the PV + electrolyser used a 73 % efficient electrolyser. Despite the similarity in efficiency there are very different design considerations. Any PV + electrolyser system will have to ensure that the standalone components are current and potential matched.

Photocathode + photoanode systems would require both electrodes to be facing the sun, doubling the area required compared to tandem devices.

A recent review by Ager *et al*. has compared the STH efficiency of spontaneous solar water splitting devices going back to 1977.[89] The STH efficiency is given by:[90,91]

$$STH = \frac{(1.23\ V)(J_{op})}{P_{in}} \qquad (1.4)$$

where J_{op} is the operational photocurrent density (mA cm^{-2}) and P_{in} is the incident irradiance (mW cm^{-2}). Devices which split water spontaneously require no external applied bias. Due to the lack of standardized testing conditions in the solar water splitting field the results must be accepted as approximate. Most devices are fabricated using inorganic non-metal oxide semiconductors. Electrode arrangements range from having at least one semiconductor-liquid junction to photovoltaic-based electrosysthetic cells (PV + electrolyser). The top performing device was an AlGaAs/Si PV with Pt (HER) and IrO_2 (OER) electrodes (a PV + electrolyser device) which achieved a STH of 18.3 % over 14 hours.[92] There are seven other reports of devices with efficiency over 10 %, and almost all are stable for 1-24 hours. This summary is an estimate but indicates that there is still a significant distance to go in terms of reaching the predicted efficiencies from the studies described above.

In addition to this study, researchers at the Joint Center for Artificial Photosynthesis (JCAP) have also conducted numerous studies on other aspects of water splitting systems using a physics and multi-phase model where charge and species transport, fluid flow and electrochemical reactions are considered. This model has been used to characterize different device structures,[93] variability of solar irradiation and temperature effects,[94] different membrane separators,[95,96] and the effects of catalyst coverage on a photoelectrode.[97]

Other studies examined potential large-scale hydrogen production facilities.[98–100] Technologies considered have been mentioned above (tandem device + electrocatalyst and photoanode + photocathode systems) as well as photocatalyst suspensions.

Designs considered include single and dual bed particle suspensions, fixed panel arrays, and arrays that track sunlight and concentrate it on the photoelectrode. Use of particle suspensions is a very simple and low cost route to produce hydrogen and oxygen from water. The predicted cost of H_2 via this route is \$1.60-\$3.20 per kg of H_2, below the U.S. Department of Energy target of \$4 per kg of H_2.[100] This is on par with the cost of producing hydrogen by steam methane reforming which costs \$1-\$5 per kg H_2.[101]

There are safety issues with these systems, however. A system using a single particle capable of splitting water requires separation of the produced gases for purity and to avoid explosive mixtures of H_2 and O_2 (4 % H_2 in O_2 or air).[33] Facilities employing panel arrays (photoelectrodes) would be more expensive at \$4.10 per kg H_2 for a tracking concentrator system and \$10.40 for fixed panels, but are safer and could produce purer fuel. Use of membranes, impermeable to gas but not ions, between hydrogen and oxygen evolving compartments could increase safety.[99] This type of system, also called an integrated PEC device is seen as a good compromise between technological maturity and cost (Figure 1.10).[102]

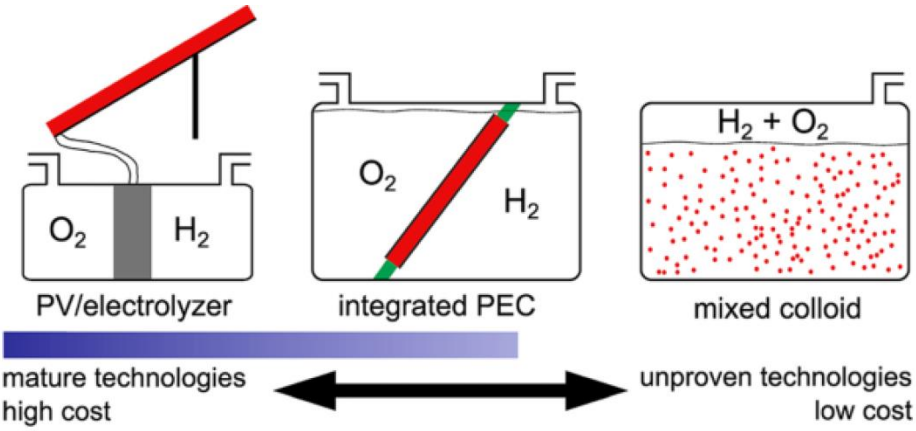

Figure 1.10 Schematic of three device architectures available for solar-driven water splitting, ordered according to their relative technological maturity and projected costs to manufacture. Reprinted with permission from ref. [102]. Copyright 2014 American Chemical.

1.4. Brief Summary of Photoelectrode Materials

1.4.1. Titanium Dioxide

The first demonstration of photoassisted water splitting was made by Honda and Fujishima using a TiO_2 photoelectrode and a platinum black counter electrode in 1972.[103] To this day, TiO_2 continues to be one of the most heavily researched semiconducting materials for water splitting due to its low cost and high chemical stability. TiO_2 is an n-type semiconductor meaning that oxidation reactions are promoted under illumination because holes accumulate at the surface. TiO_2 can be employed as either a photocatalyst dispersed in solution[104] or deposited on an electrode to be used in a photoelectrochemical system.

There are some drawbacks to its use, however. The band gap of TiO_2 is 3.2 eV which means UV light is needed to excite electrons from the valence band to conduction band. The efficiency of a TiO_2 only device is greatly hampered because UV light only accounts for 10 % of the solar spectrum. The conduction band edge of TiO_2 is positive relative to the proton reduction level so either a bias or a complementary photoelectrode also is required.

Some of these limitations can be overcome by manipulation of the morphology or doping with other elements. Mor *et al.* have shown that titania nanotube arrays greatly enhance photocurrent due to increased surface area and decreased path length for electron diffusion.[105] Nanotube arrays were prepared by anodization (10 V) of a titanium sheet in an HF + acetic acid electrolyte mixture. The highest photocurrent was obtained for nanotubes prepared at 5°C had the thickest walls (34 nm) and were longer (224 nm) than tubes prepared at higher temperatures due to temperature dependence of the chemical etching (by HF) and solubility of the product. Above 1 $V_{Ag/AgCl}$ photocurrents reached 17 mA cm^{-2} but only under UV illumination (100 mW cm^{-2}, 320-400 nm). The decrease in photocurrent with tube thickness is due to the fact that as the scale of the material decreases the space charge layer decreases and so does the strength of the internal electric field which results in less effective charge separation.

By treating TiO_2 with different gases at high temperature, the band gap can be tuned to extend absorbance to visible wavelengths. Hoang *et al*. have shown that a hydrogen and nitrogenation co-treatment extends the absorption edge of TiO_2 to 570 nm compared to 420 nm for pristine TiO_2.[106] Nitrogen doping raises the valence band while hydrogen gas treatment increase the concentration of Ti^{3+} present in the bulk which introduces a new level below the conduction band.

1.4.2. Silicon

Silicon has a band gap of 1.1 eV and can be either p- or n-doped. A significant portion of the visible spectrum is absorbed by silicon. The small band gap also means that a single layer Si device cannot split water but the conduction band is positioned well for proton reduction. Two methods for making Si photoelectrodes involve either nano/microwires (N/MW) or multijunction devices. Nano or microwire devices have the advantage of high surface area for light absorption and redox reactions as well as decreasing the distance charge carriers have to travel which reduces the recombination rate. Multijunction solar cells are stacks of differently doped Si semiconductors, which allows the band gaps to be varied, increasing the portion of sunlight absorbed, and complementary band edges which extend the redox power of the device.

Microwires of silicon (Si MWs) have been shown to be an improvement over planar electrodes.[107–109] Si MW (p-type) with diameter ≤ 2 μm have been shown to have large minority carrier (electron) diffusion lengths of 10 μm[110] to 30 μm.[111] It is also possible to use lower quality material (higher impurity concentration leads to higher possibility of recombination) as, following photogeneration, charge carriers only need to travel a short distance to reach the electrode surface and participate in electrochemical reaction. Microwires embedded in membranes have been envisioned for unassisted solar water splitting (no additional bias applied).[112] Membranes with ionically or electronically and ionically conducting (nafion and nafion/PEDOT:poly(styrenesulfonate) (PSS)) materials have been considered.[96,113,114]

Surface oxidation of silicon can occur over time and research into protecting the surface focuses on small organic molecules or metal oxides, such as TiO_2 and

Fe_2O_3.[115-117] In addition to increasing stability some of these material combinations have been shown to reduce sensitivity to pH.[115] Seo *et al*. showed that Si|R|TiO_2|Pt, where R is a $Ph(OMe)_2$, has an onset potential of +207 mV_{RHE} for proton reduction in 0.5 M H_2SO_4 under 1 sun illumination (100 mW cm^{-2}, AM 1.5G) and high stability to air storage.[118]

1.4.3. Compound Semiconductors

Compound semiconductors are alloys of group 13 and 15 elements and also called III-V semiconductors. One of the first examples for solar water splitting using a compound semiconductor is of p-$GaInP_2$ tandem with p-/n-GaAs.[119] The bandgap of p-$GaInP_2$ is 1.83 eV; theoretically this semiconductor could split water on its own. Unfortunately, it valence band is a few hundred millivolts too negative to oxidize water. Use of p-/n-GaAs as an underlayer extends the energy of photogenerated holes to levels where water oxidation is possible. As an additional benefit, the band gap of p-/n-GaAs is 1.42 eV allowing lower energy infrared light to be absorbed. This device achieved a photocurrent of 120 mA cm^{-2} (decaying to 105 mA cm^{-2} over 20 hours) and solar to hydrogen conversion of 12.4 %. In an attempt to split water with p-$GaInP_2$ on its own and to reduce some of the complexity and cost of this device, present efforts are focused on lowering valence band edge through surface modification with small molecules[120] and transition metals.[121]

GaP is also a useful compound semiconductor because its band edges are positioned for water oxidation and proton reduction. The band gap of GaP is 2.26 eV and p-GaP is very stable under acidic condition.[122] Hole injection in the film can be accomplished using dye-sensitization which improves the performance under visible light.[123] Similar to silicon, the stability has been further improved by modifying the surface with methyl groups.[124]

1.4.4. Iron Oxide

Iron oxide is another metal oxide semiconductor that has received much attention in the literature, specifically hematite (α-Fe_2O_3). Like TiO_2, α-Fe_2O_3 is inexpensive and

robust. Hematite is an n-type semiconductor with band edges positioned for water oxidation but not proton reduction. It also has a band gap of 2.2 eV making it more active in the visible region than TiO_2. Some of the disadvantages of hematite are its low molar absorptivity ($\alpha \sim 8 \times 10^4$ cm^{-1} at $\lambda = 550$ nm)[31,32] requiring thick films, short hole diffusion length (2-4 nm)[125] and poor oxygen evolution reaction kinetics.[126]

The performance of α-Fe_2O_3 can be improved by using nanostructured films and employing an oxygen evolution catalyst. Grätzel *et al*. have shown high photocurrent with nanostructured α-Fe_2O_3 following deposition of IrO_2, an excellent OER catalyst.[126] Films were prepared by atmospheric pressure chemical vapor deposition, using $Fe(CO)_5$ as a source, and achieved currents of 3 mA cm^{-2}. The photocurrent of nanostructured α-Fe_2O_3 exceeds the photocurrent obtained by single crystal, planar electrodes by two orders of magnitude.[127]

Smith *et al*. have shown that planar films can be prepared with lower temperature techniques.[128] Planar films were prepared by spin coating a solution of iron(III) 2-ethylhexanoate followed by irradiation with 185 and 254 nm light. Annealing at 500°C or greater produced crystalline films but annealing at 100°C produced films that displayed electrocatalytic (no illumination) properties in 0.1 M KOH. Transition metal electrodes are typically subjected to high temperatures in order to form the crystal phase of interest so this research provides a method for forming films on more substrates (plastics that decompose at high temperature for example).

1.4.5. Organic Semiconductors

Several early studies on photoelectrolysis with organic semiconductors were undertaken by Abe and co-workers.[129] Their work focused on p/n bilayers of small organic molecules and fullerenes (Figure 1.11). The organic materials used were either p-type (phtalocyanine with cobalt (CoPc), zinc (ZnPc), or non-metallated (H_2Pc)) or n-type 3,4,9,10-perylenetetracarboxylic acid bisbenzimidazole (PTCBI).[130–132] Fullerenes used were n-type and consisted of C_{60} or its soluble derivative PCBM. By alternating which layer was deposited first, the bilayer could act as a photoanode or photocathode. For example an indium tin oxide (ITO)/C_{60}/H_2Pc electrode acts as a photoanode and has

been used to oxidize thiols[133] and an ITO/H_2Pc/C_{60} electrode acts as a photocathode and has been used to reduce ferricyanide, $[Fe(III)(CN)_6]^{3-}$.[134]

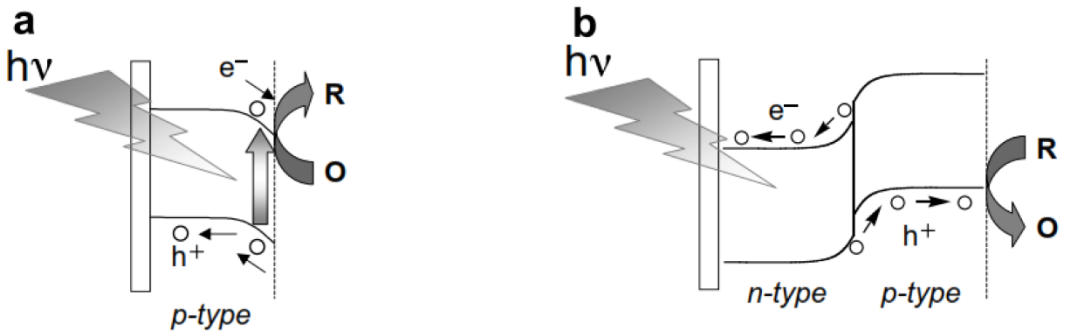

Figure 1.11 A schematic of the photoinduced reaction at a p-type semiconductor/water interface in a single layer (a) as well as the p/n bilayer (b). R and O denote reductant and oxidant, respectively. Reprinted with permission from ref. [129], with permission from Elsevier.

In the area of solar water-splitting Abe demonstrated that an ITO/H_2Pc/C_{60} electrode can reduce protons when a Pt catalyst is used.[135] The photoactive material was deposited by vapor phase deposition and had a final thickness of H_2Pc = 75 nm and C_{60} = 125 nm. Platinum was photoelectrochemically deposited from a $H_2PtCl_6^{2-}$ solution. Hydrogen evolution was achieved in a phosphoric acid electrolyte solution (pH 2) under white light intensity of 100 mW cm^{-2}. A total of 333.5 µL of H_2 was produced over 3 hours at an applied bias of -0.1 $V_{Ag/AgCl(sat.)}$. The proton reduction potential at pH 2 is -0.32 $V_{Ag/AgCl(sat.)}$ meaning 0.22 V was gained by illumination. A two compartment system consisting of an ITO/H_2Pc/C_{60}/Pt photocathode in phosphoric acid solution (pH 2) in one half and an ITO/PTCBI/H_2Pc photoanode in a KOH (pH 11) and thiol solution was constructed to demonstrate full photoelectrolysis with organic material.[136] The two compartments were separated by a salt bridge (agar and KNO_3). Without any applied bias, 2.5 mL of H_2 was produced over 30 hours.

The photocathodic activity at conjugated polymers for water splitting applications has resurfaced as an area of interest, as demonstrated by a number of recent reports, in which multiple layers are employed to increase photocurrent or photostability. For example, Lanzani *et al*. demonstrated that P3HT:PCBM films on ITO generates stable,

unbiased, photocurrent in the sub-μA cm^{-2} range in aqueous NaCl.[137] The observation of gas bubbles on the film led to the conclusion that the photocurrent was due to proton reduction at the P3HT:PCBM bulk heterojunction (BHJ) electrode and oxidation of Cl^- at the counter electrode. Bourgeteau *et al.* used the deposition of TiO_2/MoS_3 layers on top of P3HT:PCBM coated on PEDOT:PSS to promote photocathodic hydrogen evolution.[138] Photocurrents of 200 μA cm^{-2} at 0 V_{NHE} in 0.5 M H_2SO_4 were obtained upon employment of MoS_3 co-catalyst, stabilized with TiO_2. Gustafson *et al.* studied photocurrent of ITO-polyethylene terephthalate (PET)/PEDOT:PSS/P3HT:PCBM films, employing sputtered Pt on top of the BHJ film,[139] and demonstrated that by changing the underlying hole transport layer (PEDOT:PSS) to an electron transport layer (ZnO) the electrode behaviour changed from photocathodic to photoanodic. Guerroero *et al*. demonstrated dual photoanode (ITO/ZnO/P3HT:PCBM) and photocathode (ITO/PEDOT:PSS/P3HT:PCBM) behavior in organic solvents and obtained photocurrents up to 4 mA cm^{-2} and 1.5 mA cm^{-2}, respectively.[140] Hydrogen evolution was also achieved in acidified acetonitrile in the presence of a cobalt-containing, organometallic catalyst (cobaloxime). Recently, Haro *et al*. employed an insoluble cross-linkable PEDOT:PSS hole transport underneath a P3HT:PCBM BHJ, onto which a low-temperature processable TiO_x interfacial layer is deposited followed by sputtered uniform Pt Layer. These multilayer systems achieve photocurrents up to 1 mA cm^{-2} and a H_2 generation rate of 1.5 μmol h^{-1} cm^{-2}.[141]

1.5. Characterization Techniques

1.5.1. Photoelectrochemical Cell

Photoelectrochemical measurements require a specialized cell in order to keep the atmosphere in the cell contained (in other words, air tight) and have at least one flat face or a window to allow illumination of the working electrode. The cell used for the work in this thesis was designed and built in-house (Figure 1.12). Typically, quartz is used to make PEC cells because it transmits UV and visible light but borosilicate glass was used for the cell in Figure 1.12 because P3HT (the material used to make the photoelectrodes) primarily absorbs visible light.

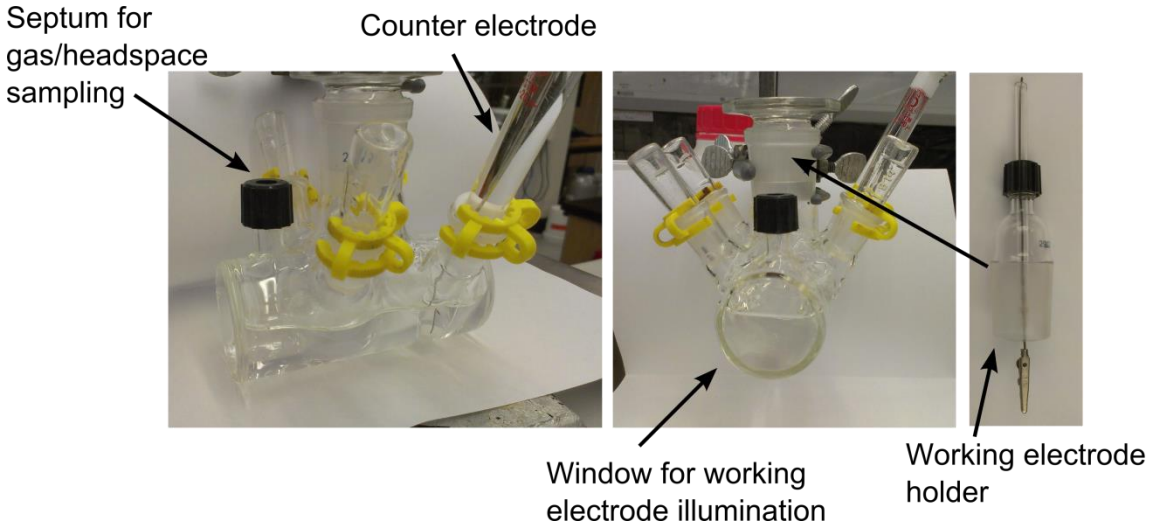

Figure 1.12 Glass cell used photoelectrochemical measurements. The working electrode is illuminated through a window at the front of the cell. Along each side are two 14/20 ground glass ports for a counter electrode, reference electrode and two other accessories (other probes or a nitrogen line for example). The working electrode hangs in the center.

1.5.2. Linear Sweep and Cyclic Voltammetry

Linear sweep voltammetry is a dynamic electrochemical method where the current at a working electrode is measured in response to a linearly applied potential (measured with respect to a reference electrode). The potentials scanned in linear sweep voltammetry are between two points. Cyclic voltammetry is an extension of linear sweep voltammetry where, after reaching a defined endpoint in the scan, the direction of the scan is changed. Cyclic voltammetry makes it possible to measure the reversibility of an electroactive species.

The cyclic voltammogram of a P3HT coated glassy carbon electrode in 0.1 M tetrabutylammonium perchlorate (TBAP)/acetonitrile (MeCN) is shown in Figure 1.13. The potentials are reported with respect to the ferrocene/ferrocenium (Fc^+/Fc) redox couple, a common standard for non-aqueous electrochemistry.[142] The film is initially in its neutral and insulating state (potentials < 0 V vs. Fc^+/Fc). As the potential is scanned to the right (larger, positive values) the film begins to oxidize as indicated by a large increase in current. The onset of oxidation ($E_{ox,onset}$) represents the ionization potential

(IP) of the polymer, the lowest potential that can remove an electron from the material, which is equivalent to the HOMO level. $E_{ox,onset}$ can be approximated by extrapolating the linear parts the voltammogram (Figure 1.13).[74,143]

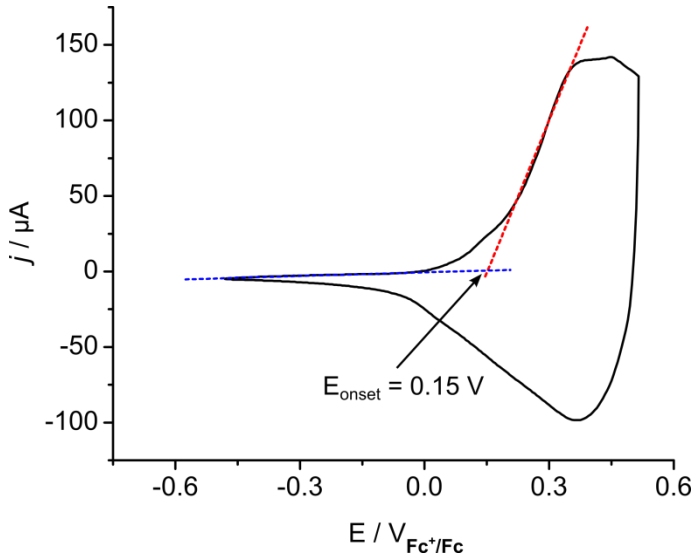

Figure 1.13 CV of P3HT coated glassy carbon electrode in 0.1 M tetrabutylammonium perchlorate, scan rate was 100 mV s^{-1}.

The IP (in units of eV) can be calculated from:

$$IP = -(4.8\ eV + E_{ox,onset}) \qquad (1.5)$$

The value 4.8 eV is the IP of ferrocene or the vacuum level position of the ferrocene/ferrocenium redox couple[144] and $E_{ox,onset}$ is obtained from Figure 1.13.

1.5.3. Electrochemical Impedance Spectroscopy

Electrochemical impedance spectroscopy (EIS) is an alternating current technique that is used to determine reaction mechanisms at electrode surfaces and properties of films coating electrodes. In a typical three electrode cell, a time varying potential is applied to the working electrode and the current response is measured. The dynamic nature of the potential-current relationship results in the measurement of the impedance of the system.

In the context of semiconductors, EIS is used to measure the flat band potential (E_{fb}). Flat band potential is the applied potential where the energy levels of the semiconductor (CB, VB, E_F) are flat while in contact with a redox containing electrolyte solution (Figure 1.14). When the bands are flat there is no electric field inside the surface of the semiconductor and, therefore, no depletion region. Without an internal electric field to separate charge, E_{fb} represents the limit where illumination of the electrode will produce a photocurrent. Consider the band structure of an n-type semiconductor pictured in Figure 1.14B. The applied potential, E (in units of volts, V), equals the flat band potential, E_{fb}. When $E > E_{fb}$ (the applied potential is more positive than E_{fb}), a depletion layer forms and photocurrent will be generated when the semiconductor is illuminated. When $E < E_{fb}$, the band bending is reversed (compared to Figure 1.14A) and electrons will begin to accumulate at the interface.

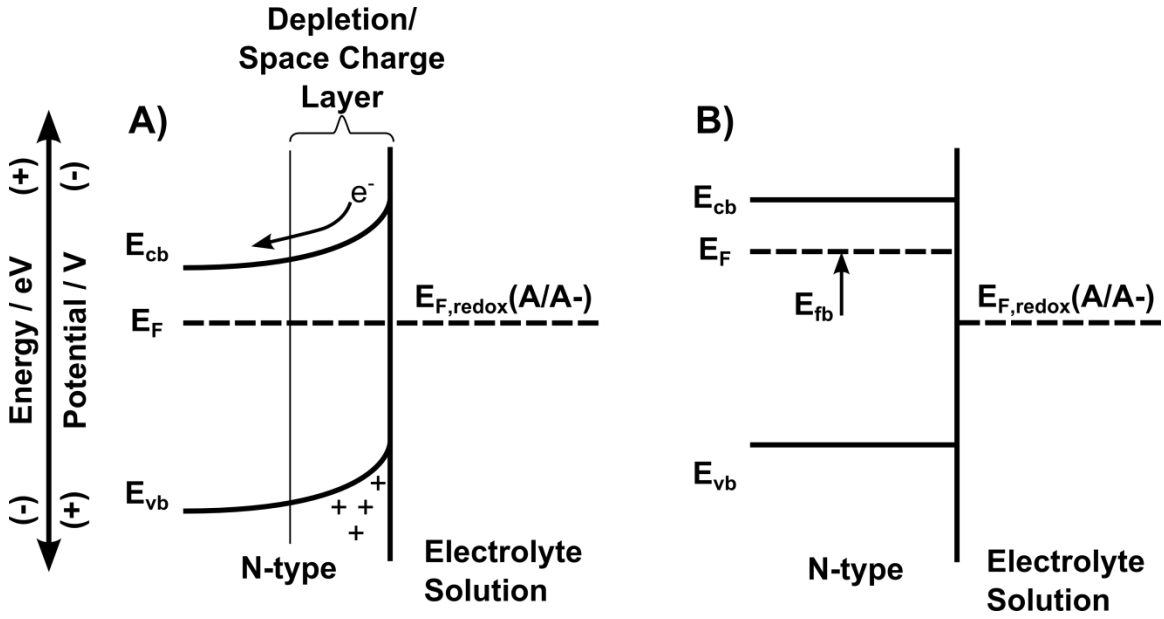

Figure 1.14 Band structure of an n-type semiconductor in contact with an electrolyte solution containing a redox couple (A/A^-) when there is no applied potential (A) and when the applied potential = E_{fb} (B). E_{cb}, E_{vb}, and E_F are the energy levels of the valence band, conduction band, and Fermi level respectively.

The value of E_{fb} is extracted from EIS data using a Mott-Schottky plot (C_{SC}^{-2} vs. E, the applied potential) and the Mott-Schottky relation given in Equation (1.6).

$$\frac{1}{C_{SC}^2} = \frac{2}{\varepsilon\varepsilon_o A^2 qN}\left(E - E_{fb} - \frac{k_B T}{q}\right) \quad \textbf{(1.6)}$$

where C_{SC} is the space charge layer capacitance (μF cm^{-2}), N is the number of charge carriers (cm^{-3}), ε_0 the permittivity of free space, ε is the dielectric constant of the material, A is the electrode area (cm^2), q is the charge of an electron, E is the applied potential (V), k_B is Boltzmann's constant, and T is the temperature in Kelvin (K). In a Mott-Schottky plot the value of E_{fb} is obtained by extrapolating the linear part of the curve to $C_{SC}^{-2} = 0$. C_{SC} is calculated using Equation (1.7):

$$C_{SC} = \frac{-1}{2\pi f Z_I} \quad \textbf{(1.7)}$$

Where Z_I is the imaginary impedance (y-axis of the Nyquist plot) and f is the frequency (Hz). The capacitance calculated from the imaginary impedance can be assigned to the space charge layer because it is the only one that contributes significantly to the total capacitance (C_{tot}). The total capacitance is calculated from a series combination, Equation (1.8):

$$\frac{1}{C_{tot}} = \frac{1}{C_{SC}} + \frac{1}{C_H} + \frac{1}{C_{Gouy}} + \frac{1}{C_{bulk}} \quad \textbf{(1.8)}$$

where C_H is the capacitance of the Helmholtz layer, C_{Gouy} is the capacitance of the Gouy layer, and C_{bulk} is the capacitance in the bulk of the material. Each layer is pictured in Figure 1.15. The bulk regions are neglected due to lack of charge accumulation. The Gouy layer is a space charge layer in solution due to excess of either cations or anions. If the electrolyte concentration is ≥ 0.01 M there is no contribution to the capacitance by the Gouy layer. The high concentration of the electrolyte (≥ 0.01 M) The Helmholtz double layer formed by two planar sheets of charge, one sheet consisting of free charges in the solid electrode and another sheet made up of adsorbed ions or ions in solution. With metal electrodes, the majority of the potential drop in the system is across this layer. The space charge layer is several orders of magnitude larger than the

Helmholtz layer and C_H can be neglected because capacitance is inversely proportional to the distance between the plates (thickness of layers in this case).

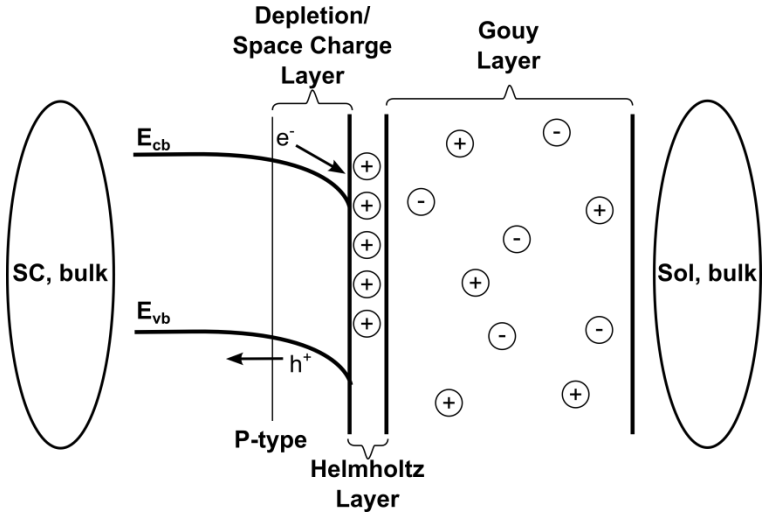

Figure 1.15 All regions that can contribute to the total capacitance when a p-type semiconductor is in contact with an electrolyte solution. SC,bulk and Sol,bulk represent the bulk of the semiconductor and solution, respectively. E_{cb} and E_{vb} are the energy levels of the valence band and conduction band, respectively.

1.5.4. Spectroelectrochemistry

Spectroelectrochemistry (SEC) is a very useful technique that combines spectroscopic information with the ability to fix the oxidation state of a thin solid film or redox couple in solution. In a typical setup, a Pt or Au mesh is used as a working electrode for redox couples in solution or ITO coated glass slides with a thin film of the material of interest. A Pt wire counter electrode and appropriate reference electrode (non-aqueous or aqueous) are used in a typical three electrode cell. The cell includes a cuvette where the working electrode is placed, a separate compartment for a counter electrode, and a tube extending half way down the cuvette for bubbling the solution (Figure 1.16).

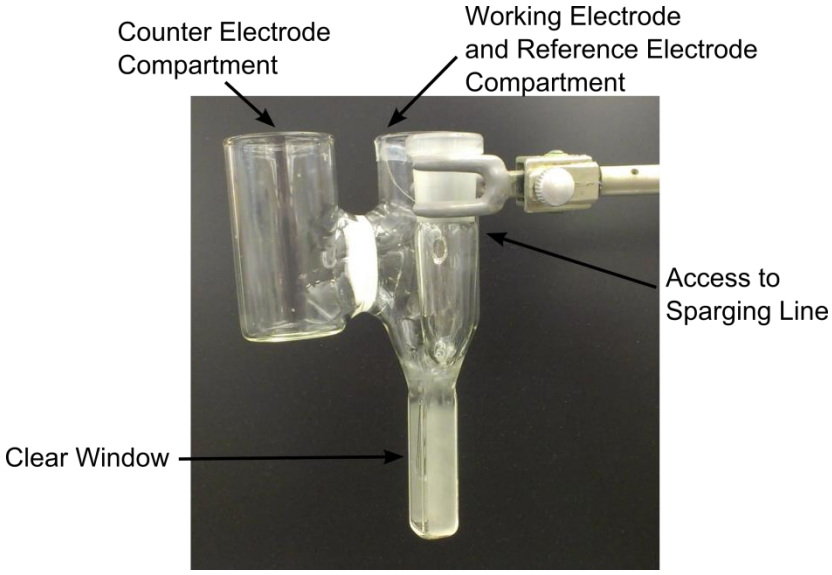

Figure 1.16 The cell used in spectroelectrochemical experiments. The cell contains three openings. The counter electrode compartment is separated from the working and reference electrode compartment by a glass frit.

In the context of conjugated polymers, SEC has been used to observe the introduction of states within the band gap due to oxidation.[145] Under ambient conditions a thin polymer film will be in its neutral or oxidized state, depending on the reduction potential of the polymer. Placing the film in a solution containing a chemical oxidant might offer some control over the polymer's oxidation state, but multiple oxidants of different strength would be required to obtain a series of spectra. Electrochemistry offers the ability to dial in the oxidation state of the conjugated polymer by controlling the potential, which is especially useful because two distinct charge carriers are formed at different levels of oxidation.

Polarons and bipolarons are generated along the polymer backbone during oxidation. A polaron is a radical cation (in the case of oxidation) formed along the polymer backbone when an electron is removed. Bipolarons are formed when the electrons of two polarons combine or one polaron is oxidized as the potential is made more anodic (positive) or a stronger oxidant is used. Both charge carriers can be identified by UV-Vis-NIR spectroscopy. The UV-visible absorbance of the polymer decreases and is replaced by peaks in the NIR as the polymer is oxidized (Figure 1.17). The band gap states introduced due to polaron and bipolaron formation provide lower

energy pathways for electron transfer from the HOMO and therefore lower energy photons are absorbed.

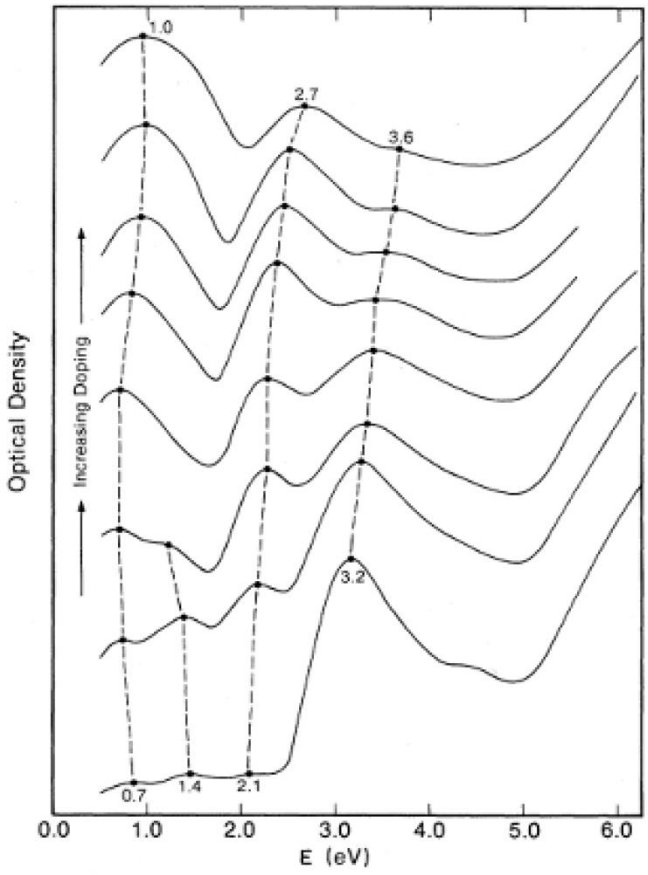

Figure 1.17 Evolution of the optical-absorption spectrum of polypyrrole from a neutral film to oxidized and fully doped. The doping level is increased by applying an increasing, positive potential. The concentration of perchlorate anions from bottom curve (almost neutral PPy) to the top curve (33 mol % doping level). Reprinted figure with permission from ref. [145]. Copyright 1984 by the American Physical Society.

1.5.5. Gas Chromatography

The most common technique for analysing PEC cell head space for hydrogen or oxygen is with gas chromatography (GC) and the most common analyser is a thermal conductivity detector (TCD).[146] GC is used so that all gases in the cell can be separated out. Also, a syringe with a gas tight valve is used. While sampling the cell headspace

then injecting into the GC, the needle is open to air and some oxygen and nitrogen is detected. TCD is used because it is non-selective detector. Other common GC detectors are flame ionization detector (FID) and electron-capture detector (ECD). FID is used to detect organic molecules and hydrogen is used as the fuel for the flame so hydrogen detection is impossible. ECD is selective for halogen containing compounds.

1.6. Thesis Scope

In the preceding decades, research into photoelectrochemical water splitting has focused on the use of inorganic materials. Conjugated polymers have received comparatively little attention despite good visible absorption and band edges suited for proton reduction. Conjugated polymers also have strong light absorption, requiring only thin films and are solution processable and can be coated onto many different substrates at room temperature. This thesis research focuses on using single layer P3HT photocathodes for proton reduction.

Chapter 2 examines the characteristics of a P3HT photocathode in aqueous acid without the use of any HER catalyst. Films are prepared on both glassy carbon and ITO. The dependence of the photocurrent and photon conversion efficiency as a function of thickness and incident light power are determined. Spectroelectrochemisty was also performed in order to determine if the polymer remains neutral and semiconducting under the conditions of photoelectrolysis. A mechanism for the photocurrent is proposed based on these results and photoluminescence spectroscopy of films in contact with aqueous acid and deionized water.

A HER catalyst (Pt) is employed in Chapter 3 and Chapter 4. P3HT is thermodynamically able to reduce protons but kinetically this may be difficult to accomplish. The use of a HER catalyst should improve the electron transfer from the photo excited polymer to protons in solution. In Chapter 3 nanoparticles are formed on P3HT photocathodes by photoelectrochemical deposition. In Chapter 4, platinum is dispersed in solution in the form of a colloid and an electron relay (methyl viologen) is used to transfer charge between the polymer and the catalyst.

Chapter 2.

Aqueous Photocathode Activity of Regioregular Poly(3-hexylthiophene)

This chapter is reproduced from: Graeme Suppes, Edward Ballard and Steven Holdcroft, *Polymer Chemistry*, **2013**, Vol. 4(20), 5345-5350 with permission from The Royal Society of Chemistry. E. Ballard assisted in making thickness dependence measurements in Section 2.3.2.

2.1. Introduction

The current average rate of energy consumption on Earth is approximately 14 TW.[84] Energy from the sun is on the order of 120, 000 TW so it is not surprising, therefore, that strategies to capture as much of this energy as possible, and as inexpensively as possible, are gaining increasing momentum. In the solar energy sector, the photovoltaic (PV) industry is regarded as undergoing the fastest growth.[147] The PV industry is currently dominated by inorganic-based semiconductor materials. However, organic semiconductors are being intensely investigated because they offer potential attributes of low cost and low mass, and are easy to process as ultrathin films, compared to inorganic-based counterparts.[148–150] Another application area of interest for photoactive semiconductors is their employment as photoelectrodes in photoelectrochemical systems, which use solar radiation to drive specific chemical reactions to produce energy carriers, products, or destroy unwanted reagents.[151–154] As with inorganic semiconductors, organic semiconductor analogues are being investigated for photoactivity in solution to drive desired reactions. Examples include hydrogen production, CO_2 reduction, and degradation of organic pollutants.[153,155–157] π-Conjugated polymers are prime candidates for photoelectrode activity because they absorb visible light, and generate electrons and holes with significant redox power upon irradiation. π-

Conjugated polymers are typically p-type semiconductors, which means that during illumination in an electrochemical cell, electrons flow towards the semiconductor/electrolyte interface and result in electrochemical reduction reactions.

A ubiquitous example of a π-conjugated polymer is poly(3-hexylthiophene) (P3HT).[158] In PV devices, P3HT can provide power conversion efficiencies (PCEs) up to 6.5 % in conjunction with an electron acceptor .[159] The first report of P3HT being used as a photocathode in a photoelectrochemical (PEC) cell was reported by El-Rashiedy and Holdcroft.[160] It was discovered that application of a potential bias more negative than the Fermi energy [+0.3 V_{SCE}], in aqueous solution, resulted in a depletion layer at the polymer/solution interface, and that upon photoexcitation a photocathodic current was produced. Photovoltages generated were linearly related to the pH of the solution, in accord with the variation in reduction potential of the H^+/H_2 couple. Photocurrent and quantum efficiency, while dependent on the solution pH, irradiation intensity, excitation wavelength, and film thickness were, however, low. More recently, Yang *et al.* constructed PEC cells based on Langmuir-Blodgett (LB) films of P3HT.[161,162] Sub-μA cm^{-2} photocurrents were reported that increase by at least an order of magnitude upon incorporation of mono-metallofullerenes. Cathodic photocurrents were further increased by the introduction of oxygen or other electron acceptors into solution. Mechanisms for cathodic photocurrent generation, in the presence of methyl viologen, were proposed for films composed of P3HT and fullerene (C_{60}) or metallofullerene ($Dy@C_{82}$) and showed that PEC is useful way to gain insight into solar cell performance and design. More recently still, Abe *et al.* reported photoanode activity of a composite, P3HT/PCBM, in aqueous solution which was further enhanced in combination with a p-type zinc phthalocyanine surface modification.[163] The authors determined, based on transmission electron microscopy and PEC measurements, that photogenerated holes accumulate at the solid/solution interface due to maldistribution of P3HT towards the surface of the film.

Work carried by El-Rashiedy *et al*.[160] investigated the use of regiorandom (RRa) P3HT as a photocathode in aqueous solution. RRa-P3HT is prepared by oxidative polymerization using ferric chloride and possesses < 70 % head-to-tail couplings.[160] It is widely known that increasing the regioregularity of P3HT modifies the polymer's optical

properties and greatly enhances charge carrier mobility,[164] which may partly explain the low photocurrents and photo-efficiencies originally observed. In this report I demonstrate significantly enhanced photocurrents of regioregular (RR) P3HT in aqueous solutions when used in a photoelectrochemical cell according to Figure 2.1. I examined the electrochemistry of P3HT films in aqueous and non-aqueous solution in order to gain insight into the mechanism of photocathodic activity.

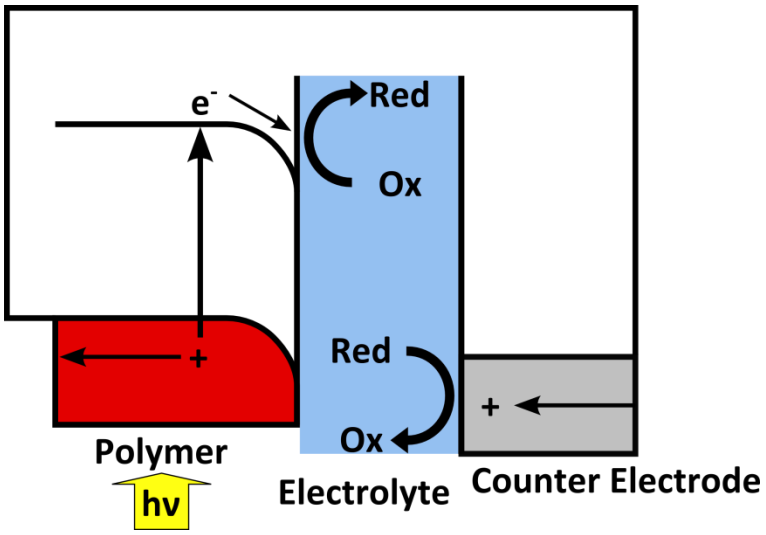

Figure 2.1 Photocathode activity of P3HT.

2.2. Experimental

2.2.1. Materials

Materials were used as received without any further purification. The monomer, 3-hexylthiophene, was purchased from Rieke Metals. Dodecylmagnesium bromide (1.0 M in ether), N-bromosuccinimide, and Ni(dppe)Cl_2 were purchased from Aldrich. Regioregular P3HT was prepared according to the GRIM method.[165,166] Preparation of the 2,5-dibromothiophene was carried out following a literature procedure.[165]

2.2.2. Regioregular P3HT Synthesis

To 80 mL of dry THF, 2,5-dibromo-3-hexylthiophene (7.86 g, 24.11 mmol) and dodecylmagnesium bromide (1.0 M in ether, 24 mL) were added. The solution was stirred at reflux for 1 hour. The catalyst, Ni(dppe)Cl_2 (64 mg, 0.12 mmol), was added and the solution was stirred for 45 minutes at reflux. After cooling to room temperature, the polymer was precipitated into 1 L of methanol. The solid was purified by Soxhlet extraction using successively methanol, hexane, and chloroform. The polymer dissolved in the chloroform fraction and was collected by rotary evaporation of the solvent. Molecular weight of the polymer were determined by gel permeation chromatography, GPC, (Mn = 31.7 kDa, PDI = 1.2). The degree of regioregularity was determined from ^{1}H NMR and found to ≥ 98 % HT-HT coupling (Figure A-1). Yield: 62 %.[164,167]

2.2.3. Thin Film Preparation

Solutions of (RR) P3HT in dichlorobenzene (10, 20, 25, 30, 35 and 40 mg mL^{-1}) were stirred and heated overnight at 60° C and spin cast at room temperature onto indium-tin oxide (ITO) coated glass (Ω ~ 10 ohms) in a glove box at 1000 rpm for 60 s to prepare films of variable thickness. The films were solvent annealed under a petri dish for 30 min followed by thermal annealing inside a glove box (H_2O and O_2 < 0.1 ppm) at 150° C for 30 min.

2.2.4. Characterization

Absorption spectra were recorded on a Cary 300 Bio UV-visible spectrophotometer. Photoluminescence (PL) spectra were obtained using a Photon Technology International PTI Felix32 system. Film Thicknesses were determined using an Alpha-Step IQ profilometer (KLA-Tencor). A Xe/Hg 200W lamp was used as the light source in combination with an AM1.5D filter (Photon Technology International LPS-250B.) and neutral density filters to achieve 100 mW cm^{-2}. The incident light power was measured using a broadband power meter 841-PE (Newport) equipped with an Ophir thermal detector head (3A-P-SH-V1). The cell configuration was designed to irradiate the polymer/electrolyte interface through the electrolyte. A water filter was placed in front of the electrochemical cell to remove excess heat. Electrochemical measurements were

performed using a Pine Bipotentiostat (AFC-BP1) and the data processed using Aftermath Scientific Data Organization Software (ASTP-B01 Module). Photoelectrochemical measurements were performed in a 3-electrode cell using an Ag/AgCl (sat. KCl) (0.199 V + 0.059 * pH relative to NHE) reference electrode and a platinum foil counter electrode in 0.1 M H_2SO_4 (unless otherwise stated).

2.3. Discussion and Results

2.3.1. P3HT Band Edge Determination: CV, UV-Visible Absorbance, and EIS

Films of RR-P3HT possess a broad absorption between 350 and 650 nm and an absorption maximum at ~550 nm. A UV-visible spectrum is shown in Figure 2.2 (inset). From the onset of the absorption (665 nm), the optical band gap (E_g) is estimated to 1.8 eV. RR-P3HT was deposited on a glassy carbon electrode and voltammetry was performed with a Pt counter electrode and a silver wire reference in 0.1 M TBAP / acetonitrile. As shown in Figure 2.2, the onset potential corresponding to the reduction and oxidation of RR-P3HT is -2.23 V and -0.01 V, respectively, vs. Fc^+/Fc , from which the energy levels of the valence band (E_{VB}) and conduction band (E_{CB}) are estimated to be -5.22 eV and -3.00 eV, respectively. [168] For any redox couple lower than E_{CB}, electrons promoted to the CB of RR-P3HT have sufficient energy to drive the reduction of material with a higher (more positive) redox couple.

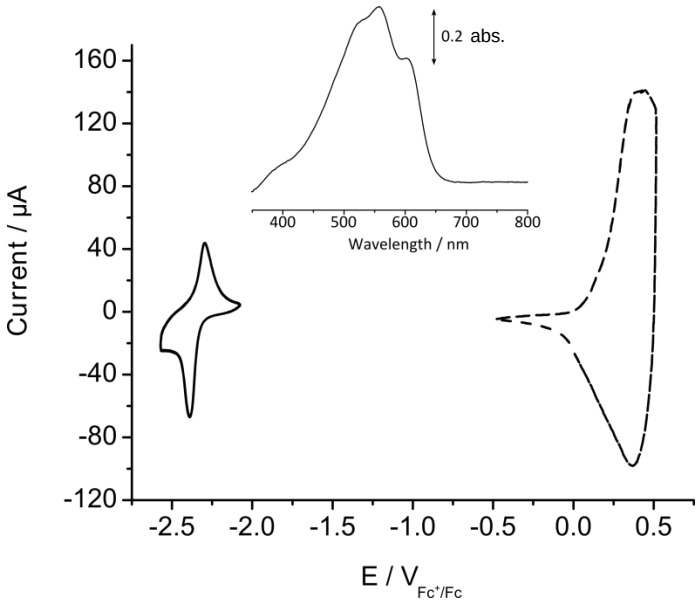

Figure 2.2 Cyclic voltammogram of P3HT coated on glassy carbon in 0.1 M TBAP-MeCN at a scan rate of 100 mV s^{-1}. The dashed and solid line represents the oxidation and reduction, respectively, of the neutral polymer Inset: UV-visible absorbance of a 100 nm thick film on ITO-coated glass. The scale bar indicates the absorbance.

Electrochemical impedance spectroscopy (EIS) was used to obtain a Mott-Schottky plot for RR-P3HT films (Figure 2.3). The plot consists of a linear portion with a negative slope, which is characteristic of a p-type semiconductor. Using the Mott-Schottky equation (Equation (1.6), the intercept with the x-axis and the slope, the flat band potential (E_{fb}) and the charge carrier density (N) was estimated. The parameters and constants in the Mott-Schottky equation are the dielectric constant, ε (3 in this study); [169,170] the permittivity of free space, ε_0; the charge of an electron, q, the Boltzmann constant, k_B; and the applied potential , E. For RR-P3HT in 0.1 M H_2SO_4, E_{fb} is ~+0.15 V (at 25 °C) (Ag/AgCl,sat.), or -4.7 eV. N was calculated to be 1.0×10^{17} cm^{-3}. The charge carrier density obtained for RR-P3HT is on the same order of magnitude reported for other conjugated polymers, including polybithiophene (3.5×10^{17} cm^{-3}), poly(4,4″-dimethoxy-3′-methyl-2′,5′,2″-terthiophene) (1.18×10^{16} cm^{-3}), and poly(3,4-dimethoxythiophene)/poly(styrene sulfonate) (2.6×10^{17} cm^{-3}).[171–173]

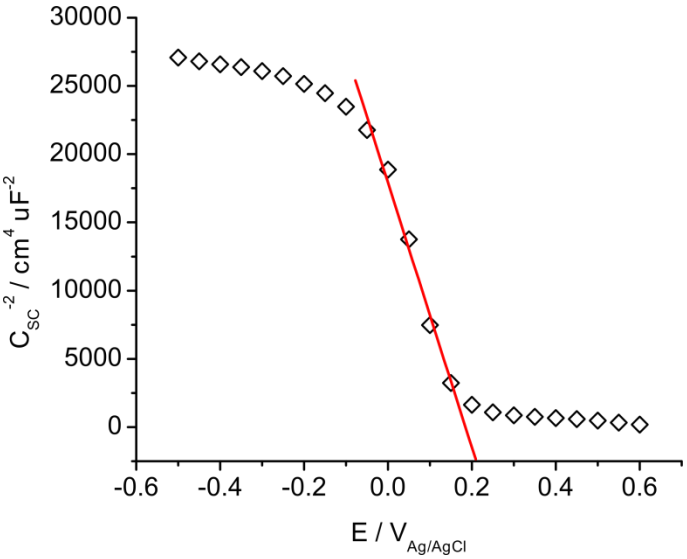

Figure 2.3 Mott-Schottky plot of RR-P3HT obtained using electrochemical impedance spectroscopy in 0.1 M H_2SO_4 (aq.), recorded in the dark at 100 kHz. Geometric area of working electrode is 0.07 cm^2.

2.3.2. P3HT Photoelectrochemistry in Aqueous Acid

A typical photo-assisted current-voltage curve for P3HT-coated ITO in 0.1 M H_2SO_4 is shown in Figure 2.4. A cathodic photocurrent (J_{ph}) is observed under illumination and increases with increasing applied negative potential. This current-voltage response is characteristic of a p-type semiconductor. A photocurrent density of ~20 µA cm^{-2} is measured at -0.4 $V_{Ag/AgCl}$. A plot of photocurrent at -0.2 $V_{Ag/AgCl}$ vs. thickness is plotted in Figure 2.5. The thinnest films studied (40 nm) yield a photocurrent of ~6 µA cm^{-2}, which increases to 10 µA cm^{-2} at -0.2 V with increasing thickness (250 nm), approaching a limiting value. A plot of transmittance of light vs. thickness, also shown in Figure 2.5, illustrates that light penetration at the polymer/electrolyte interface falls to 10 % of its original value over a distance of 130 nm. As the thickness of the film is increased, the number of photoactive units increases, explaining both the increase in photocurrent and decrease in transmittance. The electrical resistance of the film, however, also increases with film thickness, which may be responsible for the limiting value of the photocurrent. Furthermore, as photo-generated excitons in P3HT films possess relatively short diffusion lengths (≤ 10 nm),[174,175] excitons generated deeper into a thick film, i.e., more than an exciton diffusion length away from the space charge layer that exists at the P3HT/electrolyte interface, are unlikely to reach that interface. These

results are similar to other thickness dependant studies on RRa-P3HT and P3HT/metalofullerene composites .[160,161,176]

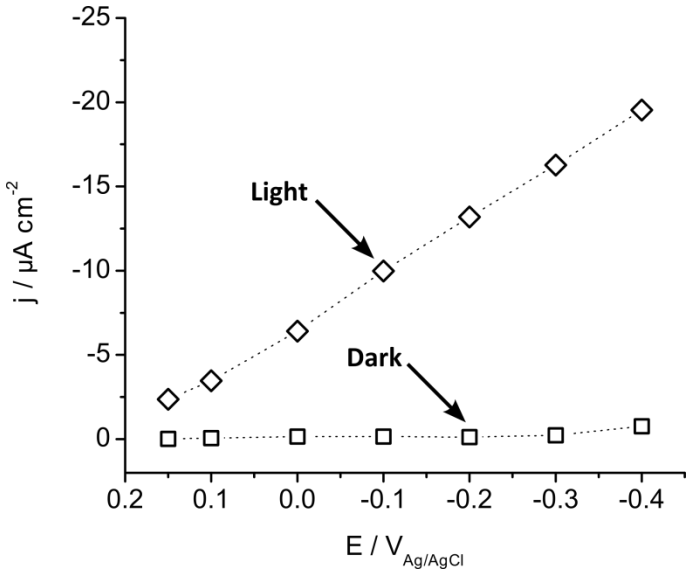

Figure 2.4 **Current-voltage plots of RR-P3HT (film thickness 126 nm) on ITO-glass in the dark and under illumination in 0.1 M H_2SO_4 (aq.). Light intensity was 100 mW cm^{-2} (AM 1.5D).**

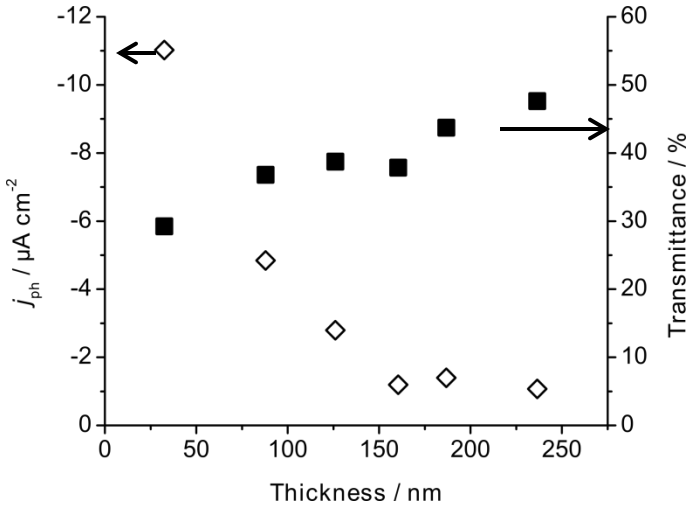

Figure 2.5 Dependence of the photocurrent (empty diamonds) and transmittance (solid squares) on the film thickness of RR-P3HT coated ITO. For photocurrent measurements Light intensity was 100 mW cm^{-2} (AM 1.5D) in 0.1 M H_2SO_4 (aq.) at E = -0.2 V (Ag/AgCl). Thin film transmittance data at λ_{max} 550 nm.

The incident photon conversion efficiency (IPCE) was calculated from the photocurrent at -0.2 $V_{Ag/AgCl}$ using Equation (2.1), where j_{ph} is the photocurrent (A cm^{-2}), λ is the wavelength of incident light (nm), I_0 is the incident power absorbed (W cm^{-2}), and the constant, 1240, has units of W A^{-1} nm^{-1}. A plot of IPCE vs. film thickness is shown in Figure 2.6. An IPCE of 0.55 % was observed for the thinnest films studied, but this dropped to 0.2 % for film thicknesses > 100 nm. The IPCEs are two orders of magnitude lower than observed for solid state, *bilayer*, organic PV devices (30-40 %)[177,178] that incorporate an electron accepting layer, but similar to *single layer* component organic PV devices (0.5 %).[4] The plateau in efficiency for films > 100 nm thick is considered to be due to the limited depth of light penetration and the inability of excitons formed deep in the polymer film reaching the polymer/electrolyte interface. The relationship between the IPCE and incident power, recorded at -0.2 $V_{Ag/AgCl}$ and 550 nm, is shown in Figure 2.7. Increasing the incident power increases the photocurrent but decreases the efficiency. With higher incident power, a greater number of excitons are generated, increasing the photocurrent. The likelihood of exciton recombination, however, also increases with increasing exciton population.

$$IPCE(\%) = \frac{1240 j_{ph}}{\lambda I_0} \times 100 \qquad \textbf{(2.1)}$$

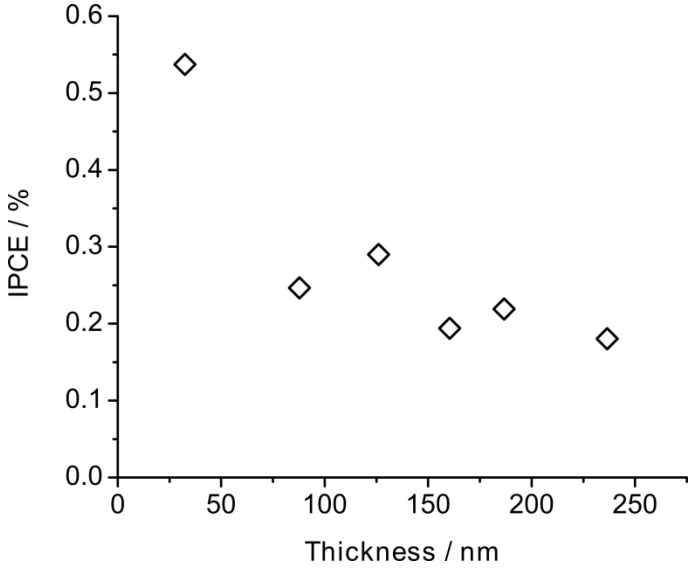

Figure 2.6 **Dependence of quantum efficiency on film thickness of RR-P3HT films under illumination of 550 nm light. Light intensity was 100 mW cm^{-2} (AM 1.5D) in 0.1 M H_2SO_4 (aq.) at E = -0.2 $V_{Ag/AgCl}$.**

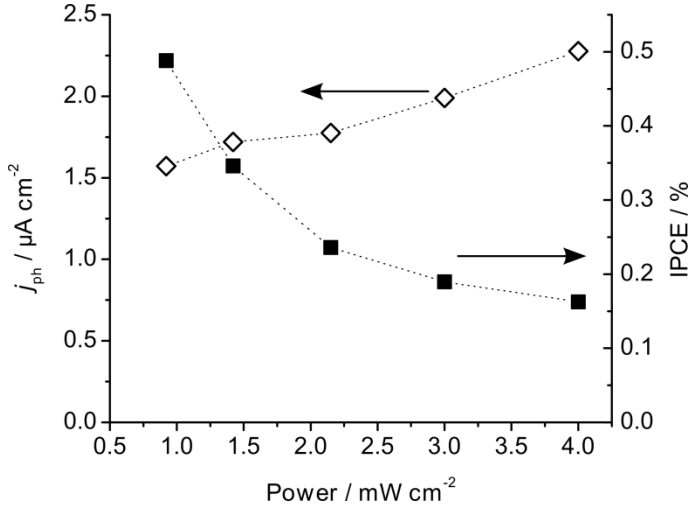

Figure 2.7 **Dependence of quantum efficiency and photocurrent of RR-P3HT coated ITO electrodes on incident 550 nm light power. Electrodes were biased at -0.2 $V_{Ag/AgCl}$ in 0.1 M H_2SO_4 (aq.).**

2.3.3. Thin Film Spectroelectrochemistry and Fluorescence

The photocurrents produced are stable and no degradation of the material is observed after hours of irradiation. The photocurrent is clearly due to photoelectrolysis of solution species and not, for example, due to a simple irreversible photoelectrochemical reduction of the film. This assertion is supported by considering the charge required to completely and irreversibly reduce the film and by spectroelectrochemistry. I calculated that 168 μC of Coulombic charge is needed to completely reduce a 100 nm thick P3HT film on a 1.5 mm radius disk, assuming 1.5 e^- per 4 thiophene units for n-doping,[179] and a polymer density of 1.10 g cm^{-3}.[180] Thinner films would require proportionally less. However, over a period of two hours photoelectrolysis, > 30 000 μC of cathodic photocurrent are typically passed, much larger than that possible due to electrochemical reduction or degradation of the film. Moreover, the films are electrochemically inactive in the absence of light in aqueous solution, indicating the films do not undergo irreversible electrochemical reduction in aqueous solution. In fact, even the characteristic electrochemically-induced oxidation and re-reduction cycles of P3HT that are typically observed in non-aqueous electrolytes are completely suppressed in aqueous solution, as illustrated in Figure 2.8. In non-aqueous electrolyte, such as acetonitrile, swelling of the polymer allows counter ions to penetrate into the film and balance charge formed during oxidation. Oxidation of the polymer occurs at positive potentials and the absorbance in the visible region decreases due to the formation of polaronic/bipolaronic states in the band (Figure 2.8A). In contrast, electrochemical activity in aqueous solution (Figure 2.8B) is completely suppressed, the polymer resists oxidation, and no change in absorbance is detected. More relevant to this study, P3HT films are electrochemically inactive at negative potentials, as determined by cyclic voltammetry and spectroelectrochemistry (Figure 2.8C). The apparent lack of electrochemical activity in aqueous solution is attributed to the hydrophobicity of the P3HT which prevents swelling and access of the electrolyte into the film.

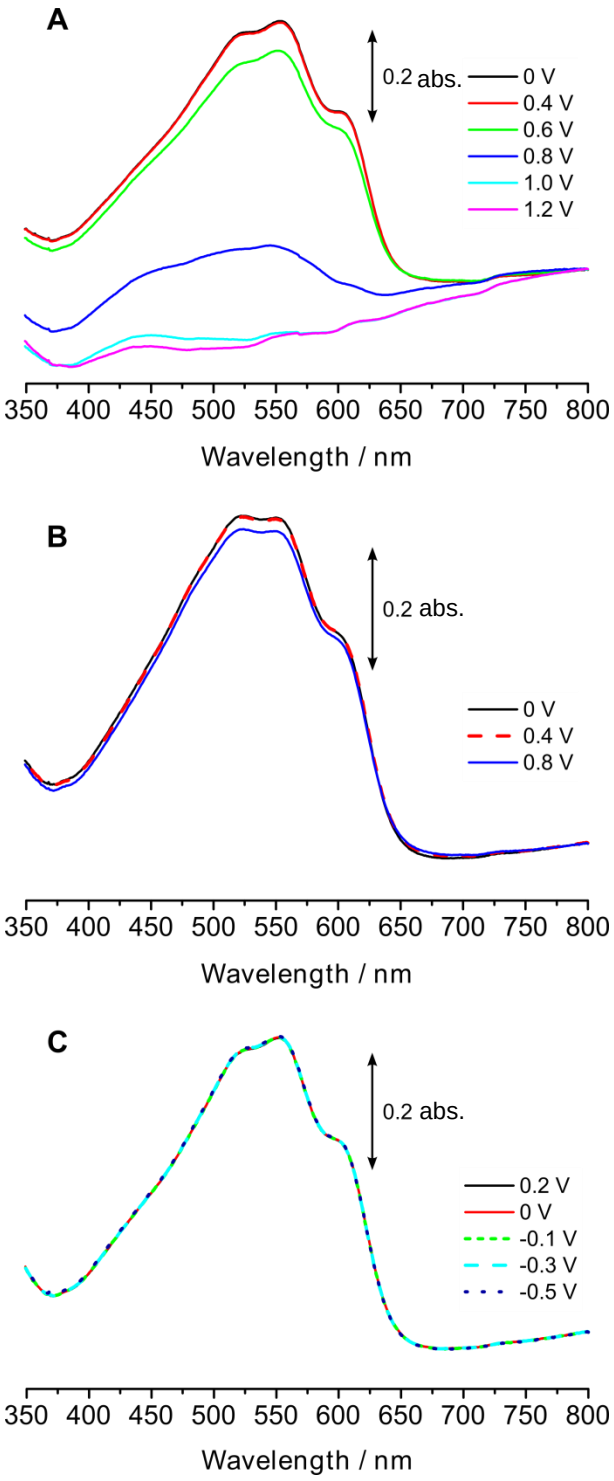

Figure 2.8 **Spectroelectrochemistry of RR-P3HT (~100 nm thick) coated ITO electrodes in (A) 0.1 M TBAP-MeCN at positive potentials, (B) 0.1 M H_2SO_4 (aq.) at positive potentials, and (C) 0.1 M H_2SO_4 (aq.) at negative potentials, *vs.* Ag/AgCl (sat.). The indicated potentials were applied for 2 min. before and while recording the spectra.**

Since oxygen is rigorously excluded from the apparatus, the most reasonable explanation for the origin of a continuous photoelectrolytic current is the reduction of protons to dihydrogen. Electrons in the conduction band of P3HT have sufficient reductive power to reduce protons.[15] However, I have yet to succeed in detecting hydrogen gas as a product because the photocurrents and quantity of gas produced is too small. For example, cumulative charge passed over two hours under illumination of P3HT (-0.7 V vs. Ag/AgCl, 100 mW/cm^2 irradiation) corresponds to only 3.8 µL of generated hydrogen.

A mechanism for photoelectrochemical hydrogen evolution at conjugated polymers films has not been addressed in the literature. However, It is well documented that polythiophenes are susceptible to protonation. Original work in this area reports that protonation of a thiophene oligomer is observed when strong acid is introduced into a solution of the oligomer,[181] as evidenced by a new single peak in the proton NMR spectrum. A red shift in the UV-visible absorption is also reported, similar to that observed for electrochemical and chemical oxidation of conjugated polythiophenes.[182,183] Sulfonic acid derivatives of poly 3-alkylthiophenes also exhibit absorption peaks above 800 nm without electrochemical or chemical oxidation.[184] These peaks are similar to polaron/bipolaron peaks observed during electrochemical oxidation but are attributed to protonation of the polymer or “self-acid doping”. An attempt to observe protonation of RR-P3HT in contact with different concentrations of acids in aqueous and non-aqueous solutions was carried out using UV-visible absorption spectroscopy. Spectra are shown in Figure 2.9. As can be observed in Figure 2.9A, the absorbance of RR-P3HT films remains unchanged when immersed in solutions of pH 7 to 1.4. I interpreted these observations to mean that RR-P3HT is too hydrophobic to allow access of acid into the film, as in the case of electrochemical analysis in aqueous solutions, rather than an inherent tendency of the polymer not to protonate. In fact, the same experiments performed in acetonitrile, in which films swell and allow acid to penetrate, shows a clear reduction of the band associated with the π-π^* transition (see Figure 2.9B), indicative of protonation.

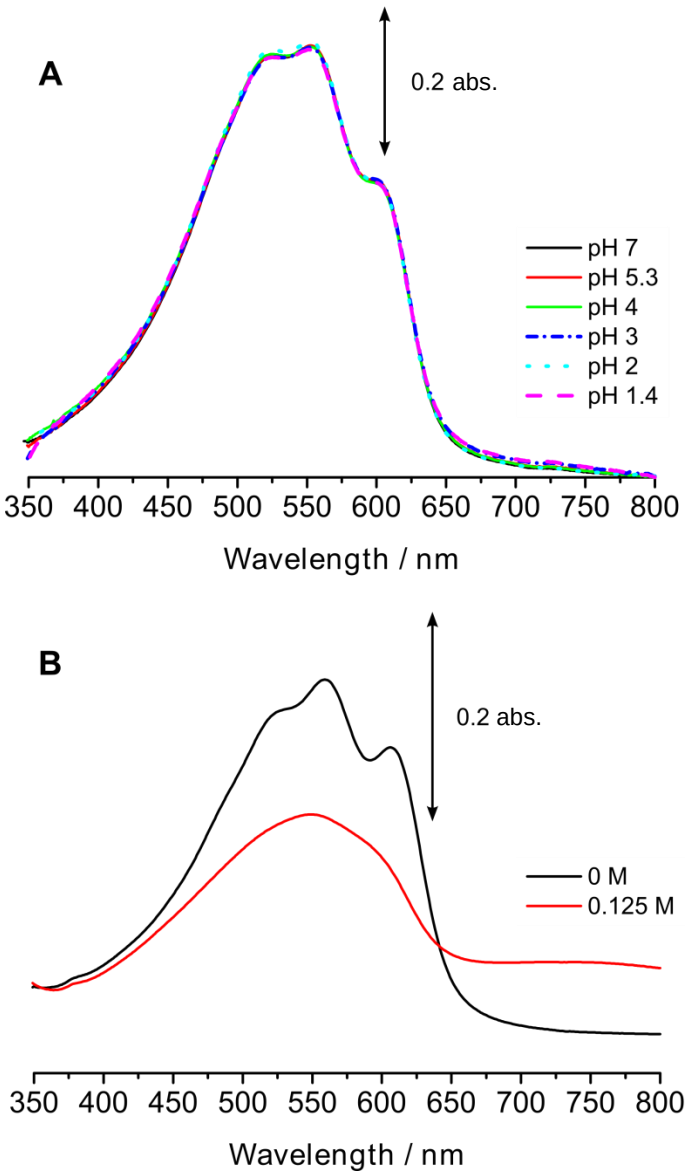

Figure 2.9. UV-visible absorbance of RR-P3HT films in solution. The effects of proton concentration on absorbance are observed in (A) aqueous solution with different concentration of H_2SO_4 and (B) H_2SO_4 in MeCN.

Notwithstanding the observation that the RR-P3HT appears impenetrable to aqueous acid, the possibility that protonation occurs at the polymer film's surface, at the polymer/electrolyte interface, cannot be disregarded—it is simply not detectable by transmission absorption spectroscopy. However, I noted that the fluorescence intensity of films of RR-P3HT decreases substantially upon exposure to aqueous acid solution (Figure 2.10). Given that photogenerated excitons are quenched by protonated

π-conjugated species, and that excitons can diffuse through the film, this is interpreted as indirect evidence for the existence of protonated species at the polymer/electrolyte interface.

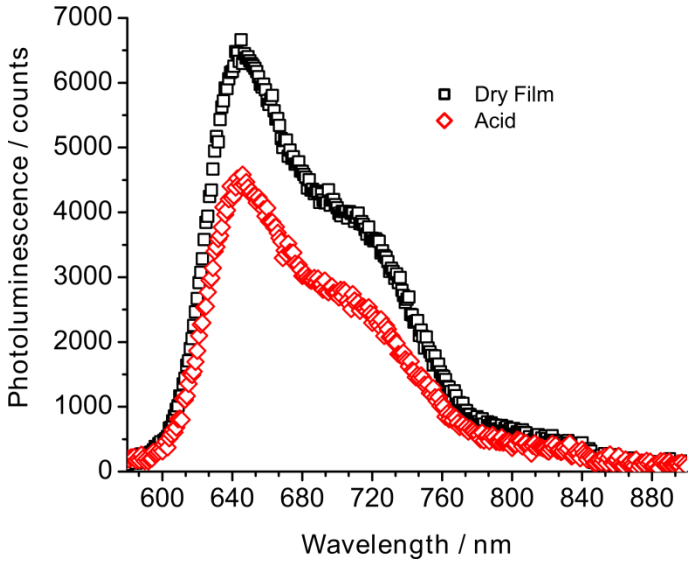

Figure 2.10 Photoluminescence spectra of RR-P3HT films. Upper spectrum (squares), dry films; lower spectrum (diamonds), the same film in contact with 0.1 M H_2SO_4. Excitation wavelength, 550 nm.

I propose a mechanism to explain the photocathodic activity of RR-P3HT in aqueous solution, illustrated in Figure 2.11. This mechanism is based is on the known self-doping phenomenon of poly(3-thienyl)alkanesulfonic acids,[185] and on protonation studies of oligomers[181] which is reported to occur through the addition of hydrogen at the α-site of the thiophene ring. In this mechanism, protonated P3HT at the polymer/electrolyte interface receives electrons that are photogenerated in the bulk of the film, resulting in the release of hydrogen and reformation of the neutral polymer at the surface. The latter is subsequently reprotonated, and primed for the next reduction cycle, while photogenerated holes in the film migrate to the anode to complete the circuit.

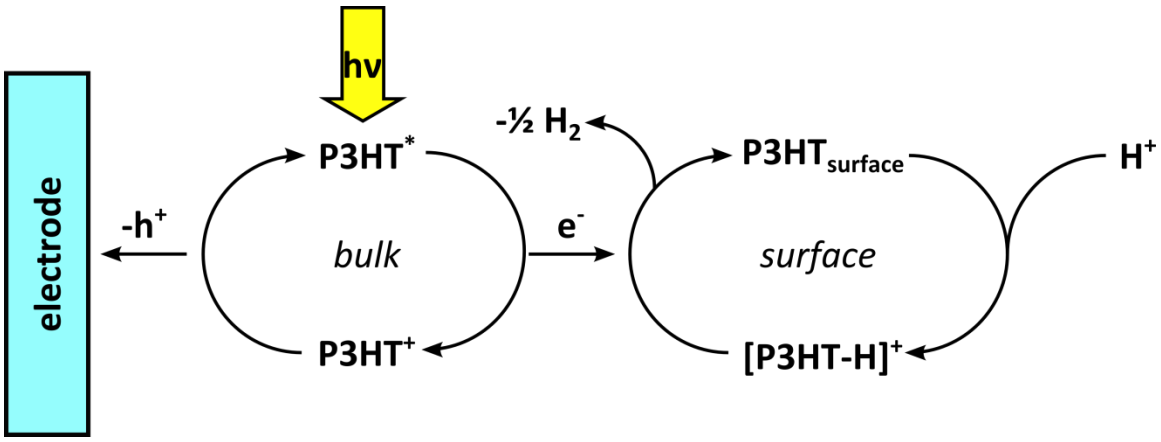

Figure 2.11 Proposed mechanism of RR-P3HT photocathodic activity in aqueous solution.

2.4. Conclusions

RR-P3HT is photoelectrochemically active in aqueous solution yielding tens of μA cm^{-2} of photocurrent. Thicker films provide larger photocurrents but at reduced power efficiencies. Photocurrents and power efficiencies are 10 times greater than RRa-polymer analogues. Spectroscopic and electrochemical evidence suggests RR-P3HT is protonated at the polymer/electrolyte interface, leading to the speculation that photocathode activity of RR-P3HT originates from reduction of the protonated surface, with subsequent elimination of molecular hydrogen. Elucidation of the mechanism and rate-determining steps should provide the insights needed to increase photo-conversion efficiencies.

Despite favourable thermodynamics, photogenerated electrons on P3HT failed to produce H_2. Lack of H_2 may indicate that a catalyst that promotes proton reduction, such as platinum, is needed. Most photoelectrochemical or photochemical systems require a catalyst in order to carry out solar water splitting.[186] Catalysts can be deposited physically (spin or spray coating) or electrochemically by photoelectrochemical reduction of metal, or metal-containing ions in solution. The most common catalyst used for hydrogen evolution is platinum and I use it as a co-catalyst with P3HT (Chapter 3 and Chapter 4). In addition to achieving hydrogen generation it is important to demonstrate

that polymer photoelectrodes are compatible with common materials and techniques for performing solar water splitting.

Chapter 3.

Photoelectrochemical Hydrogen Evolution: Single Layer Conjugated Polymer Films Bearing Surface-Deposited Platinum Nanoparticles

Sections of this chapter have been reproduced in part with permission from: Graeme M. Suppes, Patrick J. Fortin, and Steven Holdcroft, Journal of the Electrochemical Society, 2015, Vol. 162(8), H551-H556. Copyright 2015, The Electrochemical Society. The work presented in this chapter was my (G. Suppes) contribution to the paper.

3.1. Introduction

Photoelectrochemistry (PEC) of redox species in aqueous solutions has undergone a resurgence of interest due to a desire to develop inexpensive, renewable fuels. In the seminal work of Fujishima and Honda, oxygen and hydrogen gas were produced upon the photo-assisted electrolysis of water at an illuminated n-type TiO_2 electrode and Pt black counter electrode.[103] PEC of n-type TiO_2 has two main drawbacks. The first is that, whereas, photo-generated "holes" arising from the valence band are sufficiently energetic (thermodynamically) to oxidize water to dioxygen, conduction band electrons are insufficiently energetic to reduce water to dihydrogen, hence the requirement to negatively bias the counter electrode. The second drawback is that TiO_2 absorbs a relatively small fraction of the solar spectrum due to its large band gap (~3 eV); the "solar" efficiencies obtained are, therefore, relatively low. As a consequence, research effort is being directed to the study of other inorganic semiconductors including alternative metal oxides,[187–190] silicon and other compound semiconductors,[109,119,191,192] and composites of the two,[193–195] with the intention of

enhancing photoelectrochemical water splitting reaction kinetics and solar-to-fuel efficiencies.

An alternate strategy to employing a single semiconductor to generate electrons and holes that simultaneously split water photoelectrochemically is to design individual n- and p-type semiconductors with the specific task of oxidizing and reducing water, respectively. Using this approach dioxygen is evolved at photoanodes and dihydrogen at photocathodes[196,197] or from tandem semiconductor devices.[88,198] Another approach fosters consideration of materials other than metal oxides and inorganic semiconductors.[113,199–202] Organic semiconducting polymers would appear prime candidates for photocathode materials because they absorb visible light, are typically p-type, meaning that during illumination electrons flow towards the electrode surface, and they participate actively in electron transfer reactions. Optoelectronic studies of poly(3-hexylthiophene) (P3HT) indicate that the LUMO energy levels (-3.1 eV, -1.4 V_{NHE} at pH 0) possess sufficient reductive power to reduce protons to water (0 V_{NHE}), whereas the HOMO energy levels (-5.1 eV, 0.6 V_{NHE} at pH 0) is insufficient oxidize water to oxygen (1.23 V_{NHE}).[203,204] Moreover, there is a plethora of research using organic polymers in photovoltaic devices from which to learn.

Examples of conjugated organic polymers used in sacrificial water splitting systems can be found as early as 1985 wherein it was reported that irradiation of a suspension of poly(p-phenylene) in the presence of diethylamine led to the photoreduction of protons to hydrogen gas.[205] It was subsequently reported, using a photoelectrochemical system, that regiorandom P3HT exhibited photocathode activity in aqueous solutions and that photocurrent could be increased by incorporation of electron acceptors, such as fullerene.[160] The importance of the stereochemistry of these polymers was later realized; it was demonstrated that improving the regioregularity of P3HT greatly improved the structural organization of the polymer films and enhanced their charge conductivity.[68,206] Photoelectrochemical studies of regioregular (RR) P3HT in aqueous solution exhibited improved photocathode activity, reaching 20 μA cm^{-2} under 100 mW cm^{-2} AM 1.5D irradiation, and led to 0.55 % photon-to-current conversion efficiency, i.e. ten times greater than with regiorandom P3HT.[207]

It has been determined that the photocurrent on bare P3HT is actually due to reduction of trace oxygen, left behind even after sparging the solution with Ar for up to 2 hours.[208] Semiconducting materials used for water splitting typically need a catalyst in order to perform water oxidation or proton reduction.[186] Conducting polymers have been used as scaffolds for noble metal catalyst in order to carry out reactions such as methanol oxidation,[209,210] hydrazine oxidation,[211] as well as oxygen reduction[212] and proton reduction[213,214] but not under photoelectrochemical conditions. Polymers, such as polypyrrole,[213,215] polythiophene,[211,216] and polyaniline[209,210,217] are prepared electrochemically, wherein a monomer in an electrolyte solution is oxidized at an inert metal (or glassy carbon) electrode and reacts with other oxidized monomers (or n-mers) to "grow" the polymer film on the electrode surface. Electrochemically prepared polymer films are porous and provide a high surface area matrix for dispersing metal nanoparticles which should result in improved electrocatalytic efficiency.[212,218] Metal nanoparticles, such as Pt, Ir, or Au, can be deposited on the surface or embedded in the film using electrochemical[219] or electroless methods.[220] Several recent results using conjugated polymer photovoltaic device structures for solar water splitting are discussed in Section 1.4.5.

Given the advancements in the field that indicate an apparent need for catalysts to promote hydrogen evolution at irradiated conjugated films, a technological preference to employ a single layer film rather than the more complex, multilayer architectures (akin to organic PV devices), and that single layer organic PV efficiencies can reach relatively high values (up to 7 %),[221] I investigated the aqueous PEC of Pt nanoparticles (Pt NPs) deposited on single layer polymer films (Figure 3.1).

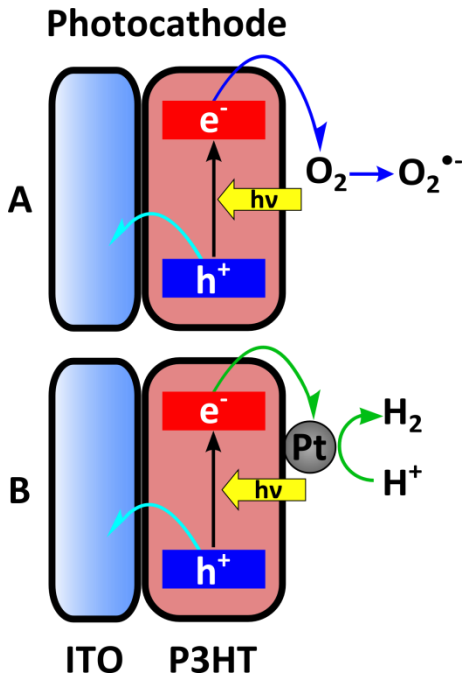

Figure 3.1 **Photoelectrochemical setup for single layer poly(3-hexylthiophene) (P3HT) photocathodes (100 nm thick) with a platinum counter electrode. Light absorption leads to excitation of electrons from the valence band to the conduction band. In the absence of an electrocatalyst photogenerated electrons carry out the reduction of O_2 ($O_2 + e^- \rightarrow O_2^{\bullet -}$) (A). Pt nanoparticles deposited on P3HT enhances the photocurrent, generating hydrogen (B).**

3.2. Experimental

3.2.1. Materials

P3HT was purchased from Rieke Metals (RMI-001E, MW = 69,000 g mol^{-1}, regioregularity ≥ 96 %). K_2PtCl_6 (Johnson Matthey), chlorobenzene (Sigma-Aldrich), H_2SO_4 (Anachmia), NaOH (BDH chemicals), NaCl (Fisher), Na_2SO_3 (Fisher) were all used as received. All aqueous solutions were prepared using ultrapure water obtained from a Milli-Q water purification system (18 MΩ, EMD Millipore). Indium tin oxide (ITO) coated glass slides (Merck Display Technologies Ltd.) were cleaned by sequential sonication in each of the following solutions: isopropyl alcohol, acetone, H_2O: H_2O_2: NH_4OH (5:1:1) solution and distilled water.

3.2.2. Film Preparation

Films were prepared from a 20 mg mL^{-1} solution using P3HT (Rieke) dissolved in chlorobenzene. Film thicknesses were determined using an Alpha-Step IQ profilometer (KLA-Tencor). Silver conductive paste (MG Chemicals, 8331-14G) was used to connect a wire to the ITO electrode after wiping away a small part of the polymer with a cotton tipped applicator (Puritan). The edges of the film were completely covered with an electronically insulating and chemically resistant epoxy (T20-3004 HVGR50, Epoxies, Etc.).

3.2.3. Characterization

Photoelectrochemistry. The light source was a 200 W Xe/Hg lamp (Uhsio America, Inc.), used in combination with a 300-700 nm band pass filter (FSQ-KG3, Newport Corp.) and neutral density filters (Thorlabs Inc.), to achieve 100 mW cm^{-2} irradiation, as measured using a broadband power meter (841-PE, Newport Corporation) equipped with an Ophir thermal detector head (3A-P-SH-V1). The cell configuration was designed to allow irradiation of the polymer–electrolyte interface through the electrolyte. A water filter was placed in front of the electrochemical cell to remove excess heat. Electrochemical measurements were performed using a Pine Bipotentiostat (AFC-BP1). PEC measurements were performed in a 3-electrode configuration using a saturated standard calomel electrode (SCE) (+0.24 V vs. NHE) and a Pt wire as the reference and counter electrodes, respectively. Solutions were sparged with argon (Praxair, purity 99.999 %) for 1.5 to 2 hours in a glass PEC cell and sealed under a flow of argon. Pt was photoelectrochemically-deposited onto P3HT-coated ITO electrodes from K_2PtCl_6 in 1 M H_2SO_4 solutions under 100 mW cm^{-2} irradiation. Concentration of K_2PtCl_6, applied potential and time of deposition were varied.

Hydrogen Gas Detection. The headspace in the electrochemical cell was sampled using a 5 mL syringe, fitted with a gas tight valve (Series A-2, VICI Precision Sampling), and analyzed using an Agilent Technologies 6890N GC system equipped with a thermal conductivity detector. A 2.13 m Agilent J&W GC packed column in stainless steel tubing was used (inner diameter of 2 mm, HayeSep N packing material,

60/80 mesh size). Argon was used as a carrier gas at a flow rate of 30 mL min^{-1} under 46.2 psi.

Microscopy. Scanning electron micrographs were collected using a FEI Dualbeam 235 SEM set to an accelerating voltage of 5 kV and spot size 3. Films were prepared on ITO as described above and fixed to an aluminum stub using carbon tape (SPI supplies). The system is equipped with an energy dispersive X-ray system (EDAX) for elemental analysis.

3.3. Results

3.3.1. Pt Deposition on P3HT Photocathodes

In contrast to the one-electron reduction reactions of oxygen and MV^{2+}, any mechanism leading to hydrogen evolution at an illuminated conjugated polymer must be congruent with two one-electron transfer events that lead to a juxtaposition of C-H bonds (each formed by electron transfer to H^+), and which combines to eliminate H_2. H_2 elimination from a polymer backbone would appear to be a highly speculative and unlikely process. In order to differentiate photo-absorption and charge separation processes from the electrocatalytic event, the use of Pt nanoparticles (Pt NPs) deposited on the surface of P3HT-coated ITO electrodes was investigated with the intent on establishing that an electrocatalyst is significant in the PEC at P3HT films.

To deposit Pt NPs, I used the photoreductive power of P3HT; the reduction of $PtCl_6^{2-}$ anion is 0.49 V_{SCE},[222] which lies substantially below the conduction band edge of P3HT. Hence, irradiation (100 mW cm^{-2}, 300-700 nm) of P3HT, under negative biases vs. SCE in 0.1 mM K_2PtCl_6/1 M H_2SO_4, resulted in the generation of photocurrent (> 10 µA cm^{-2}) as shown in Figure 3.2, which is attributed to reduction of $PtCl_6^{2-}$. In the absence of $PtCl_6^{2-}$ the photocurrent is << 1 µA cm^{-2}. Moreover, SEM micrographs of the resultant polymer film (Figure 3.3A) reveal the surface deposition of NPs, the composition of which, is proved to be Pt using energy dispersive X-ray for elemental analysis (Figure A-3 and A-4). The amount of Pt deposited (typically sub-µg cm^{-2}) was

controlled by adjusting the charge passed. A P3HT film without platinum is shown in Figure 3.3B and is featureless at the same magnification.

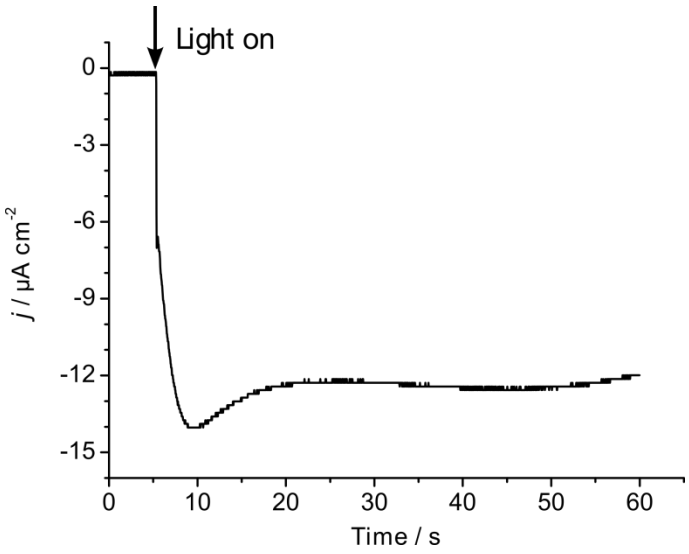

Figure 3.2 Photoelectrolysis of a P3HT-coated ITO electrode in 0.1 mM K_2PtCl_6 / 1 M H_2SO_4. A potential of -0.1 V_{SCE} was applied for 1 minute. Light intensity: 100 mW cm^{-2} (300-700 nm), blocked for the first 5 seconds.

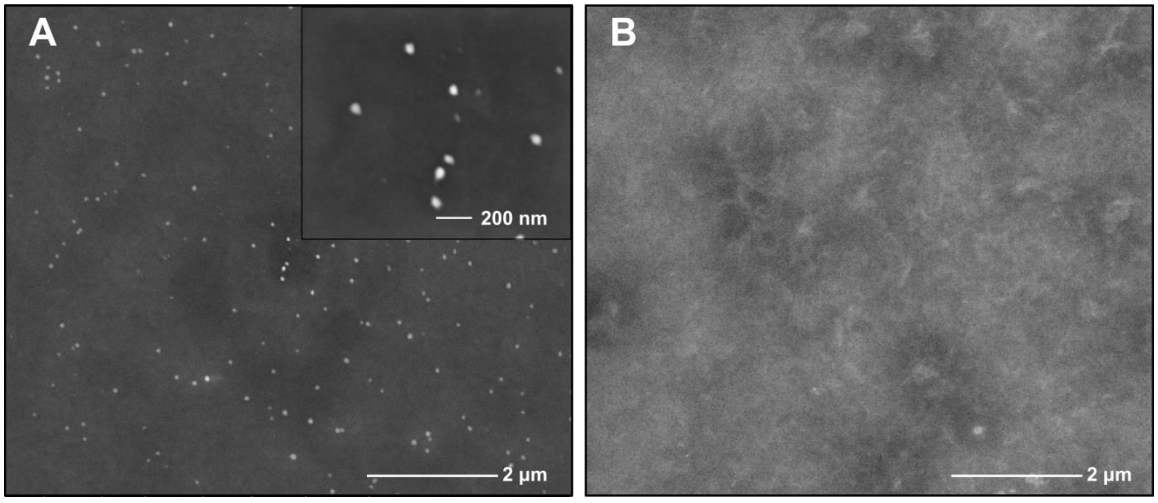

Figure 3.3 SEM micrograph of (A) P3HT-Pt and (B) P3HT coated ITO. Pt loading, 0.23 μg cm^{-2}. Inset: magnified view.

Deposition of Pt NPs was optimized by changing the concentration of K_2PtCl_6 used, the time of deposition and the applied potential. As described in the experimental section, the deposition solution was K_2PtCl_6/1 M H_2SO_4 and the light intensity was

100 mW cm^{-2} (300-700 nm). Deposition time was varied from 60 s to 300 s, concentration of K_2PtCl_6 was 0 mM, 0.1 mM, 0.25 mM, or 0.5 mM, and applied potential was -0.1 V_{SCE} or -0.3 V_{SCE}. Figure 3.4 shows the chopped linear sweep voltammetry (LSV) of P3HT-Pt NP films in 0.1 M H_2SO_4. Rather than perform one experiment in the dark and one under illumination, blocking and unblocking the light source allows that information to be collected in one linear sweep. When the light source is unblocked current transients can give information about charge generation and recombination (*vide infra*).

These films are prepared (Pt NPs deposited) at -0.3 V_{SCE}. When the deposition time is 0 s, 60 s, and 100 s the amount of deposited Pt is 0 µg cm^{-2}, 0.54 µg cm^{-2}, and 2.48 µg cm^{-2}, respectively. The platinum loading is calculated from the charge passed during deposition and it is assumed that 100 % of the current is due to $PtCl_6^{2-}$ reduction.

The P3HT and P3HT-Pt NP films respond very quickly to illumination changes as the light source is blocked/unblocked. Films with Pt show a much higher photocurrent than Pt-free films but as the deposition time is increased I observed an increase in the dark current. Without illumination the current should decrease to very low values due to the loss of photo-generated charge carriers. The appearance of current without illumination implies another pathway for charge transfer such as contact of Pt with the underlying ITO electrode or exposure of the ITO to the solution. The fact that the dark current increases with Pt loading seems to indicate some deposition on the ITO.

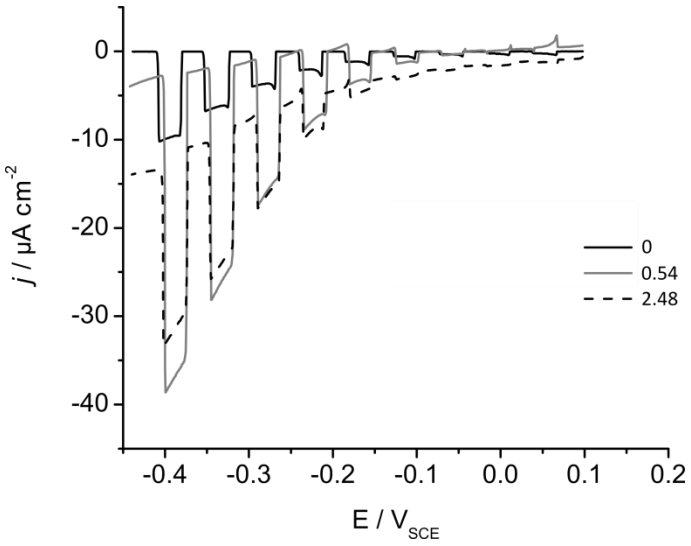

Figure 3.4 Linear sweep voltammetry (LSV) of P3HT-Pt with various loading (0, 0.54, and 2.48 µg cm^{-2}) in 0.1 M H_2SO_4. Light intensity was 100 mW cm^{-2} over 300-700 nm (bandpass filter). The scan rate was 5 mV s^{-1} and the light source was blocked every 5 seconds. A platinum wire was used as a counter electrode. The different Pt loadings were achieved by varying the time of photoelectrolysis (at -0.3 V_{SCE}) in the deposition solution.

A similar trend is also observed when the deposition time is held constant but the concentration of K_2PtCl_6 is varied. Figure 3.5 shows the chopped LSV for P3HT-Pt NP films in 0.1 M H_2SO_4. These films are prepared (Pt NPs deposited) at -0.3 V_{SCE}. When the concentration of K_2PtCl_6 is 0 mM, 0.1 mM, 0.25 mM, and 0.5 mM the amount of deposited Pt is 0 µg cm^{-2}, 0.54 µg cm^{-2}, 2.01 µg cm^{-2}, and 2.83 µg cm^{-2}, respectively. Again, as the amount of deposited platinum increases so does the dark current.

These results imply that in order to have good P3HT-Pt NP films deposition should be carried out using low concentration of K_2PtCl_6 (≤ 0.1 mM) and for short duration under 100 mM cm^{-2} (300-700 nm) illumination. A good film is one where any current generated under illumination is due to photoelectron transfer from the polymer to the metal nanoparticle.

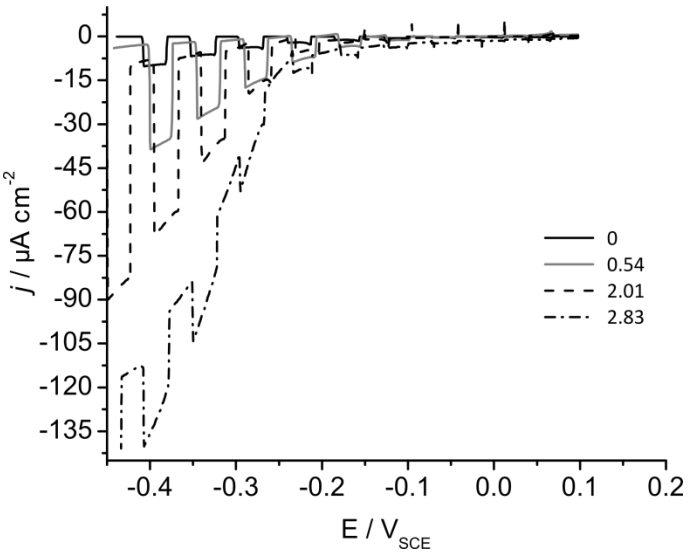

Figure 3.5 LSV of P3HT-Pt NP films with different loading (0. 0.54, 2.01, and 2.83 µg cm^{-2}) in 0.1 M H_2SO_4 at 5 mV s^{-1}. The different Pt loadings were achieved by varying the concentration of Pt in the deposition solution and applying a potential of -0.3 V_{SCE} for 60 seconds under illumination.

The accuracy of the platinum loading calculation may be affected by proton reduction when the deposition potential is -0.3 V_{SCE}. The proton reduction potential is -0.26 V_{SCE} in 1 M H_2SO_4 (pH 0.3). A portion of the photocurrent, and therefore charge passed, may be due to proton reduction at deposited Pt NPs. Figure 3.6 compares the photocurrent to the calculated amount of platinum deposited for P3HT-Pt NP films. When the deposition is carried out at -0.1 V_{SCE} the calculated amount of platinum deposited is in the range of 0.2-0.4 µg cm^{-2} and a deposition potential of -0.3 V_{SCE} results in a range of 2.6-4.2 µg cm^{-2} (deposition time was 60 seconds for all cases). The photocurrent produced when these films are biased at -0.24 V_{SCE} in 0.1 M H_2SO_4 and illuminated with 100 mW cm^{-2} (300-700 nm) light is approximately 30 µA cm^{-2} (0.2-0.4 µg cm^{-2}) and 60 µA cm^{-2} (2.6-4.2 µg cm^{-2}). The amount of platinum deposited, according to the calculation, increases by an order of magnitude but the photocurrent only doubles.

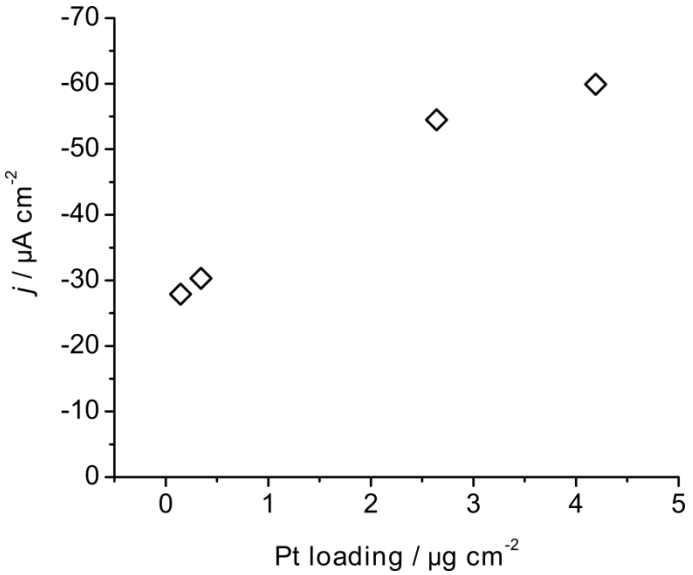

Figure 3.6 Photocurrent vs. platinum loading of P3HT-Pt coated ITO in 0.1 M H_2SO_4 at -0.24 V_{SCE}. Light intensity was 100 mW cm^{-2} over 300-700 nm (bandpass filter). Platinum deposition conditions: Photoelectrochemical deposition at -0.1 V_{SCE} (~9 µA cm^{-2}) and -0.3 V_{SCE} (~120 µA cm^{-2}), 60 s in 0.1 mM K_2PtCl_6/1 M H_2SO_4, light intensity was 100 mW cm^{-2} over 300-700 nm (bandpass filter). A platinum wire and SCE were used as a counter and reference electrode, respectively.

Finally, it can be deduced how well charge is transferred between the P3HT and the platinum NPs by comparing the flatband potential (E_{fb}) with the onset of photocurrent. Recall that E_{fb} is the applied potential required to flatten the conduction and valence band of a semiconductor electrode following contact with solution containing a redox couple (see Section 1.5.3). For a p-type semiconductor a photocathodic current should be produced when any potential more negative than E_{fb} is applied. Figure 3.7A shows the Mott-Schottky plot of a P3HT coated ITO at 100 kHz in 0.1 M H_2SO_4 and under dark conditions. The linear portion of the curve has a negative slope as expected for p-type semiconductors and extrapolation to the x-axis reveals E_{fb} = 65 mV_{SCE}.

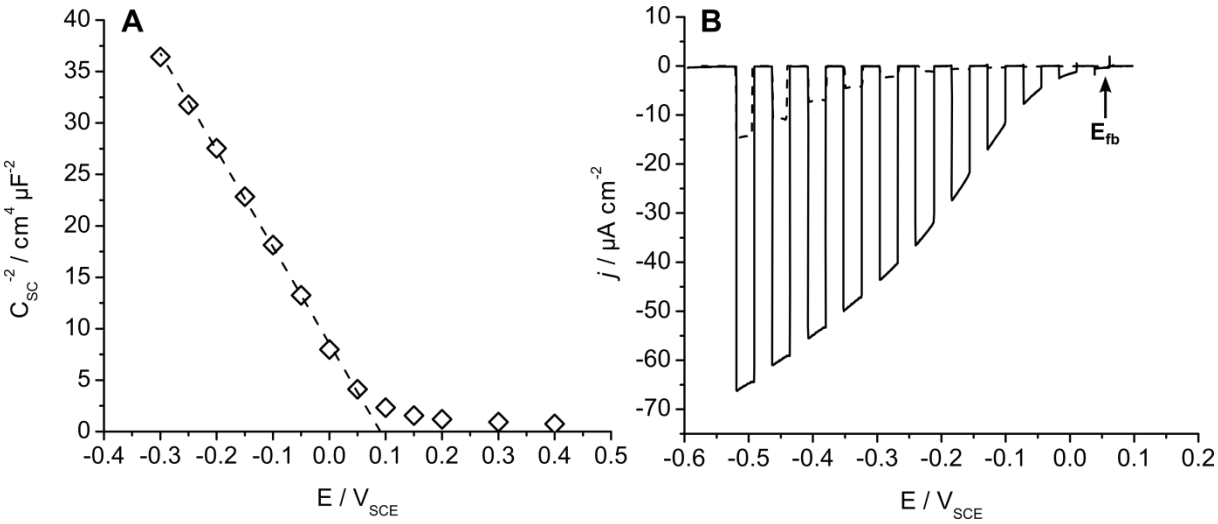

Figure 3.7 Mott–Schottky (A) plot of P3HT coated ITO obtained using electrochemical impedance spectroscopy in 0.1 M H_2SO_4 under dark conditions at 100 kHz. E_{fb} measured is 65 mV_{SCE}. Linear sweep voltammogram (B) of a P3HT-Pt NP (0.34 μg cm^{-2}) film (solid line) and a P3HT film (dashed line) in 0.1 M H_2SO_4 with scan rate 5 mV s^{-1}. Light intensity: 100 mW cm^{-2} (300-700 nm). The light source was blocked every 5 seconds. The arrow points to E = 65 mV_{SCE}.

Figure 3.7B shows the chopped LSV of a P3HT-Pt NP (0.34 μg cm^{-2}) film in 0.1 M H_2SO_4. Chopped LSV gives a qualitative estimate of E_{fb}.[140] The potential where photocurrent begins in Figure 3.7B coincides closely with E_{fb} calculated from EIS for Pt free films indicating that photogenerated electrons are transferred easily to the Pt NPs. LSV of films without Pt NPs also show a photocurrent onset near the calculated E_{fb}. This photocurrent is most likely due to reduction of O_2 as determined by other work done by the Holdcroft lab.[208]

Other photoelectrode materials, such as hematite (α-Fe_2O_3), require the application of a large overpotential before generating photocurrent which has been shown to be due to charging of surface states.[223–225] Klahr *et al*. determined E_{fb} in a pH 7 solution (phosphate buffer) to be 0.25 $V_{Ag/AgCl}$ but photocurrent onset was just above 0.6 $V_{Ag/AgCl}$.[223] The onset can be cathodically shifted (for water oxidation photoelectrodes) by use of a catalyst, such as IrO_2[126] or cobalt-phosphate,[225,226] but some overpotential still exists.

A closer inspection of the light on-off cycle at a single potential (-0.24 V_{SCE}) is shown in Figure 3.8. A high transient cathodic current is observed for the first on/off cycle for P3HT-Pt NP and P3HT films and is not present for subsequent cycles of P3HT-Pt NP films. This transient is present for P3HT films but with a reduced magnitude (Figure 3.8 inset). The first cycle transient current may be due to oxidation of trapped charges caused by some oxidation of the film when exposed to air and light during the cell setup or from any unreacted material in the case of P3HT-Pt NP films. Transient anodic current in n-type metal oxide semiconductors used for oxygen evolution (water oxidation) is due to slow electron transfer kinetics at the surface.[227–229] When initially illuminated photogenerated electrons and holes separate and produce a large current. Hole accumulation at the surface, for n-type semiconductors, due to slow transfer kinetics with water and recombination with electrons increases until a steady state is reached. A similar explanation could be applied to transient currents observed for P3TH photocathodes. When Pt NPs are used the transient cathodic current is negligible, indicating photogenerated electrons are consumed as soon as they reach the surface.

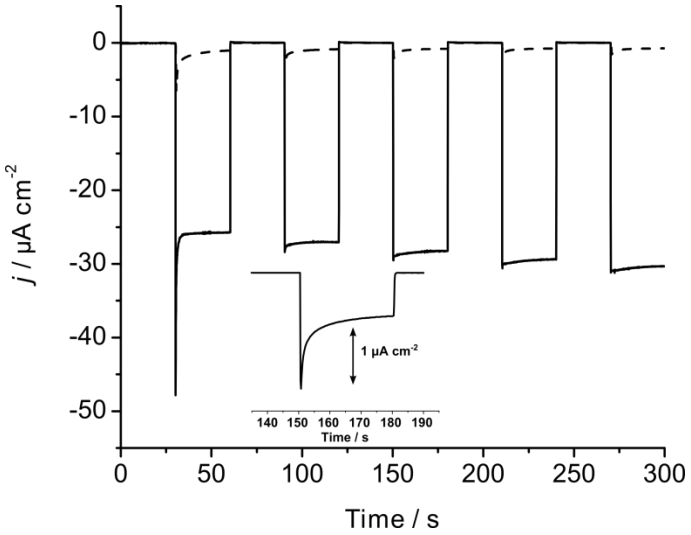

Figure 3.8 J-t curve for a (solid line) P3HT-Pt NP (0.34 µg cm^{-2}) and a (broken line) P3HT coated ITO electrode in 0.1 M H_2SO_4 at -0.24 V_{SCE}. Light intensity was 100 mW cm^{-2} (300-700 nm). Inset: close up of one of the P3HT electrode's light on/off cycles.

Deposition of platinum on P3HT is possible with low concentrations of K_2PtCl_6 (0.1 mM) and short electrolysis times (~60 seconds). By applying a potential slightly more negative than the flat band potential of P3HT in 0.1 M H_2SO_4 (-0.1 V_{SCE} and

+0.065 V_{SCE}, respectively) sub-µg cm^{-2} amounts of Pt are deposited. These P3HT-Pt NP films produce high photocurrents (relative to un-platinized films) which quickly decreases to almost zero when the light source is interrupted.

3.3.2. Photocurrent versus pH

To ensure that platinum is being deposited and useable as a co-catalyst, the pH dependence of the photocurrent was examined. Figure 3.9 shows the effect of pH on photocurrent of a P3HT-Pt NP film with 0.34 µg cm^{-2} of platinum deposited. As expected the photocurrent increases with decreasing pH. For P3HT-Pt films prepared by deposition of Pt at -0.1 V_{SCE}, either a slight increase or no increase in photocurrent (result from several films) is observed when pH is decreased from 1.2 to 0.3. The Figure 3.9 inset shows the chopped LSV of a P3HT film without Pt. The film shows a similar response to changes in pH but produces significantly lower photocurrent.

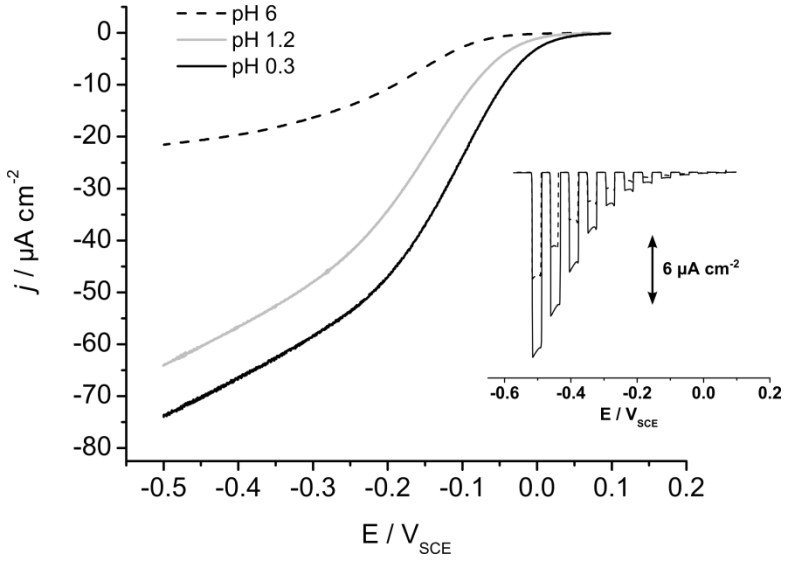

Figure 3.9 LSV of a P3HT-Pt NP (0.34 µg cm^{-2}) coated ITO electrode in 0.1 M NaCl (pH 6.0), 0.1 M H_2SO_4 (pH 1.2), and 1 M H_2SO_4 (pH 0.3). Light intensity was 100 mW cm^{-2} over 300-700 nm (bandpass filter). The scan rate was 5 mV s^{-1}. A Platinum wire was used as a counter electrode. Inset: LSV of a P3HT coated ITO in 0.1 M H_2SO_4 at pH 6 and pH 0.3 with the same scan rate and light intensity.

The similarity in the photocurrent at low pH may be due to saturation of the surface by protons and the limited number of charge carriers a semiconductor possess.

This non-linear response of the photocurrent with concentration was seen when methyl viologen (MV^{2+}) was used as an electron acceptor in solution (Section 4.3.1). As the concentration of MV^{2+} was increased from 5 mM to 10 mM the photocurrent changed only slightly and eventually becomes independent of concentration. Other photoelectrodes display a similar behaviour in response to pH changes.[230–232]

3.3.3. Hydrogen Evolution at P3HT-Pt NP Films

Irradiation of the P3HT-Pt NP films (0.38 µg cm^{-2} Pt) on ITO, in 0.1 M H_2SO_4, yields significantly higher photocurrent compared to pristine P3HT-coated ITO films. Gas bubbles accumulate on the illuminated P3HT-Pt NP surface, and H_2 generation is confirmed through GC analysis of the headspace (Figure 3.10 inset). Chronocoulometric measurements in 0.1 M H_2SO_4 at -0.24 V_{SCE} under illumination (100 mW cm^{-2}, 300-700 nm) were performed and the cell headspace analysed for H_2 by GC every hour for six hours. The charge passed was equivalent to 1.1 µmoles H_2, assuming 100 % current-to-gas efficiency. The H_2 measured by GC was ~0.7 µmoles. The change in photocurrent over time and total hydrogen produced are shown in Figure 3.11.

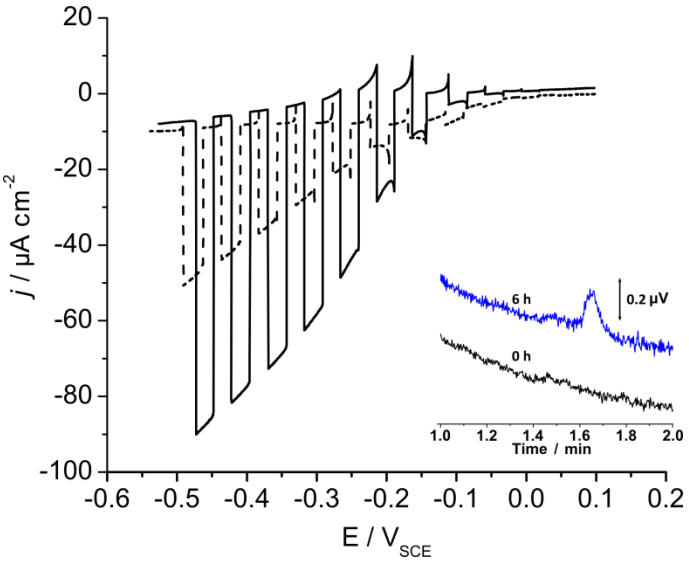

Figure 3.10 Linear sweep voltammogram of a P3HT-Pt NP electrode (0.38 µg cm^{-2} Pt) before (solid line) and after (dashed line) 6 hours of photoelectrolysis at -0.24 V_{SCE} in 0.1 M H_2SO_4. Scan rate was 5 mV s^{-1}, light intensity: 100 mW cm^{-2} (300-700 nm). The light source was blocked every 5 seconds. Inset: GC trace of the photoelectrochemical cell head space before and after illuminating P3HT-Pt NP (0.38 µg cm^{-2}) for 6 h in 0.1 M H_2SO_4 at -0.24 V_{SCE}.

The photocurrent at P3HT-Pt NP films steadily decays with prolonged PEC, and the rate of H_2 generation falls accordingly. The LSV of the P3HT-Pt NP film (Figure 3.10) shows that in addition to photocurrent loss there is also a slight increase in the dark current. The UV-visible absorbance of P3HT-Pt NP films was recorded before and after prolonged photoelectrolysis (Figure 3.12). The UV-visible absorbance of the P3HT film shows no change over 6 h of electrolysis, indicating the polymer film *was not* irreversibly photo-oxidized, as has been observed for P3HT films exposed under ambient illumination under non-PEC conditions.[233] One possibility for the decrease in photocurrent is the result of loss of Pt NPs through physical detachment from the surface—a phenomenon that could be addressed by adopting strategies that make use of stronger interactions between the polymer and Pt. Another explanation is that the P3HT film reacts with any trace oxygen, left after sparging or produced from the counter electrode, which would reduce the photoactivity of the film but not oxidize it.[233–235]

Chronocoulometric measurements in 0.1 M H_2SO_4 at -0.24 V_{SCE} were carried out using an ITO and a P3HT-coated ITO electrode without Pt. The current measured using

a blank ITO was on the order of nA cm^{-2} and became positive after the first hour. P3HT without Pt produced a photocurrent of ~2 µA cm^{-2} under 100 mW cm^{-2} (300-700 nm) illumination. No H_2 was detected by GC for either sample. Interestingly, the photocurrent of the P3HT coated ITO did not decay over the 4 hours unlike all samples with Pt. A P3HT-Pt NP film was tested under the same conditions but without illumination. The current produced under dark conditions was < 1 µA cm^{-2} and no H_2 was detected after 5 hours.

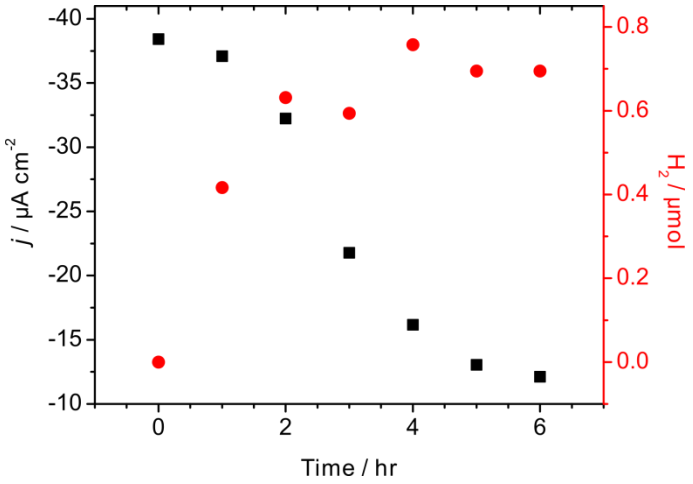

Figure 3.11 **Photocurrent (black squares) and H_2 measured (red circles) at a P3HT-Pt NP (0.38 µg cm^{-2}) electrode (biased at -0.24 V_{SCE} in 0.1 M H_2SO_4). Light intensity: 100 mW cm^{-2} (300-700 nm).**

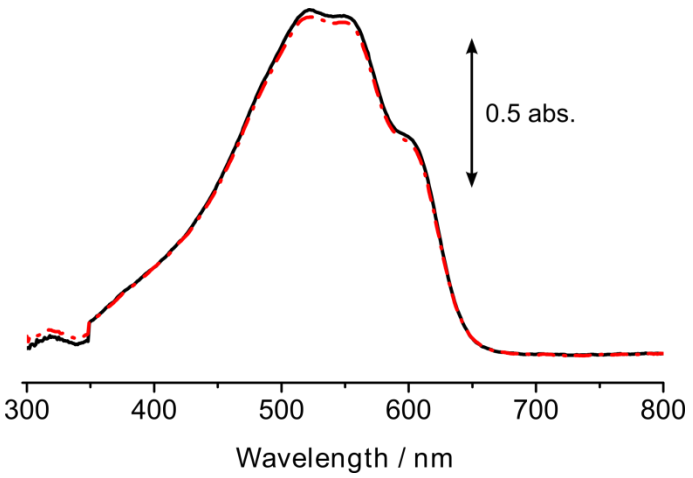

Figure 3.12 **UV visible absorbance of a P3HT-Pt (0.38 µg cm^{-2}) film before (black solid line) and after (red dashed line) constant potential electrolysis at -0.24 V_{SCE} under illumination (6 hours in 0.1 M H_2SO_4).**

3.3.4. Control Experiments

Previous reports have shown that poly(3,4-ethylenedioxthiophene) is photocatalytically active for oxygen[236] and proton[237] reduction but more recent research indicates that reduction may actually occur at the gold electrode on which the polymer is deposited.[238] Several control experiments were performed to elucidate the relationship between P3HT, ITO, and deposited platinum. It is important to be confident that any hydrogen observed is due to proton reduction at platinum on P3HT and not from platinum deposited on the ITO backing material. First, platinum was deposited onto blank ITO then coated with P3HT to see the effect of a platinum substrate on P3HT photocurrent. Second, P3HT-Pt films (platinum photoelectrochemically deposited on P3HT) were rinsed with $CHCl_3$ to remove P3HT and their linear sweep voltammograms in 0.1 M H_2SO_4 were compared to blank ITO and ITO-Pt.

Figure 3.13 shows the chopped light LSV of P3HT with and without platinum pre-deposited on the ITO in 0.1 M H_2SO_4, the inset shows the CV of ITO and ITO-Pt (1.2 µg cm^{-2}) electrodes prior to coating with P3HT. Both films still show a photocurrent when illuminated but performance of films with Pt underneath is greatly reduced. The appearance of significant dark current is similar to films were a large amount of platinum was used in the deposition (Figure 3.5, 0.5 mM K_2PtCl_6). The dark current observed here could mean that the dark currents observed for films in Figure 3.4 and Figure 3.5 could be due to platinum deposition directly on the ITO. The decrease in photocurrent for P3HT(ITO-Pt) compared to P3HT(ITO) was not expected and could mean the platinum under layer quenches the excitation of P3HT. Film thickness was measured and found to be similar to P3HT films without a Pt underlayer, eliminating the possibility of a thinner film being responsible for the decrease in photocurrent.

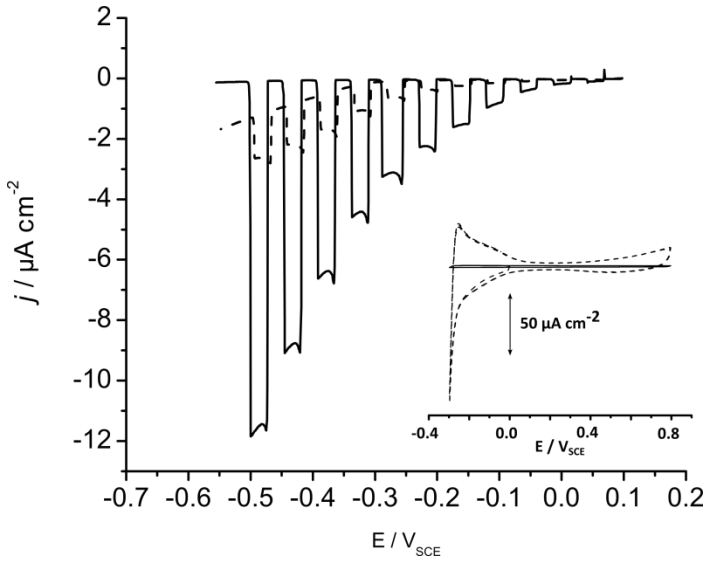

Figure 3.13 LSV of P3HT coated onto ITO and ITO-Pt (1.2 µg cm^{-2}) in 0.1 M H_2SO_4. Light intensity was 100 mW cm^{-2} over 300-700 nm (bandpass filter). The scan rate was 5 mV s^{-1} and the light source was blocked every 5 seconds. A platinum wire was used as a counter electrode. The inset shows the CV of a ITO electrode with platinum electrochemically deposited and a blank ITO in 0.1 M H_2SO_4. The scan rate was 100 mV s^{-1} and a platinum wire was used as a counter electrode.

Experiments were performed to confirm that the photocurrent was a result of PEC at the P3HT-Pt NP/electrolyte interface, not underlying ITO. In these experiments, P3HT-Pt NP films were rinsed with $CHCl_3$ to remove P3HT (and the overlying Pt). Linear sweep voltammograms of the electrodes in 0.1 M H_2SO_4 were compared to blank ITO and to ITO electrodes onto which Pt had been directly electrochemically deposited. Figure 3.14A shows the voltammogram of a P3HT-Pt NP film (0.43 µg cm^{-2} and 2.38 µg cm^{-2} Pt) and a blank ITO electrode under chopped light conditions. Both P3HT-Pt NP films are prepared by photoreduction of $PtCl_6^{2-}$ using a light intensity of 100 mW cm^{-2} (300-700 nm) at -0.1 V_{SCE} for 60 seconds in 0.1 mM and 0.5 mM K_2PtCl_6 which results in 0.43 µg cm^{-2} and 2.38 µg cm^{-2}, respectively, of deposited Pt. The P3HT-Pt NP film with 0.43 µg cm^{-2} yields a large photocurrent but no dark current. When the loading is increased to 2.38 µg cm^{-2}, however, we see the appearance of dark current below -0.25 V_{SCE}. ITO films subject to the same illumination conditions show no photocurrent response. P3HT is easily removed by rinsing the films with $CHCl_3$. If Pt had been depositing directly on the ITO its presence would have been observable, by electrochemistry, after removal of P3HT. Voltammetry of the rinsed film, Pt(0.42), (Figure

3.14B) shows a I-V curve similar to a blank ITO, indicating no Pt deposition under the P3HT film. A large reduction current is recorded for the film with the higher platinum loading, Pt(2.38), following removal of the P3HT in $CHCl_3$. The I-V curve of an ITO electrode having Pt directly deposited on to it (0.28 µg cm^{-2}), shown for comparison, exhibits a large onset of dark current at -0.24 V_{SCE}. The similarity between the I-V response of Pt(2.38) and an ITO-Pt electrode provides evidence that Pt is deposited on the surface of P3HT-coated ITO electrode and not the underlying ITO.

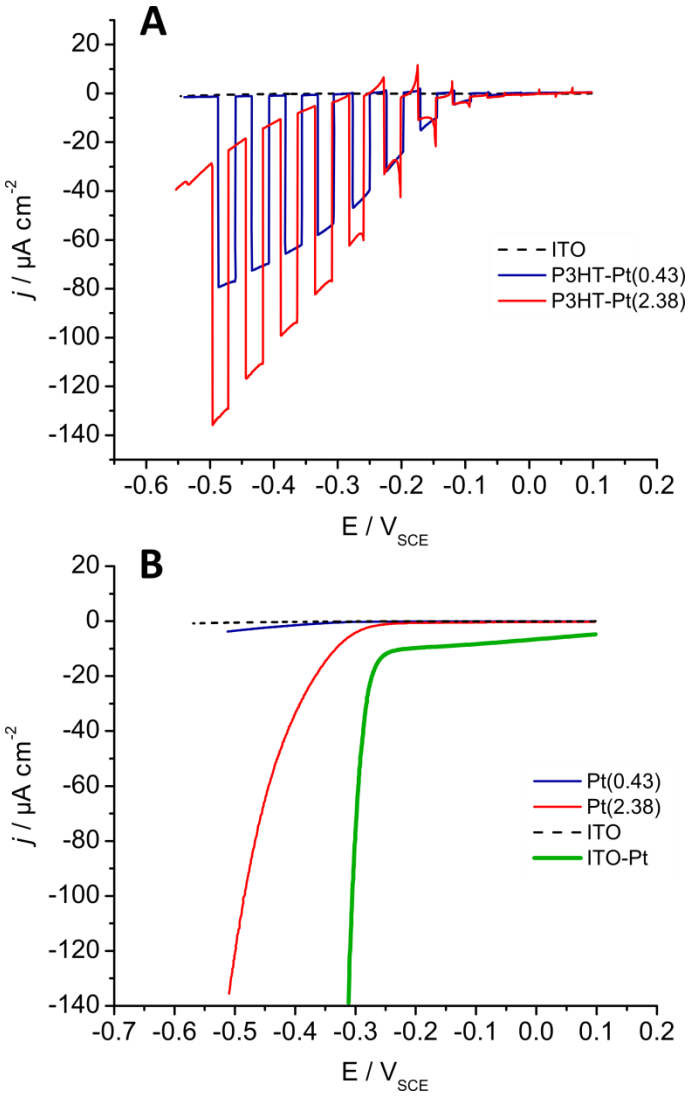

Figure 3.14 **Voltammetry of P3HT-Pt NP (0.43 µg cm^{-2} and 2.38 µg cm^{-2}) in 0.1 M H_2SO_4 before (A) and after (B) rinsing the film with $CHCl_3$. In (A), the P3HT-Pt NP films are compared to a blank ITO electrode under illumination. Light intensity: 100 mW cm^{-2} (300-700 nm), blocked every 5 seconds. In (B), the P3HT has been removed by rinsing the electrode in $CHCl_3$ and is compared to a blank ITO electrode and an ITO-Pt (0.28 µg cm^{-2}) electrode. The scan rate was 5 mV s^{-1} for both (A) and (B).**

3.4. Conclusion

I demonstrated that Pt can be deposited (photoelectrochemically) on to P3HT coated ITO as a co-catalyst for proton reduction. Low loadings of Pt NPs

(0.2-0.4 μg cm^{-2}) result in photocurrents of ~ 30 μA cm^{-2} at -0.24 V_{SCE} and production of H_2 in 0.1 M H_2SO_4 solution. Increasing either the time of deposition or the concentration of platinum source (K_2PtCl_6) resulted in high dark currents due to deposition of Pt directly on ITO. The photocurrents produced are several orders of magnitude lower than what is possible with inorganic photoelectrodes (see Section 1.4) but show that a P3HT photoelectrode is compatible with a commonly used hydrogen evolution catalyst.

Photoelectrolysis of P3HT/Pt NP films resulted in H_2 production but the rate decays quickly and after a few hours hydrogen production ceases. The loss of photocurrent is possibly due to the loss of Pt NPs from the surface or degradation of P3HT photoactivity through reactions with trace amounts of O_2 in solution. The size of platinum NPs can be tuned by including an organic additive, such as polyvinylpyrrolidone.[239] The presence of an organic additive is thought to help the adsorption of metal ions at the surface on metal electrodes. Its presence here may additionally help to anchor the Pt NP to the polymer film. Methods to protect the film from O_2 should also be considered. Air stability of organic polymer solar cells has been shown to be enhanced significantly when a TiO_2 layer is deposited between the active material and the metal cathode.[240] The polymer itself can be made more resilient to the presence of oxygen by increasing the ionization potential (make the polymer harder to oxidize) which has been shown for poly carbazole derivatives.[241] Incorporation of TiO_2 and/or new polymers is discussed in more detail in Chapter 5.

Chapter 4.

Poly (3-hexylthiophene) as a Photosensitizer in a Hydrogen Generating, Multicomponent System

4.1. Introduction

Multicomponent systems take advantage of the chemical reactions between several different types of materials that, when acting in concert, lead to the conversion of light energy into chemical energy. These systems are almost exclusively homogenous (i.e., all components are dissolved or dispersed in water), consisting of a soluble sensitizer (light absorber), charge relay, and a dispersion of noble metal as a gas evolution catalyst. Tris(2,2′-bipyridene)ruthenium(II) dichloride ($Ru(bpy)_3Cl_2$) was the most common choice of sensitizer for early investigators, with more modern examples being porphyrins,[242] platinum(II) terpyridyl acetylide,[243] and CdSe/CdS nanostructures.[244] Platinum colloid is a common choice for hydrogen evolution catalyst and it can be stabilized with a variety of organic materials, such as polyvinylalcohol and sodium citrate.[245] An electron relay is necessary to transfer charge between the photosensitizer and the catalyst because electronically excited $Ru(bipy)_3^{2+}$ does not carry out proton reduction itself. Methyl viologen (MV^{2+}, Figure 4.1) is a common choice as it is known that $*Ru(bipy)_3^{2+}$ can reduce MV^{2+}.[246,247] In addition, it is well established that hydrogen is evolved in the presence of a platinum catalyst following MV^{2+} reduction to its cation radical ($MV^{+\bullet}$):[248]

$$MV^{+\bullet} + H^+ \underset{Pt}{\leftrightarrow} MV^{2+} + \frac{1}{2}H_2 \qquad (4.1)$$

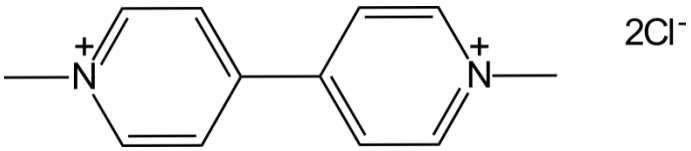

Figure 4.1 Methyl viologen dichloride

Multicomponent systems have a few disadvantages. They are designed to carry out only hydrogen or oxygen evolution reaction, HER and OER, respectively, (i.e., not full water splitting). A sacrificial electron donor or acceptor is necessary to reduce or oxidize the photosensitizer following charge transfer to the relay.

One early system reported by Moradpour *et al.*, consisted of 6 µmol $Ru(bpy)_3Cl_2$ as a photosensitizer, 0.06 mmol MV^{2+} as an electron relay, 2 µmol of platinum or gold colloid as HER catalyst, and 0.6 mmol ethylenediaminetetraacetic acid (EDTA) as a sacrificial electron donor in 30 mL of buffer solution (Figure 4.2).[249] Hydrogen production was highest at pH 4-5 but decreased at higher (pH 7) and lower (pH 3) values. At neutral pH, the water reduction potential is very similar to the MV^{2+} reduction potential (E_{H^+/H_2} = -0.42 V_{NHE} vs. $E_{MV^{2+}/MV^{+\bullet}}$ = -0.44 V_{NHE})[250] and would result in a decrease of electron transfer between the $MV^{+\bullet}$ and Pt catalyst. Hydrogenation of MV^{2+} in acidic solutions was suspected but a decrease in the luminescence quenching of $Ru(bipy)_3^{2+*}$ by MV^{2+} was detected by transient absorption spectroscopy. No hydrogen was produced when one of the components was removed from the system.

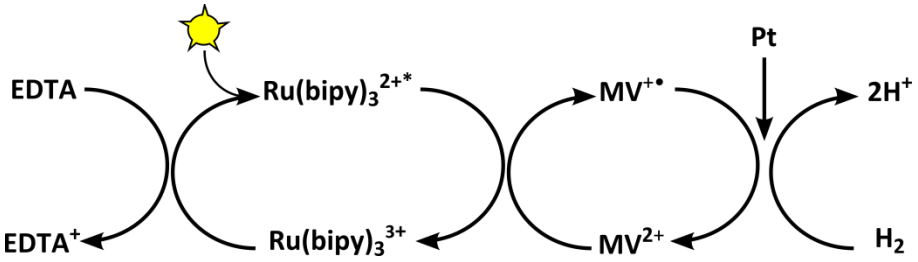

Figure 4.2 Multicomponent system described by Moradpour *et al.*[249] All components (except H_2) are dissolved/dispersed in a buffer solution.

A nearly opposite trend of H_2 evolved vs. pH was shown by Grätzel *et al.* when triethanolamine (TEOA) was employed as an electron donor.[251] Using transient absorption spectroscopy to observe $MV^{+\bullet}$ (λ = 632.3 nm), $TEOA^+$ was found to oxidize

$MV^{+\bullet}$ back to MV^{2+} following electron donation to $Ru(bipy)_3^{2+*}$ at pH 5. Hydrogen generation was not observed at pH 9 because at high pH the water reduction potential is too negative compared to the $MV^{2+}/MV^{+\bullet}$ redox couple (same reason as Moradpour *et al*.[249]). The transient absorption signal of $MV^{+\bullet}$ does not, however, decay as it does at lower pH. At pH 5, the signal decays to zero in approximately 5 µs whereas at pH 9 there is no decay. The difference in transient absorption is speculated to be due to the acid/base chemistry of $TEOA^+$ which is deprotonated to a neutral molecule, at high pH, and does not react with the cation radical. McLendon *et al.* also showed a pH dependence of the electron donor with EDTA.[252] Reduction of $Ru(bipy)_3^{3+}$ by EDTA was diminished at pH < 4, possibly due to protonation of EDTA. Following this report were many papers detailing the dependence of Pt colloid size,[253] solution pH, and viologen reduction potential on the hydrogen evolution efficiency of the system.[252,254] These reports show that this system is very complex.

This chapter examines the use of a single layer photoelectrode (poly 3-hexylthiophene (P3HT) coated on indium tin oxide (ITO) electrodes) in place of the soluble sensitizer (Figure 4.3). The main advantage is that this system no longer requires a sacrificial reductant because photogenerated holes are collected by the ITO. During photoexcitation, electrons are excited to P3HT's LUMO leaving holes in the HOMO. Excitons diffuse to the surface where electrons are accepted by the MV^{2+} in solution and holes diffuse to the back electrode contact. The semiconductor film remains neutral and does not require a reducing agent to be made available again to perform photoreduction of the electron relay.

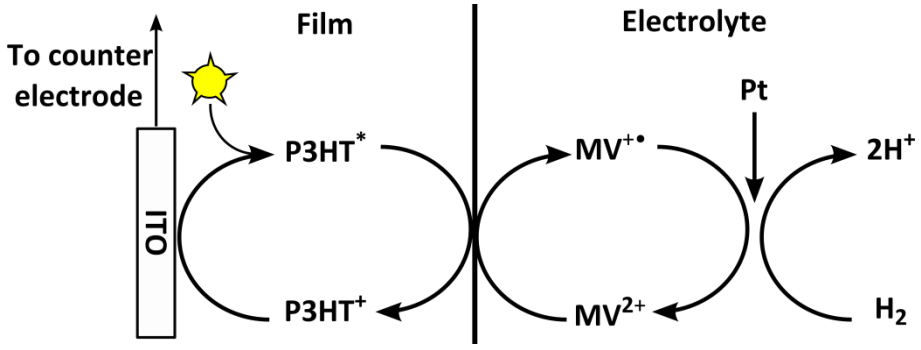

Figure 4.3 Multicomponent system where the soluble photosensitizer has been replaced with a P3HT photocathode.

4.2. Experimental

4.2.1. Materials

Regioregular P3HT was synthesized according to a literature procedure (details of the synthesis are presented in Section 2.2.2).[165] The number-average molecular weight of the polymer was 31,700 kDa with a polydispersity index (PDI) of 1.2 as determined by gel permeation chromatography using tetrahydrofuran (Sigma-Aldrich, HPLC grade) eluent, three Waters μStyragel columns at 40°C, a Waters 1515 isocratic HPLC pump, a Waters 2414 differential refractometer, and a Waters 2487 dual UV absorbance detector (λ = 254 nm). Polystyrene standards (Waters) were used for calibration. The degree of head-to-tail regioregularity was determined to be 94 % by ^{1}H NMR spectroscopic analysis (Figure A-1), according to standard literature procedure.[164,167]

A colloidal solution of Pt was synthesized following a published method.[255,256] A solution of 7.8 mg H_2PtCl_6 (Sigma-Aldrich) in 49 mL of ultrapure water was prepared and brought to a boil using an oil bath. Once boiling, 1 mL of 0.84 M sodium citrate solution was added. The mixture was left to reflux for 45 minutes. After 45 minutes the mixture had become dark grey and was allowed to cool in an ice bath before storing it in a fridge. Nanoparticles were characterized by UV-visible absorbance spectroscopy of the solutions (Figure A-2).[256,257]

Chlorobenzene (Sigma-Aldrich), methyl viologen dichloride hydrate (Sigma-Aldrich), Na_2SO_4, and H_2SO_4 (Anachemia) were used as received. Aqueous solutions were prepared using water obtained from a Milli-Q water purification system (18 MΩ, EMD Millipore). ITO coated glass slides (Merck Display Technologies Ltd.) were cleaned by sequential sonication in each of the following solutions: isopropyl alcohol, acetone, H_2O: H_2O_2: NH_4OH (5:1:1) solution and distilled water.

4.2.2. Film Preparation

Films for P3HT-O_2 photoelectrochemistry were prepared from a 20 mg mL^{-1} chlorobenzene solution that had been stirred overnight at 65˚C. The solution was

spin-cast onto chemically cleaned ITO in a glove box (H_2O < 0.1 ppm, O_2 < 1 ppm) at 1000 rpm for 1 minute, affording polymer films ~100 nm thick. Silver conductive paste (MG Chemicals, 8331-14G) was used to connect a wire to the ITO electrode after wiping away a small part of the polymer with a cotton tipped applicator (Puritan). The edges of the film were completely covered with an electronically insulating and chemically resistant epoxy (T20-3004 HVGR50, Epoxies, Etc.)

4.2.3. Characterization

Photoelectrochemistry. The light source was a 200 W Xe/Hg lamp (Uhsio America, Inc.), used in combination with a 300-700 nm band pass filter (FSQ-KG3, Newport Corp.) and neutral density filters (Thorlabs Inc.), to achieve 100 mW cm^{-2} irradiation, as measured using a broadband power meter (841-PE, Newport Corporation) equipped with an Ophir thermal detector head (3A-P-SH-V1). The cell configuration was designed to allow irradiation of the polymer–electrolyte interface through the electrolyte. A water filter was placed in front of the electrochemical cell to remove excess heat. Electrochemical measurements were performed using a Pine Bipotentiostat (AFC-BP1). Photoelectrochemical (PEC) measurements were performed in a 3-electrode configuration (Figure 4.4) using a saturated standard calomel electrode (SCE) (+0.24 V vs. NHE) and a Pt wire as the reference and counter electrodes, respectively. Solutions were sparged with argon (Praxair, purity 99.999 %) for 1.5 to 2 hours in a glass PEC cell and sealed under a flow of argon. Solution pH was measured using a (Metrohm 848 Titrino Plus and pH electrode, model number 6.0262.100).

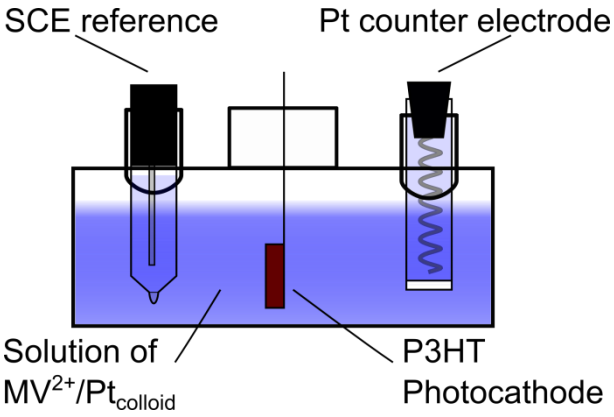

Figure 4.4 **Three-electrode cell configuration used for experiments. The counter electrode compartment is separated from the main body of the cell by a glass frit.**

Hydrogen Gas Detection. The headspace in the electrochemical cell was sampled using a 5 mL syringe, fitted with a gas tight valve (Series A-2, VICI Precision Sampling), and analyzed using an Agilent Technologies 6890N GC system equipped with a thermal conductivity detector. A 2.13 m Agilent J&W GC packed column in stainless steel tubing was used (inner diameter of 2 mm, HayeSep N packing material, 60/80 mesh size). Argon was used as a carrier gas at a flow rate of 30 mL min^{-1} under 46.2 psi.

4.3. Results and Discussion

4.3.1. Photoelectrochemical Reduction of MV^{2+} at P3HT Photocathodes

The energy level of the $MV^{2+}/MV^{+\bullet}$ redox couple lies below the LUMO energy level of P3HT as determined from literature.[203,204] The literature value of $MV^{2+}/MV^{+\bullet}$ is -0.44 V_{NHE} which corresponds to a vacuum energy level of -4.1 eV. The conduction band/LUMO level of P3HT was determined to be -3.1 eV (see Section 2.3.1). Photogenerated electrons in P3HT are, therefore, thermodynamically able to reduce MV^{2+} to $MV^{+\bullet}$. It has been described above that $MV^{+\bullet}$ can transfer an electron to colloidal Pt. MV^{2+} is regenerated and proton reduction, forming hydrogen gas, is carried out on the Pt colloid. Figure 4.5 shows the steps in this process.

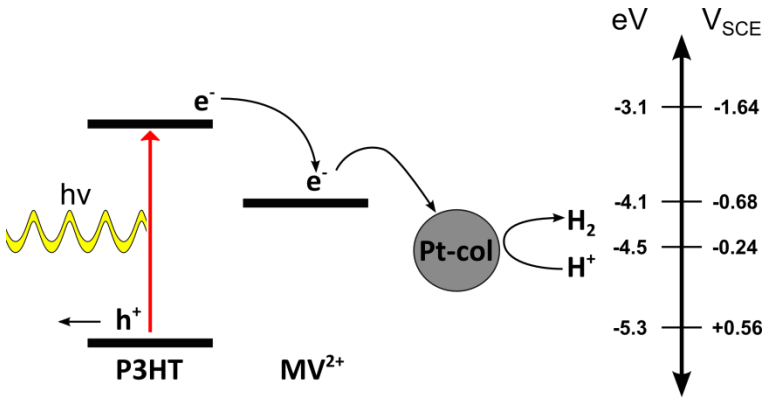

Figure 4.5 Energy level diagram of P3HT's HOMO and LUMO, methyl viologen (MV^{2+}), and proton reduction at a platinum colloid (Pt-col).

This section first demonstrates the ability of P3HT to reduce MV^{2+} when illuminated. The linear sweep voltammetry of a P3HT-coated ITO electrode in 0.2 mM MV^{2+}/0.1 M $NaClO_4$ (aq.) with chopped (periodically interrupted) illumination is presented in Figure 4.6**.** In the dark, the observed cathodic current is < 1 µA cm^{-2} and remains steady, showing no signs of a Faradaic process. Under illumination a significant increase in current density is observed. The photocurrent, without interruption of illumination, is shown as a dashed line in Figure 4.6. The large spike in current at -0.3 V_{SCE} (solid curve) is associated with the most rapid change in current. The stability of the photocurrent was monitored over four hours (Figure 4.7). After one hour, the cathodic current equilibrated and maintained a value of ~ 2.6 µA cm^{-2}.

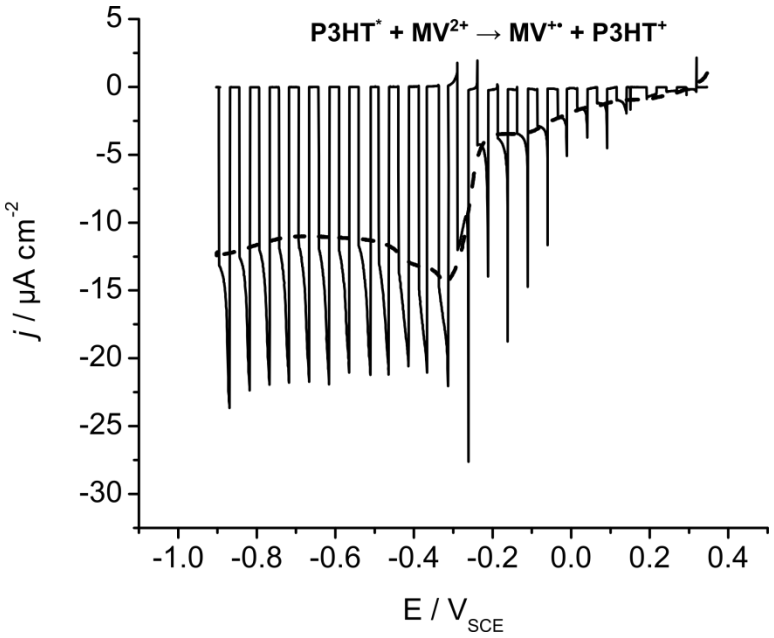

Figure 4.6 **Linear sweep voltammogram (dashed line) of a P3HT coated ITO electrode in 0.2 mM MV^{2+} / 0.1 M $NaClO_4$ obtained using a scan rate of 5 mV s^{-1} with illumination. A Pt wire was used as a counter electrode. The light intensity was 100 mW cm^{-2} (300-700 nm) and the light source was interrupted every 5 seconds (solid line). Inset: stability of the same P3HT film under illumination and constant applied potential (-0.4 V_{SCE}).**

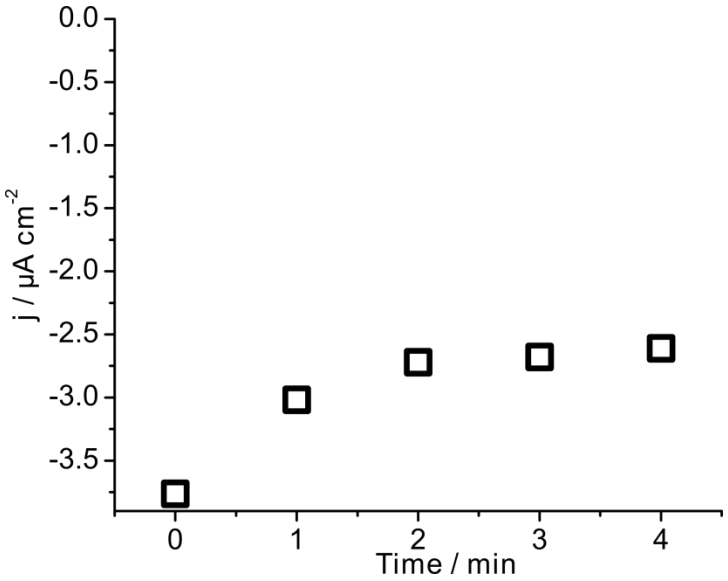

Figure 4.7 Stability of the P3HT coated ITO electrode in 0.2 mM MV^{2+} / 0.1 M $NaClO_4$ under illumination and constant applied potential (-0.4 V_{SCE}). A Pt wire was used as a counter electrode. The light intensity was 100 mW cm^{-2} (300-700 nm)

The photocurrent was found to be dependent on the MV^{2+} concentration (Figure 4.8). As the MV^{2+} concentration is increased, the photocurrent increases. The relationship between photocurrent and MV^{2+} concentration further confirms that photogenerated electrons of P3HT are able to reduce MV^{2+} to $MV^{+\bullet}$. The photocurrent increases linearly to 5 mM MV^{2+} but approaches constant value (~ 70 µA cm^{-2}) for greater concentrations, indicating saturation of the electrode surface by the electron acceptor, which has also been observed in PEC studies of P3HT:fullerene (and metalofullerene).[161] This may be due to the smaller number of charge carriers on a semiconductor when compared to metal electrodes. For example, the charge carrier density for P3HT is 10^{17} cm^{-3}.[207,258] The charge carrier density for a metal conductor such as copper is 1.43×10^{23} cm^{-3}.[259]

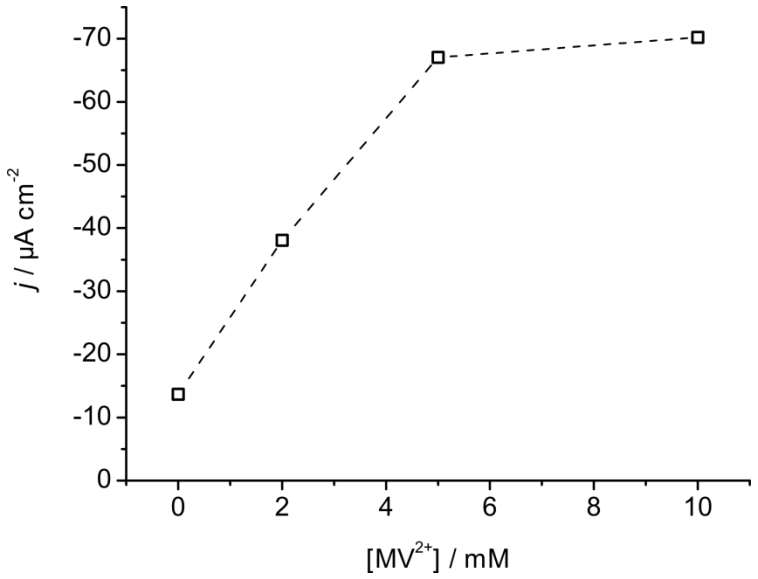

Figure 4.8 Photocurrent generated by P3HT coated glassy carbon electrode at E = -0.65 V_{SCE} in the presence of increasing amounts of methyl viologen (MV^{2+}). A platinum coil was used as a counter electrode and 0.1 M $NaClO_4$ was used as a supporting electrolyte. Incident light power was 100 mW cm^{-2} (300-700 nm).

4.3.2. Hydrogen Evolution Measurements

For chronoamperometric photoelectrolysis experiments, a concentration of 2 mM MV^{2+} was chosen. Several different conditions were used for the photoelectrolysis of the three component system. The results for P3HT films biased at -0.4 V_{SCE} at pH 7, -0.4 V_{SCE} at pH 4, and -0.2 V_{SCE} at pH 4 are presented in Figure 4.9, Figure 4.10, and Figure 4.11, respectively. The expected sequence of reactions under illumination is:

$$P3HT \xrightarrow{h\nu} P3HT^{*} \qquad (4.2)$$

$$P3HT^{*} + MV^{2+} \rightarrow P3HT^{+} + MV^{+\bullet} \qquad (4.3)$$

$$MV^{+\bullet} + H^{+} \xrightarrow{Pt_{col}} MV^{2+} + \frac{1}{2}H_2 \qquad (4.4)$$

Where P3HT* denotes the excited state of the polymer. Equation (4.3) shows that the production of the current under illumination is due to charge transfer between P3HT* and MV^{2+}. After the transfer, the hole left on $P3HT^{+}$ diffuses to the back contact (interface between P3HT and ITO) and returns the polymer to a neutral state, P3HT. Note, this process is not shown in the reaction scheme. In the dark, the reaction in Equation (4.2) does not occur and thus no current is produced in the dark (see panel A, solid line, in Figure 4.9 to Figure 4.11).

Three component systems are typically used in neutral solutions to balance the effects of an increasing overpotential for proton reduction vs. the $MV^{+\bullet}/MV^{2+}$ redox couple and the acid-base chemistry of the electron acceptor as described above (Section 4.1). In all cases the dark current (dark CV, solid line, from panel A, Figure 4.9 to Figure 4.11) is < 1 μA cm^{-2}, therefore all current produced under illumination is considered photocurrent (due to reaction of photogenerated electrons from the P3HT LUMO with an electron accepting species in solution, i.e., Equation (4.3)). Initially, the photocurrents follow the expected trend: As the pH is lowered and the applied potential is made more negative (-0.2 V_{SCE} to -0.4 V_{SCE}), the photocurrent increases (Table 4.1). This trend is expected because as the pH is lowered the proton reduction potential becomes less negative (E_{H^+/H_2} = 0 V_{NHE} at pH 0, becoming more negative by 59 mV for every pH unit increase) and is more easily reduced by $MV^{+\bullet}$ in the presence of colloidal Pt. At pH 7, for example, $E_{MV^{2+}/MV^{+\bullet}}$ = -0.44 V_{NHE} and E_{H^+/H_2} = -0.42 V_{NHE} (Section 4.1) resulting in very little driving force for electron transfer from $MV^{+\bullet}$ to Pt colloid.

Table 4.1 Initial and final photocurrent (after 4 hours of photoelectrolysis). Light intensity was 100 mW cm^{-2} (300-700 nm).

		-Current / μA cm^{-2}	
	Conditions	t = 0 hr	t = 4 hr
Figure 4.9	-0.4 V_{SCE}, pH 7	1.3	2.4
Figure 4.10	-0.4 V_{SCE}, pH 4	3	20
Figure 4.11	-0.2 V_{SCE}, pH 4	1.8	5

The cathodic photocurrent increased in all three systems over the course of four hours of photoelectrolysis (panel C in Figure 4.9, Figure 4.10, and Figure 4.11). The steady increase in current may indicate a change in the resistance of the film and/or deposition of electroactive material on the polymer (discussed later). Illumination of the film was periodically interrupted to measure the dark current. Although the current decreased when the light was blocked, the magnitude of the dark current increased with time. CVs of the films after electrolysis (panel B in Figure 4.9 to Figure 4.11) reveal that any photogenerated current is swamped by dark current. The loss of photocurrent indicates a new, lower resistance pathway for reactions at the electrode surface.

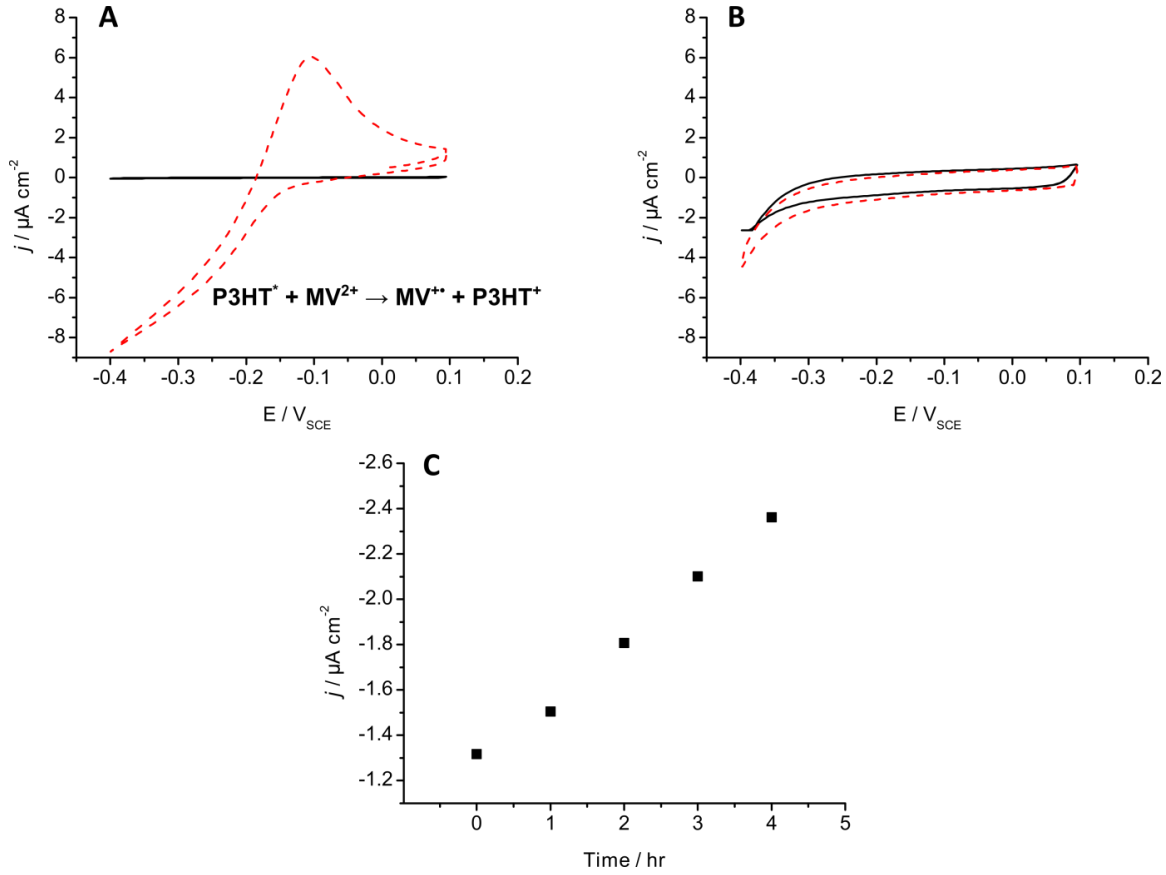

Figure 4.9 **Cyclic voltammetry of a P3HT coated ITO electrode before (A) and after (B) 4 hours of photoelectrolysis. Films were measured in the dark (solid black line) and under illumination (broken red line). Scan rate was 100 mV s^{-1}. Photoelectrolysis (C) of the same film over 4 hours at -0.4 V_{SCE}. The solution was comprised of 2 mM MV^{2+}, 0.31 mM Pt colloid, and 0.1 M Na_2SO_4, adjusted to pH 7 with H_2SO_4. The incident light power was 100 mW cm^{-2} (300-700 nm).**

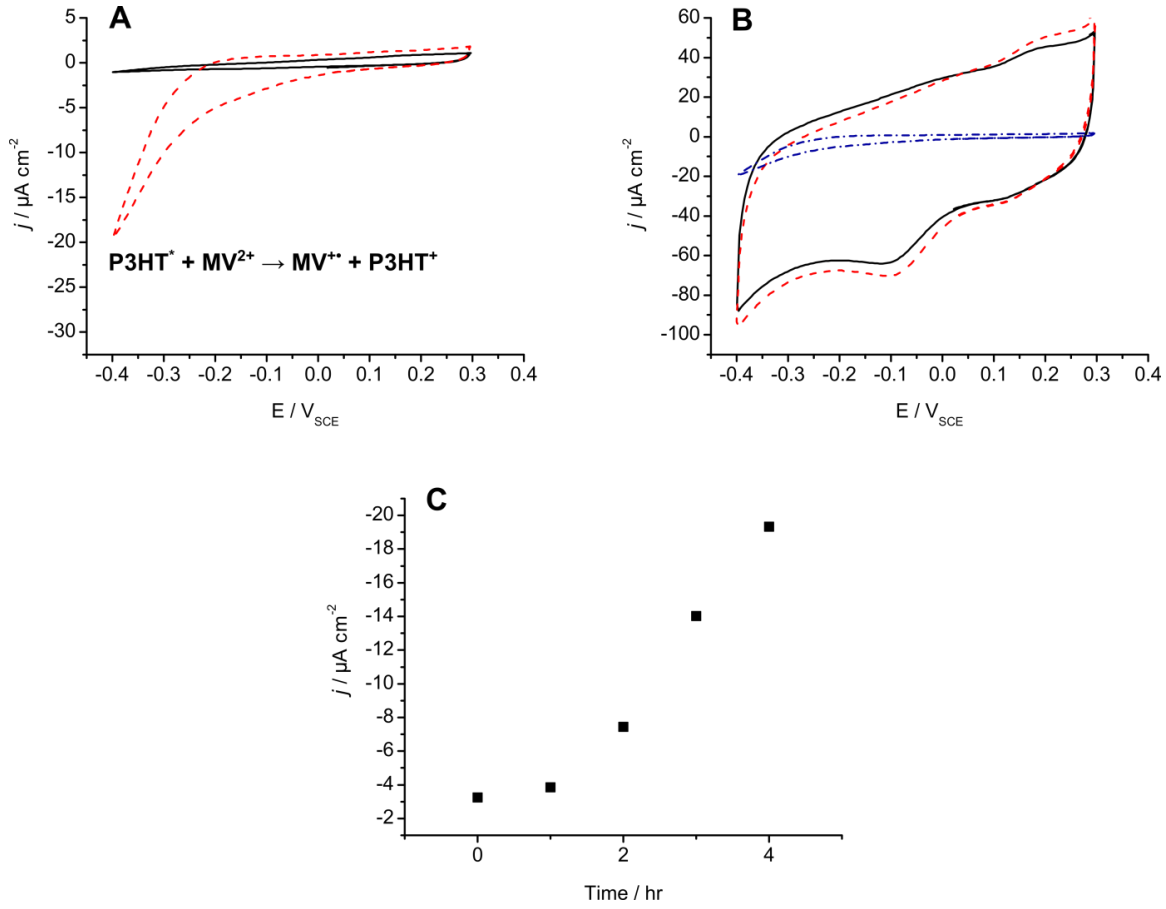

Figure 4.10 **Cyclic voltammetry of a P3HT coated ITO electrode before (A) and after (B) 4 hours of photoelectrolysis. Films were measured in the dark (solid black line) and under illumination (broken red line). The broken blue line in B shows the initial illuminated voltammogram from A. Scan rate was 100 mV s^{-1}. Photoelectrolysis (C) of the same film over 4 hours at -0.4 V_{SCE}. The solution was comprised of 2 mM MV^{2+}, 0.31 mM Pt colloid, and 0.1 M Na_2SO_4, adjusted to pH 4 with H_2SO_4. The incident light power was 100 mW cm^{-2} (300-700 nm).**

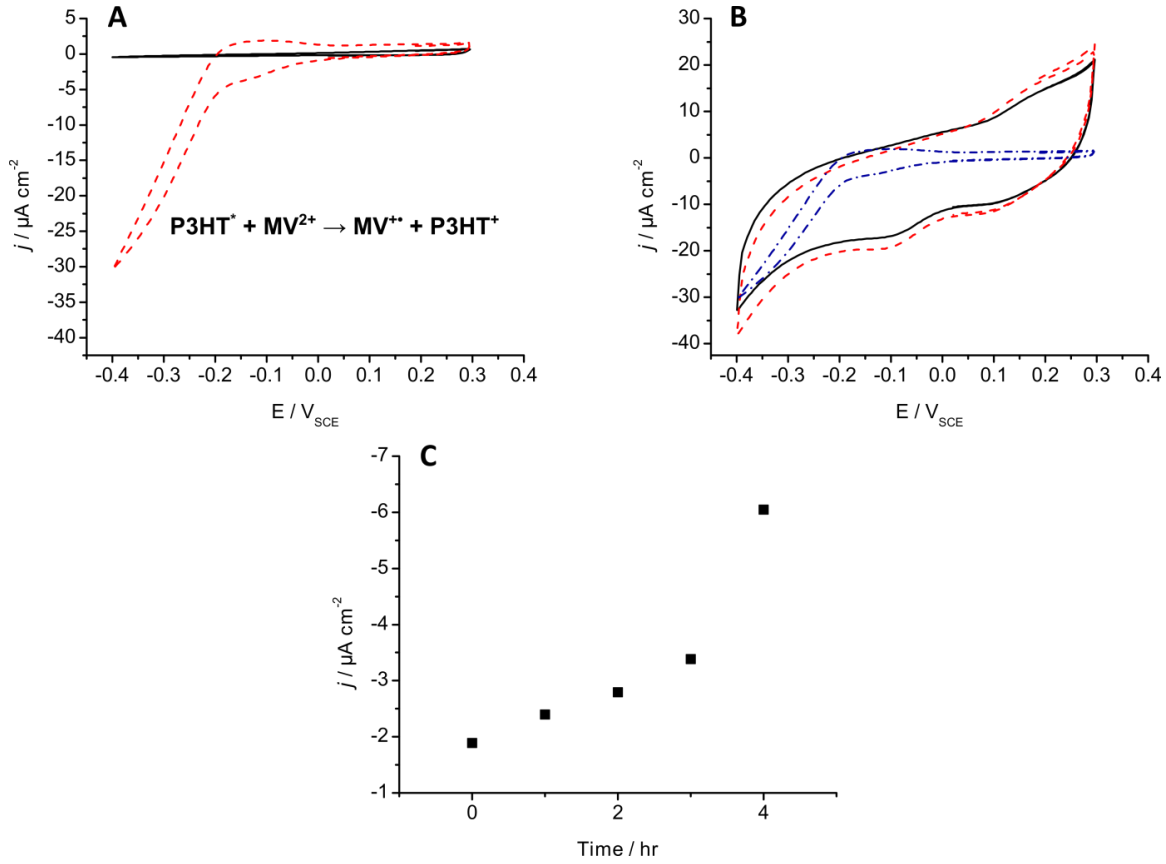

Figure 4.11 **Cyclic voltammetry of a P3HT coated ITO electrode before (A) and after (B) 4 hours of photoelectrolysis. Films were measured in the dark (solid black line) and under illumination (broken red line). The broken blue line in B shows the initial illuminated voltammogram from A. Scan rate was 100 mV s^{-1}. Photoelectrolysis (C) of the same film over 4 hours at -0.2 V_{SCE}. The solution was comprised of 2 mM MV^{2+}, 0.31 mM Pt colloid, and 0.1 M Na_2SO_4, adjusted to pH 4 with H_2SO_4. The incident light power was 100 mW cm^{-2} (300-700 nm).**

The physical appearance of the films changes as a result of electrolysis. Photographs of the P3HT electrode used to collect data shown in Figure 4.9, before and after photoelectrochemistry, are shown in Figure 4.12. The film is initially flat but can be seen to have a significant amount of bubbling following electrolysis. The nature of the bubbling is not known. Two possibilities are that water penetrates the film and remains between the ITO and P3HT or, if Pt is present on the ITO, small bubbles of hydrogen are formed. When the film is left to dry overnight the bubbles disappear.

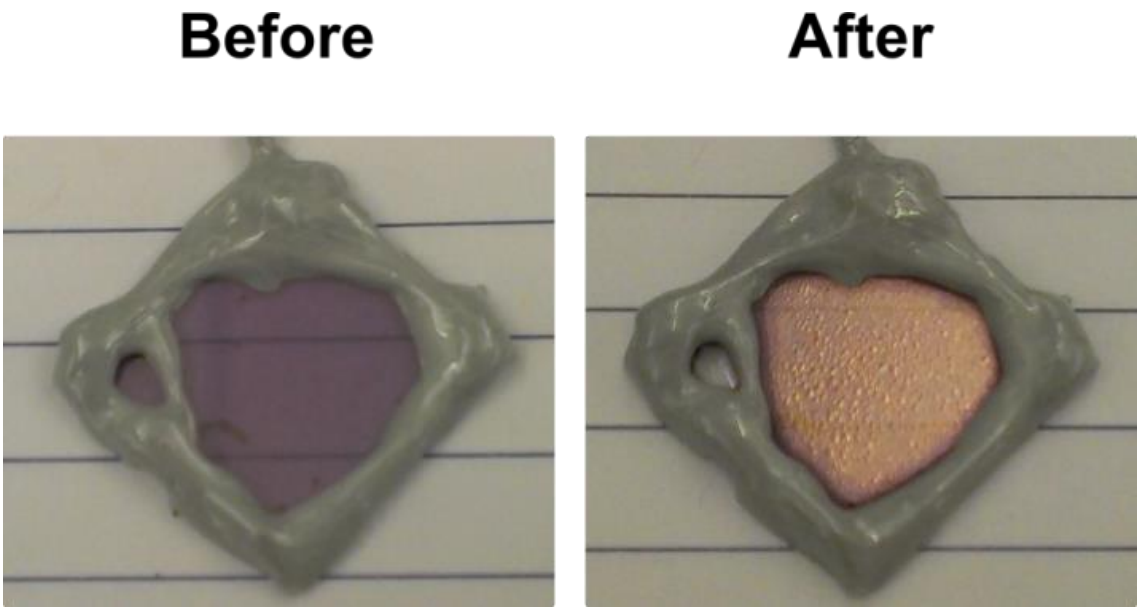

Figure 4.12 P3HT coated ITO before and after 4 hours of photoelectrolysis at -0.4 V_{SCE} in a pH 7 solution of 2 mM MV^{2+} / 0.1 M Na_2SO_4. The incident light power was 100 mW cm^{-2} (300 700 nm).

The headspace of the cell is sampled after 4 or 6 hours of constant photoelectrolysis and analyzed by gas chromatography. Figure 4.13 presents the gas chromatographs following PEC of a P3HT electrode in a MV^{2+}/Pt colloid solution at pH 7 with E_{app} = -0.4 V_{SCE} (Figure 4.13 triangles) and pH 4 with E_{app} = -0.2 V_{SCE} (Figure 4.13 circles). A sample from a cell where H_2 was produced from a platinum electrode (Figure 4.13 solid curve) and a cell that was purged with argon (Figure 4.13 squares) are shown for comparison. Using a platinum electrode in 0.1 M H_2SO_4 and applying a bias of -0.325 V_{SCE} for 5 minutes resulted in -105.8 mC of charge being passed and 0.55 µmol H_2 produced (calculated from charge assuming 100 % efficiency). A sample of the headspace produces a peak in the chromatography with a retention time of 1.178 min and is associated with dihydrogen. All gas chromatography samples taken from cells after photoelectrolysis of the P3HT electrode-MV^{2+}-Pt colloid system did not produce any dihydrogen and showed no difference when compared to samples from cells prior to photoelectrolysis. Comparing the charge passed, some hydrogen formation should have been observed. At pH 7, with applied potential of -0.4 V_{SCE} for 6 hours, -170.5 mC is passed which would translate into 0.88 µmol H_2 (assuming 100 % charge conversion efficiency). obtained by sampling the cell headspace following several experiments.

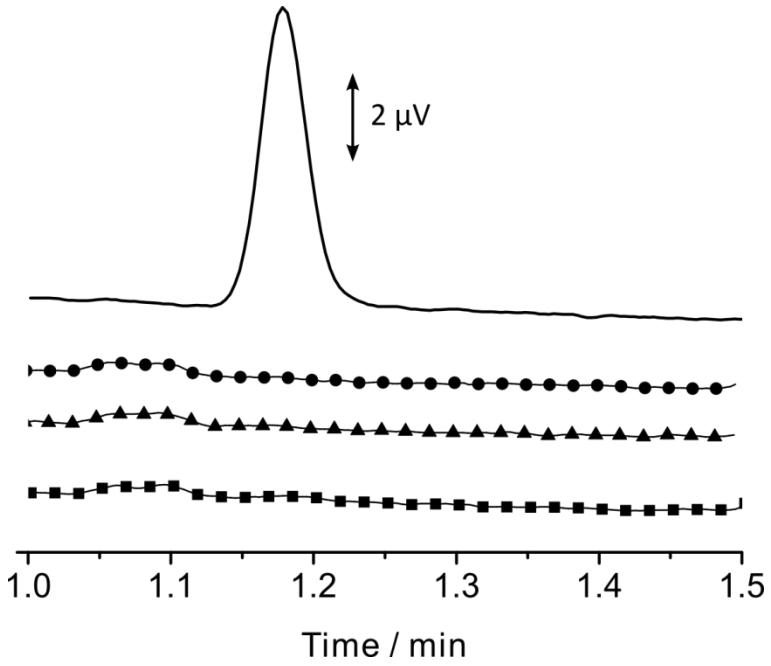

Figure 4.13 Gas chromatograph of the photoelectrochemistry cell headspace after various experiments: (solid curve) platinum electrode in 0.1 M H_2SO_4 at -0.325 V_{SCE} for 5 min (-105.8 mC, 0.55 µmol H_2); (circles) P3HT coated ITO in 2 mM MV^{2+} / 0.31 mM Pt / pH 4 at -0.2 V_{SCE} for 4 hours (-68.3 mC); (triangles) P3HT coated ITO in 2 mM MV^{2+} / 0.31 mM Pt / pH 7 at -0.4 V_{SCE} for 6 hours (-170.5 mC); (squares) empty cell prior to any photoelectrochemical measurements but after Ar sparging for 2 hours. The curves are offset for clarity.

Additional interactions of MV^{2+} and Pt colloid with the P3HT surface must be considered. Three component systems are almost exclusively homogenous except where the photosensitizer was replaced with an electrode to measure kinetics.[260,261] Introduction of a solid film may lead to issues not present in previously examined systems. Some control experiments have been performed to examine this.

Any change in the concentration of MV^{2+}, whether through degradation of the material or regeneration through the reaction of $MV^{+\bullet}$ with Pt colloid, would result in a loss of current. If MV^{2+} were absorbing on to the P3HT surface this could result in passivation of the surface. Metal deposition on the ITO or oxidation of the polymer from its semiconducting, neutral state to a conducting state would result in higher currents. Deposition of Pt was examined using glassy carbon electrodes in solutions consisting of the Pt colloid, MV^{2+}, or neither (all with supporting electrolyte). Figure 4.14 compares the

CV of a blank glassy carbon electrode in 0.31 mM Pt colloid solution with a 2 mM MV^{2+} solution. In the platinum colloid solution, the current increases with the number of scans indicating deposition of some electroactive material. The onset for deposition is approximately -0.6 V_{SCE} which is close to the onset of MV^{2+} reduction at approximately -0.5 V_{SCE}. The closeness of these potentials would make reduction of the MV^{2+} difficult to achieve without some reduction of the Pt colloid. Deposition of material was confirmed by cycling the glassy carbon electrode 0.1 M HCl (Figure 4.15), which is free of Pt colloid. Prior to polishing the electrode a CV similar to platinum is generated with a current onset of about -0.26 V_{SCE}. The potential for proton reduction in 0.1 M HCl (pH 1) is -0.3 V_{SCE} (this equation is used to convert from NHE to SCE, E_{SCE} = -0.24 V - 0.059 V * pH). After polishing with an alumina suspension the observed CV is that of a blank glassy carbon electrode.

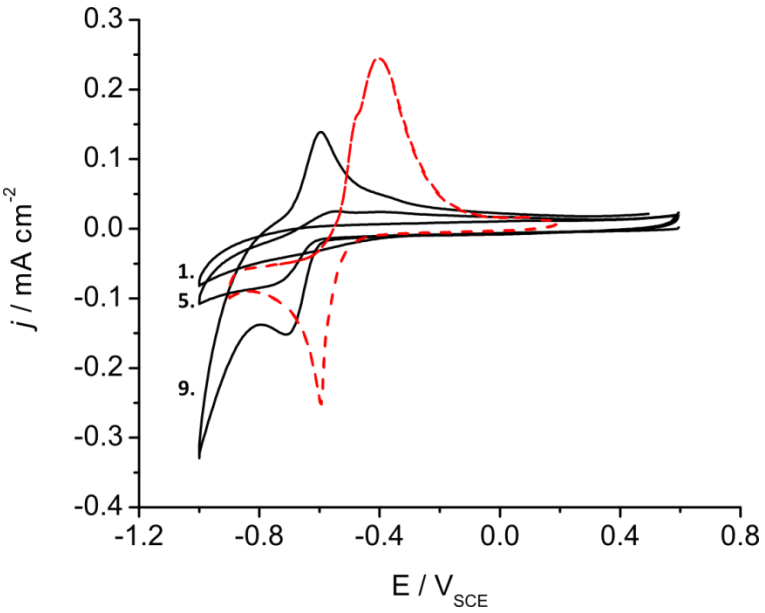

Figure 4.14 **Cyclic voltammetry of a glassy carbon electrode in 2 mM MV^{2+} / 0.1 M $NaClO_4$, scan rate 50 mV s^{-1} (red broken line) and the 1st, 5th, and 9th scan of a glassy carbon electrode in a 0.31 mM platinum colloid / 0.1 M Na_2HPO_4 / 0.1 M HCl (pH 7) solution, scan rate 100 mV s^{-1} (black solid line).**

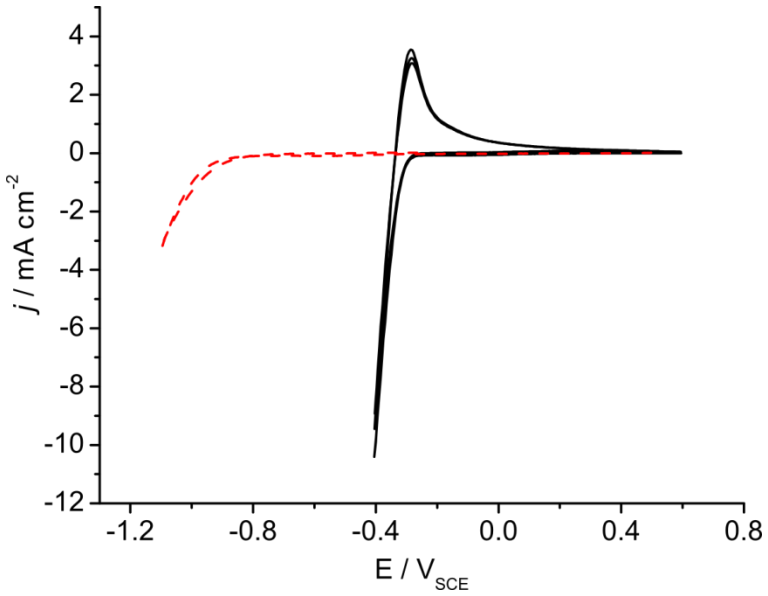

Figure 4.15 Cyclic voltammetry of a glassy carbon electrode in 0.1 M HCl before (solid black line) and after (red broken line) polishing with an alumina suspension. Scan rate 100 mV s^{-1}. The electrode was previously cycled in a solution containing platinum colloid.

4.4. Conclusion

This chapter has demonstrated that a three component system where a P3HT coated electrode is used as a photo-absorber does not produce H_2. Photocurrent generated by MV^{2+} reduction can reach 70 µA cm^{-2} with 10 mM MV^{2+} and high stability (in 0.2 mM MV^{2+}, Figure 4.6 inset). Addition of Pt colloid to the system does not produce H_2 and may be depositing on the P3HT and/or the ITO. Deposition of the catalyst directly on the film (physically or electrochemically) has been shown to work for inorganic photoelectrodes and may provide a more reliable method for producing H_2 from P3HT. Platinum in solution could also be replaced with a solid electrode. Bard *et al.* have shown that photocurrent is produced at platinum electrodes in the presence of suspended TiO_2 and an electron trap (MV^{2+}, Cu^{2+}, or Fe^{3+}).[262–264] Generation of photocurrent begins immediately when the cell is illuminated and stirred due to photogeneration of an electron-hole pair from TiO_2 followed by electron capture by the electron trap (the hole is irreversibly trapped by a sacrificial donor). The reduced electron trap is oxidized at the platinum electrode, where the current is measured. Interruption of illumination causes a slow decay as the as the reduced electron trap is oxidized and

stops immediately when the stirring is shut off. Shutting the stirring off under illumination also causes the current to drop to zero. Derivatives of methyl viologen with a more negative redox potential have been shown to produce more hydrogen when all other variables are left the same.[265] The ability of these powerful reducing agents (following electron donation from an excited photo sensitizer) may not be fully realized as these systems still require pH balancing due to the acid-base chemistry of the sacrificial electron donor.

Chapter 5.

Conclusion

This thesis has shown that poly 3-hexylthiophene (P3HT) can be employed as a photocathode for solar water splitting following deposition of a hydrogen evolution catalyst (HER) on the film. For several decades, the majority of solar water splitting research has focused on inorganic materials. Despite significant progress in using organic materials (conjugated polymers in particular) in solar cells, little has been reported for photoelectrochemistry. Conjugated polymers have large absorption coefficients, which results in the possibility of creating thinner devices. Additionally, the solubility of conjugated polymers in organic solvents allows for processing of room temperature solutions for coating a variety of substrates. In solar cell devices, the polymers are paired with an electron accepting material to improve performance but this thesis research demonstrates that a single layer device can perform proton reduction when used with a HER catalyst.

In chapter 2, I demonstrated that regioregular P3HT produces photocurrent in aqueous acid and at a higher efficiency when compared to regiorandom P3HT. A series of photoelectrochemical experiments were performed using films of varying thickness and the illumination intensity. One important result was provided by spectroelectrochemical studies of P3HT electrodes in aqueous acid and acetonitrile. In aqueous acid, P3HT remains neutral and semiconducting between potentials of 0.8 V and -0.5 V vs. Ag/AgCl (values vs. NHE) but can be oxidized above 0.4 V vs. Ag/AgCl in a non-aqueous electrolyte system. However, no H_2 was detected, implying that a HER catalyst is needed.

Chapter 3 built upon the work in Chapter 2 and demonstrated the evolution and detection of H_2 when platinum nanoparticles (Pt NPs) were employed as a HER catalyst.

Pt NPs were deposited on P3HT by photoelectrochemical reduction of $PtCl_6^{2-}$. P3HT/Pt NP photocathodes produced much higher photocurrent in 0.1 M H_2SO_4 (~ 30 μA cm^{-2}) than just P3HT alone (~ 2 μA cm^{-2}). Bubbles were observed on the surface of P3HT/Pt NP films during photoelectrolysis and H_2 generation was confirmed by gas chromatography by sampling the cell headspace above the electrodes.

Platinum as a HER catalyst was also employed in Chapter 4 but as a platinum colloid, not fixed to the film's surface. The colloid was dispersed in an aqueous solution with methyl viologen (MV^{2+}) as an electron acceptor/relay. P3HT photocathodes produce a photocurrent in solutions containing MV^{2+} because photogenerated electrons (from P3HT) have sufficient energy to reduce MV^{2+} to $MV^{+\bullet}$. Another electron transfer occurs between $MV^{+\bullet}$ and Pt colloid which has been shown to produce H_2 from proton reduction. Unfortunately, no H_2 was detected and the photocurrent produced by P3HT was quenched after a few hours of photoelectrolysis. Electrochemical experiments using glassy carbon electrodes (without any polymer film) in the Pt colloid solution indicate deposition of platinum onto the electrode is occurring.

Research in the Holdcroft group indicates that trace amounts O_2 (< 0.01 ppm) may be present in aqueous solutions even after 2 hours or sparging with argon or nitrogen.[208] Furthermore, O_2 is known to be detrimental to P3HT performance in the context of photovoltaic (PV) devices and has also been shown to degrade the photocurrent produced through photoelectrolysis in aqueous solutions. Two strategies to mitigate the effect of O_2 are to protect the polymer film with TiO_2 and/or use a polymer that is more air stable (higher ionization potential).

Lee *et al*.[240] have shown that the air stability of a P3HT:phenyl-C61-butyric acid methyl ester (PCBM) PV device can be improved by including a layer of TiO_x between the active layer and the metal cathode. Oxygen vacancies present in TiO_2 cause it to be a good scavenger for oxygen.[266] The TiO_x layer was produced using a sol-gel and resulted in Ti:O = 1:1.34 ratio (measured by XPS) rather than the 1:2 ratio expected for TiO_2. Devices with and without TiO_x layers were stored in air for over 100 hours and their photon conversion efficiency (PCE) was measured periodically. The PCE of devices without TiO_x layers degraded by over 2 orders of magnitude in this time but devices with

TiO_x only degraded by approximately a factor of 2 (both devices had an initial PCE = 4 %).

In addition to air stability, TiO_x layers could improve performance when an HER catalyst is used. Bourgeteau *et al*.[138] have shown the P3HT:PCBM photoelectrodes produce hydrogen only when both TiO_2 and MoS_3 are present. Cobaloxime is a cobalt containing coordination compound HER catalyst (Figure 5.1) that is typically only active in organic solvents (such as acetonitrile).[267] Lakadamyail *et al*.[268] have shown that cobaloxime can be anchored to TiO_2 particles and produce hydrogen in water and in the presence of oxygen. The TiO_2-cobaloxime system was dispersed in solution but it may be possible to use the anchoring technique to deposit the cobalt catalyst on a TiO_2 film.

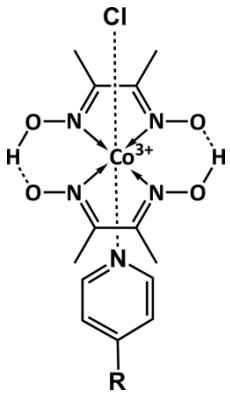

Figure 5.1 The structure of cobaloxime, where R = H or PHO_3^-. PHO_3^- is used for anchoring to the TiO_2 nanoparticles.[268]

Modeling results by Jin *et al*.[96] have shown that a large pH gradient can develop near the surface of the photoelectrodes. The pH near the surface of the photocathode can be as high as 13.5, even when the solution is buffered to pH 9.2. A decrease in pH is observed at the photoanode and the system experiences a voltage loss due to the pH gradient. One possible method of maintaining the pH at the surface of the photocathode is by employing a strongly acidic Nafion polyfluorosulphonic acid (PFSA) ionomer. The ionomer is available as a dispersion and could be mixed with TiO_2 dispersions to form films through spray and spin coating techniques. The area around a catalyst (Pt for example) should have the highest pH as that is where protons are consumed. If the catalyst is surrounded by PFSA that may make more protons available and help keep the pH stabilized.

New polymers should also be considered. Cho *et al*. synthesized a poly(2,7-carbozol derivative, poly[N-9”-hepta-decanyl-2,7-carbazole-alt-5,5-(4’-7’-di-2-thienyl-2’,1’,3’-benzothiadiazole)] (PCDTBT) (Figure 5.2) that is thermally stable in air when annealed to 150 °C and in an N_2 atmosphere when annealed to 350 °C.[241] Thermal stability was determined by observing changes in the UV-visible spectra as a function of annealing temperature. The stability of the polymer is due to the position of the HOMO level at -5.5 eV below vacuum energy level,[70] which is below the air oxidation threshold (ca. -5.27 eV).[71] Oxidation of the polymer backbone when exposed to air is accelerated when the temperature is elevated.

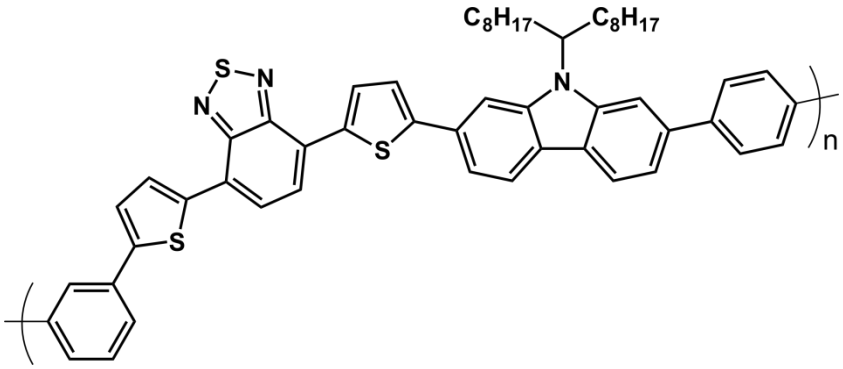

Figure 5.2 The structure of poly[N-9”-hepta-decanyl-2,7-carbazole-alt-5,5-(4’-7’-di-2-thienyl-2’,1’,3’-benzothiadiazole)] (PCDTBT).[241]

These recommendations focus heavily on the improving the stability of a polymer photocathode in the presence of O_2. Other figures of merit, such as the photocurrent and catalyst loading, will also require improvement or investigation. Protection against O_2, in my estimation, is very important as it seems that some O_2 will always be present. Any future device based on polymer photoelectrodes should be straightforward to operate and supply with water. Even if fresh, pure water is available, techniques used to remove O_2, such as freeze-pump-thaw and sparging with inert gas, may not be feasible.

References

(1) Schwendeman, I.; Hickman, R.; Soenmez, G.; Schottland, P.; Zong, K.; Welsh, D. M.; Reynolds, J. R. *Chem. Mater.* **2002**, *14*, 3118.

(2) Karabay, B.; Pekel, L. C.; Cihaner, A. *Macromolecules* **2015**, *48*, 1352.

(3) Sirringhaus, H.; Tessler, N.; Friend, R. H. *Science* **1998**, *280*, 1741.

(4) Marks, R.; Halls, J.; Bradley, D.; Friend, R.; Holmes, A. *J. Phys. Condens. Matter* **1994**, *6*, 1379.

(5) Chen, X.; Schulz, G. L.; Han, X.; Zhou, Z.; Holdcroft, S. *J. Phys. Chem. C* **2009**, *113*, 8505.

(6) Song, H.-K.; Palmore, G. T. R. *Adv. Mater.* **2006**, *18*, 1764.

(7) Wang, J.; Too, C. O.; Wallace, G. G. *J. Power Sources* **2005**, *150*, 223.

(8) Sengodu, P.; Deshmukh, A. D. *RSC Adv.* **2015**, *5*, 42109.

(9) Biso, M.; Mastragostino, M.; Montanino, M.; Passerini, S.; Soavi, F. *Electrochim. Acta* **2008**, *53*, 7967.

(10) Cuentas-Gallegos, A. K.; Lira-Cantu, M.; Casan-Pastor, N.; Gomez-Romero, P. *Adv. Funct. Mater.* **2005**, *15*, 1125.

(11) Suppes, G. M.; Cameron, C. G.; Freund, M. S. *J. Electrochem. Soc.* **2010**, *157*, A1030.

(12) Chiang, C. K.; Fincher Jr., C. R.; Park, Y. W.; Heeger, A. J.; Shirakawa, H.; Louis, E. J.; Gau, S. C.; MacDiarmid, A. G. *Phys. Rev. Lett.* **1977**, *39*, 1098.

(13) Shirakawa, H.; Louis, E. J.; MacDiarmid, A. G.; Chiang, C. K.; Heeger, A. J. *J. Chem. Soc. Chem. Commun.* **1977**, 578.

(14) Grzeszczuk, M.; Ozsakarya, R. *RSC Adv.* **2014**, *4*, 22214.

(15) Smela, E. *J. Micromechanics Microengineering* **1999**, *9*, 1.

(16) Freund, M. S.; Karp, C.; Lewis, N. S. *Inorganica Chim. Acta* **1995**, *240*, 447.

(17) Bravo-Grimaldo, E.; Hachey, S.; Cameron, C. G.; Freund, M. S. *Macromolecules* **2007**, *40*, 7166.

(18) Jen, K. Y.; Oboodi, R.; Elsenbaumer, R. L. *Polym. Mater. Sci. Eng.* **1985**, *53*, 79.

(19) Jen, K. Y.; Miller, G. G.; Elsenbaumer, R. L. *J. Chem. Soc. Chem. Commun.* **1986**, 1346.

(20) Sato, M.; Tanaka, S.; Kaeriyama, K. *J. Chem. Soc. Chem. Commun.* **1986**, 873.

(21) Hsieh, B. R.; Yu, Y.; VanLaeken, A. C.; Lee, H. *Macromolecules* **1997**, *30*, 8094.

(22) Kraft, A.; Grimsdale, A. C.; Holmes, A. B. *Angew. Chemie, Int. Ed.* **1998**, *37*, 403.

(23) Babel, A.; Jenekhe, S. A. *Synth. Met.* **2005**, *148*, 169.

(24) Yu, G.; Heeger, A. J. *J. Appl. Phys.* **1995**, *78*, 4510.

(25) Halls, J. J. M.; Walsh, C. A.; Greenham, N. C.; Marseglia, E. A.; Friend, R. H.; Moratti, S. C.; Holmes, A. B. *Nature* **1995**, *376*, 498.

(26) Zykwinska, A.; Domagala, W.; Pilawa, B.; Lapkowski, M. *Electrochim. Acta* **2005**, *50*, 1625.

(27) Moskwa, T.; Domagala, W.; Czardybon, A.; Pilawa, B.; Lapkowski, M. *Synth. Met.* **2005**, *152*, 189.

(28) Brunetti, F. G.; Kumar, R.; Wudl, F. *J. Mater. Chem.* **2010**, *20*, 2934.

(29) Subramaniyan, S.; Xin, H.; Kim, F. S.; Murari, N. M.; Courtright, B. A. E.; Jenekhe, S. A. *Macromolecules* **2014**, *47*, 4199.

(30) Hoppe, H.; Arnold, N.; Sariciftci, N. S.; Meissner, D. *Sol. Energy Mater. Sol. Cells* **2003**, *80*, 105.

(31) Beermann, N.; Vayssieres, L.; Lindquist, S.-E.; Hagfeldt, A. *J. Electrochem. Soc.* **2000**, *147*, 2456.

(32) Hamann, T. W. *Dalt. Trans.* **2012**, *41*, 7830.

(33) Weaver, J. H.; Frederikse, P. R. *CRC Handbook of Chemistry and Physics (Internet Version)*; Lide, D. R., Ed.; 96th ed.; CRC Press/Taylor and Francis: Boca Raton, FL., 2016.

(34) Halary-Wagner, E.; Wagner, F.; Hoffmann, P. *J. Electrochem. Soc.* **2004**, *151*, C571.

(35) Osterloh, F. E. *Chem. Soc. Rev.* **2013**, *42*, 2294.

(36) Patra, A.; Bendikov, M. *J. Mater. Chem.* **2010**, *20*, 422.

(37) Van Pruissen, G. W. P.; Gholamrezaie, F.; Wienk, M. M.; Janssen, R. A. J. *J. Mater. Chem.* **2012**, *22*, 20387.

(38) Dong, H.; Zhu, H.; Meng, Q.; Gong, X.; Hu, W. *Chem. Soc. Rev.* **2012**, *41*, 1754.

(39) Kanazawa, K. K.; Diaz, A. F.; Geiss, R. H.; Gill, W. D.; Kwak, J. F.; Logan, J. A.; Rabolt, J. F.; Street, G. B. *J. Chem. Soc. Chem. Commun.* **1979**, 854.

(40) Winther-Jensen, B.; Breiby, D. W.; West, K. *Synth. Met.* **2005**, *152*, 1.

(41) Hains, A. W.; Liang, Z.; Woodhouse, M. A.; Gregg, B. A. *Chem. Rev.* **2010**, *110*, 6689.

(42) Gledhill, S. E.; Scott, B.; Gregg, B. A. *J. Mater. Res.* **2005**, *20*, 3167.

(43) Gregg, B. A. *J. Phys. Chem. B* **2003**, *107*, 4688.

(44) Gregg, B. A.; Hanna, M. C. *J. Appl. Phys.* **2003**, *93*, 3605.

(45) Heeger, A. J. *Chem. Soc. Rev.* **2010**, *39*, 2354.

(46) Heeger, A. J. *Angew. Chemie, Int. Ed.* **2001**, *40*, 2591.

(47) Brabec, C. J.; Gowrisanker, S.; Halls, J. J. M.; Laird, D.; Jia, S.; Williams, S. P. *Adv. Mater.* **2010**, *22*, 3839.

(48) van der Horst, J.-W.; Bobbert, P. A.; Michels, M. A. J.; Bassler, H. *J. Chem. Phys.* **2001**, *114*, 6950.

(49) Antoniadis, H.; Abkowitz, M. A.; Osaheni, J. A.; Jenekhe, S. A.; Stolka, M. *Chem. Mater.* **1994**, *6*, 63.

(50) Sze, S. M.; Lee, M.-K. *Semiconductor Devices: Physics and Technology*; 3rd ed.; John Wiley & Sons, 2015.

(51) Hwang, I.; Scholes, G. D. *Chem. Mater.* **2011**, *23*, 610.

(52) Bredas, J.-L.; Norton, J. E.; Cornil, J.; Coropceanu, V. *Acc. Chem. Res.* **2009**, *42*, 1691.

(53) Munters, T.; Martens, T.; Goris, L.; Vrindts, V.; Manca, J.; Lutsen, L.; De

Ceuninck, W.; Vanderzande, D.; De Schepper, L.; Gelan, J.; Sariciftci, N. S.; Brabec, C. J. *Thin Solid Films* **2002**, *403-404*, 247.

(54) Vandenbergh, J.; Conings, B.; Bertho, S.; Kesters, J.; Spoltore, D.; Esiner, S.; Zhao, J.; Van Assche, G.; Wienk, M. M.; Maes, W.; Lutsen, L.; Van Mele, B.; Janssen, R. A. J.; Manca, J.; Vanderzande, D. J. M. *Macromolecules* **2011**, *44*, 8470.

(55) Tajima, K.; Suzuki, Y.; Hashimoto, K. *J. Phys. Chem. C* **2008**, *112*, 8507.

(56) Kim, Y.; Cook, S.; Tuladhar, S. M.; Choulis, S. A.; Nelson, J.; Durrant, J. R.; Bradley, D. D. C.; Giles, M.; McCulloch, I.; Ha, C.-S.; Ree, M. *Nat. Mater.* **2006**, *5*, 197.

(57) Li, G.; Shrotriya, V.; Huang, J.; Yao, Y.; Moriarty, T.; Emery, K.; Yang, Y. *Nat. Mater.* **2005**, *4*, 864.

(58) Yang, X.; Loos, J.; Veenstra, S. C.; Verhees, W. J. H.; Wienk, M. M.; Kroon, J. M.; Michels, M. A. J.; Janssen, R. A. J. *Nano Lett.* **2005**, *5*, 579.

(59) Faist, M. A.; Shoaee, S.; Tuladhar, S.; Dibb, G. F. A.; Foster, S.; Gong, W.; Kirchartz, T.; Bradley, D. D. C.; Durrant, J. R.; Nelson, J. *Adv. Energy Mater.* **2013**, *3*, 744.

(60) Alberga, D.; Perrier, A.; Ciofini, I.; Mangiatordi, G. F.; Lattanzi, G.; Adamo, C. *Phys. Chem. Chem. Phys.* **2015**, Ahead of Print.

(61) Hertel, D.; Baessler, H. *ChemPhysChem* **2008**, *9*, 666.

(62) Ma, W.; Yang, C.; Gong, X.; Lee, K.; Heeger, A. J. *Adv. Funct. Mater.* **2005**, *15*, 1617.

(63) Mihailetchi, V. D.; Xie, H.; de Boer, B.; Koster, L. J. A.; Blom, P. W. M. *Adv. Funct. Mater.* **2006**, *16*, 699.

(64) Ewbank, P. C.; Laird, D.; McCullough, R. D. In *Organic Photovoltaics: Materials, Device Physics, and Manufacturing Technologies*; Brabec, C.; Dyakonov, V.; Scherf, U., Eds.; WILEY-VCH Verlag: Weinheim, 2008; pp. 3–55.

(65) McCullough, R. D. *Adv. Mater.* **1998**, *10*, 93.

(66) Curtis, M. D. *Macromolecules* **2001**, *34*, 7905.

(67) Chen, T. A.; Rieke, R. D. *J. Am. Chem. Soc.* **1992**, *114*, 10087.

(68) McCullough, R. D.; Lowe, R. D.; Jayaraman, M.; Ewbank, P. C.; Anderson, D. L.;

Tristram-Nagle, S. *Synth. Met.* **1993**, *55*, 1198.

(69) McCullough, R. D.; Lowe, R. D.; Jayaraman, M.; Anderson, D. L. *J. Org. Chem.* **1993**, *58*, 904.

(70) Blouin, N.; Michaud, A.; Gendron, D.; Wakim, S.; Blair, E.; Neagu-Plesu, R.; Belletete, M.; Durocher, G.; Tao, Y.; Leclerc, M. *J. Am. Chem. Soc.* **2008**, *130*, 732.

(71) de Leeuw, D. M.; Simenon, M. M. J.; Brown, A. R.; Einerhand, R. E. F. *Synth. Met.* **1997**, *87*, 53.

(72) Ohkita, H.; Cook, S.; Astuti, Y.; Duffy, W.; Tierney, S.; Zhang, W.; Heeney, M.; McCulloch, I.; Nelson, J.; Bradley, D. D. C.; Durrant, J. R. *J. Am. Chem. Soc.* **2008**, *130*, 3030.

(73) Lee, J. H.; Shin, J.-H.; Song, J. Y.; Wang, W.; Schlaf, R.; Kim, K. J.; Yi, Y. *J. Phys. Chem. C* **2012**, *116*, 26342.

(74) Liao, W.-P.; Hsu, S.-C.; Lin, W.-H.; Wu, J.-J. *J. Phys. Chem. C* **2012**, *116*, 15938.

(75) Scurlock, R. D.; Wang, B.; Ogilby, P. R.; Sheats, J. R.; Clough, R. L. *J. Am. Chem. Soc.* **1995**, *117*, 10194.

(76) Xing, K. Z.; Johansson, N.; Beamson, G.; Clark, D. T.; Bredas, J. L.; Salaneck, W. R. *Adv. Mater.* **1997**, *9*, 1027.

(77) Abdou, M. S. A.; Holdcroft, S. *Macromolecules* **1993**, *26*, 2954.

(78) Nozik, A. J.; Memming, R. *J. Phys. Chem.* **1996**, *100*, 13061.

(79) Morrison, S. R. *Electrochemistry at Semiconductor and Oxidized Metal Electrodes*; Plenum Press: New York, 1980.

(80) Bard, A. J. *Science* **1980**, *207*, 139.

(81) Lewis, N. S. *Inorg. Chem.* **2005**, *44*, 6900.

(82) Kelly, J. J.; Memming, R. *J. Electrochem. Soc.* **1982**, *129*, 730.

(83) Currao, A. *Chimia* **2007**, *61*, 815.

(84) Lewis, N. S.; Crabtree, G. W. *Basic Research Needs for Solar Energy Utilization*; Lewis, N. S.; Crabtree, G. W., Eds.; Department of Energy, 2005.

(85) Walter, M. G.; Warren, E. L.; McKone, J. R.; Boettcher, S. W.; Mi, Q.; Santori, E.

A.; Lewis, N. S. *Chem. Rev.* **2010**, *110*, 6446.

(86) Li, J.; Wu, N. *Catal. Sci. Technol.* **2015**, *5*, 1360.

(87) Bolton, J. R.; Strickler, S. J.; Connolly, J. S. *Nature* **1985**, *316*, 495.

(88) Hu, S.; Xiang, C.; Haussener, S.; Berger, A. D.; Lewis, N. S. *Energy Environ. Sci.* **2013**, *6*, 2984.

(89) Ager III, J. W.; Shaner, M.; Walczak, K.; Sharp, I. D.; Ardo, S. *Energy Environ. Sci.* **2015**, *8*, 2811.

(90) Chen, Z.; Jaramillo, T. F.; Deutsch, T. G.; Kleiman-Shwarsctein, A.; Forman, A. J.; Gaillard, N.; Garland, R.; Takanabe, K.; Heske, C.; Sunkara, M.; McFarland, E. W.; Domen, K.; Miller, E. L.; Turner, J. A.; Dinh, H. N. *J. Mater. Res.* **2010**, *25*, 3.

(91) Dotan, H.; Mathews, N.; Hisatomi, T.; Grätzel, M.; Rothschild, A. *J. Phys. Chem. Lett.* **2014**, *5*, 3330.

(92) Licht, S.; Wang, B.; Mukerji, S.; Soga, T.; Umeno, M.; Tributsch, H. *J. Phys. Chem. B* **2000**, *104*, 8920.

(93) Haussener, S.; Xiang, C.; Spurgeon, J. M.; Ardo, S.; Lewis, N. S.; Weber, A. Z. *Energy Environ. Sci.* **2012**, *5*, 9922.

(94) Haussener, S.; Hu, S.; Xiang, C.; Weber, A. Z.; Lewis, N. S. *Energy Environ. Sci.* **2013**, *6*, 3605.

(95) Berger, A.; Segalman, R. A.; Newman, J. *Energy Environ. Sci.* **2014**, *7*, 1468.

(96) Jin, J.; Walczak, K.; Singh, M. R.; Karp, C.; Lewis, N. S.; Xiang, C. *Energy Environ. Sci.* **2014**, *7*, 3371.

(97) Chen, Y.; Sun, K.; Audesirk, H.; Xiang, C.; Lewis, N. S. *Energy Environ. Sci.* **2015**, *8*, 1736.

(98) Zhai, P.; Haussener, S.; Ager, J.; Sathre, R.; Walczak, K.; Greenblatt, J.; McKone, T. *Energy Environ. Sci.* **2013**, *6*, 2380.

(99) Sathre, R.; Scown, C. D.; Morrow III, W. R.; Stevens, J. C.; Sharp, I. D.; Ager III, J. W.; Walczak, K.; Houle, F. A.; Greenblatt, J. B. *Energy Environ. Sci.* **2014**, *7*, 3264.

(100) Pinaud, B. A.; Benck, J. D.; Seitz, L. C.; Forman, A. J.; Chen, Z.; Deutsch, T. G.; James, B. D.; Baum, K. N.; Baum, G. N.; Ardo, S.; Wang, H.; Miller, E.; Jaramillo, T. F. *Energy Environ. Sci.* **2013**, *6*, 1983.

(101) Conti, J. J. *Annual Energy Outlook 2011, report DOE/EIA-0383*; Washington, D.C., 2011.

(102) McKone, J. R.; Lewis, N. S.; Gray, H. B. *Chem. Mater.* **2014**, *26*, 407.

(103) Fujishima, A.; Honda, K. *Nature* **1972**, *238*, 37.

(104) Hashimoto, K.; Irie, H.; Fujishima, A. *Japanese J. Appl. Physics, Part 1 Regul. Pap. Br. Commun. Rev. Pap.* **2005**, *44*, 8269.

(105) Mor, G. K.; Shankar, K.; Paulose, M.; Varghese, O. K.; Grimes, C. A. *Nano Lett.* **2005**, *5*, 191.

(106) Hoang, S.; Berglund, S. P.; Hahn, N. T.; Bard, A. J.; Mullins, C. B. *J. Am. Chem. Soc.* **2012**, *134*, 3659.

(107) Hou, Y.; Abrams, B. L.; Vesborg, P. C. K.; Bjoerketun, M. E.; Herbst, K.; Bech, L.; Setti, A. M.; Damsgaard, C. D.; Pedersen, T.; Hansen, O.; Rossmeisl, J.; Dahl, S.; Norskov, J. K.; Chorkendorff, I. *Nat. Mater.* **2011**, *10*, 434.

(108) Warren, E. L.; Atwater, H. A.; Lewis, N. S. *J. Phys. Chem. C* **2014**, *118*, 747.

(109) Boettcher, S. W.; Warren, E. L.; Putnam, M. C.; Santori, E. A.; Turner-Evans, D.; Kelzenberg, M. D.; Walter, M. G.; McKone, J. R.; Brunschwig, B. S.; Atwater, H. A.; Lewis, N. S. *J. Am. Chem. Soc.* **2011**, *133*, 1216.

(110) Putnam, M. C.; Turner-Evans, D. B.; Kelzenberg, M. D.; Boettcher, S. W.; Lewis, N. S.; Atwater, H. A. *Appl. Phys. Lett.* **2009**, *95*, 163116/1.

(111) Kelzenberg, M. D.; Turner-Evans, D. B.; Putnam, M. C.; Boettcher, S. W.; Briggs, R. M.; Baek, J. Y.; Lewis, N. S.; Atwater, H. A. *Energy Environ. Sci.* **2011**, *4*, 866.

(112) Spurgeon, J. M.; Walter, M. G.; Zhou, J.; Kohl, P. A.; Lewis, N. S. *Energy Environ. Sci.* **2011**, *4*, 1772.

(113) McFarlane, S. L.; Day, B. A.; McEleney, K.; Freund, M. S.; Lewis, N. S. *Energy Environ. Sci.* **2011**, *4*, 1700.

(114) Bruce, J. P.; Asgari, S.; Ardo, S.; Lewis, N. S.; Oliver, D. R.; Freund, M. S. *J. Phys. Chem. C* **2014**, *118*, 27742.

(115) Hamann, T. W.; Lewis, N. S. *J. Phys. Chem. B* **2006**, *110*, 22291.

(116) Hwang, Y. J.; Boukai, A.; Yang, P. *Nano Lett.* **2009**, *9*, 410.

(117) Kargar, A.; Kim, S. J.; Allameh, P.; Choi, C.; Park, N.; Jeong, H.; Pak, Y.; Jung, G. Y.; Pan, X.; Wang, D.; Jin, S. *Adv. Funct. Mater.* **2015**, *25*, 2609.

(118) Seo, J.; Kim, H. J.; Pekarek, R. T.; Rose, M. J. *J. Am. Chem. Soc.* **2015**, *137*, 3173.

(119) Khaselev, O.; Turner, J. A. *Science* **1998**, *280* , 425.

(120) MacLeod, B. A.; Steirer, K. X.; Young, J. L.; Koldemir, U.; Sellinger, A.; Turner, J. A.; Deutsch, T. G.; Olson, D. C. *ACS Appl. Mater. Interfaces* **2015**, *7*, 11346.

(121) Bansal, A.; Turner, J. A. *J. Phys. Chem. B* **2000**, *104*, 6591.

(122) Memming, R.; Schwandt, G. *Electrochim. Acta* **1968**, *13*, 1299.

(123) Chitambar, M.; Wang, Z.; Liu, Y.; Rockett, A.; Maldonado, S. *J. Am. Chem. Soc.* **2012**, *134*, 10670.

(124) Brown, E. S.; Peczonczyk, S. L.; Wang, Z.; Maldonado, S. *J. Phys. Chem. C* **2014**, *118*, 11593.

(125) Sivula, K.; Zboril, R.; Le Formal, F.; Robert, R.; Weidenkaff, A.; Tucek, J.; Frydrych, J.; Grätzel, M. *J. Am. Chem. Soc.* **2010**, *132*, 7436.

(126) Tilley, S. D.; Cornuz, M.; Sivula, K.; Grätzel, M. *Angew. Chemie, Int. Ed.* **2010**, *49*, 6405.

(127) Dare-Edwards, M. P.; Goodenough, J. B.; Hamnett, A.; Trevellick, P. R. *J. Chem. Soc. Faraday Trans. 1 Phys. Chem. Condens. Phases* **1983**, *79*, 2027.

(128) Smith, R. D. L.; Prevot, M. S.; Fagan, R. D.; Zhang, Z.; Sedach, P. A.; Siu, M. K. J.; Trudel, S.; Berlinguette, C. P. *Science* **2013**, *340*, 60.

(129) Abe, T.; Nagai, K. *Org. Electron.* **2007**, *8*, 262.

(130) Abe, T.; Nagai, K.; Ogiwara, T.; Ogasawara, S.; Kaneko, M.; Tajiri, A.; Norimatsu, T. *J. Electroanal. Chem.* **2006**, *587*, 127.

(131) Abe, T.; Nagai, K.; Kabutomori, S.; Kaneko, M.; Tajiri, A.; Norimatsu, T. *Angew. Chemie, Int. Ed.* **2006**, *45*, 2778.

(132) Abe, T.; Kamei, Y.; Nagai, K. *Solid State Sci.* **2010**, *12*, 1136.

(133) Abe, T.; Nagai, K.; Ichinohe, H.; Shibata, T.; Tajiri, A.; Norimatsu, T. *J. Electroanal. Chem.* **2007**, *599*, 65.

(134) Abe, T.; Nagai, K.; Sekimoto, K.; Tajiri, A.; Norimatsu, T. *Electrochem. commun.* **2005**, *7*, 1129.

(135) Abe, T.; Tobinai, S.; Taira, N.; Chiba, J.; Itoh, T.; Nagai, K. *J. Phys. Chem. C* **2011**, *115*, 7701.

(136) Abe, T.; Chiba, J.; Ishidoya, M.; Nagai, K. *RSC Adv.* **2012**, *2*, 7992.

(137) Lanzarini, E.; Antognazza, M. R.; Biso, M.; Ansaldo, A.; Laudato, L.; Bruno, P.; Metrangolo, P.; Resnati, G.; Ricci, D.; Lanzani, G. *J. Phys. Chem. C* **2012**, *116*, 10944.

(138) Bourgeteau, T.; Tondelier, D.; Geffroy, B.; Brisse, R.; Laberty-Robert, C.; Campidelli, S.; de Bettignies, R.; Artero, V.; Palacin, S.; Jousselme, B. *Energy Environ. Sci.* **2013**, *6*, 2706.

(139) Gustafson, M. P.; Clark, N.; Winther-Jensen, B.; MacFarlane, D. R. *Electrochim. Acta* **2014**, *140*, 309.

(140) Guerrero, A.; Haro, M.; Bellani, S.; Antognazza, M. R.; Meda, L.; Gimenez, S.; Bisquert, J. *Energy Environ. Sci.* **2014**, *7*, 3666.

(141) Haro, M.; Solis, C.; Molina, G.; Otero, L.; Bisquert, J.; Gimenez, S.; Guerrero, A. *J. Phys. Chem. C* **2015**, *119*, 6488.

(142) Gagne, R.; Koval, C.; Lisensky, G. *Inorg. Chem.* **1980**, *19*, 2854.

(143) Johansson, T.; Mammo, W.; Svensson, M.; Andersson, M. R.; Inganaes, O. *J. Mater. Chem.* **2003**, *13*, 1316.

(144) Pommerehne, J.; Vestweber, H.; Guss, W.; Mahrt, R. F.; Baessler, H.; Porsch, M.; Daub, J. *Adv. Mater.* **1995**, *7*, 551.

(145) Bredas, J. L.; Scott, J. C.; Yakushi, K.; Street, G. B. *Phys. Rev. B Condens. Matter Mater. Phys.* **1984**, *30*, 1023.

(146) Chen, Z.; Dinh, H.; Miller, E. *Photoelectrochemical Water Splitting*; 1st ed.; Springer-Verlag: New York, 2013.

(147) Bennur, R.; Dhere, N. In *Hydrogen Fuel*; CRC Press, 2008; pp. 227–282.

(148) Hoppe, H.; Sariciftci, N. In *Photoresponsive Polymers II*; Marder, S. R.; Lee, K.-S., Eds.; Springer Berlin Heidelberg, 2008; pp. 1–86.

(149) Jenekhe, S. A. *Science* **1998**, *279*, 1903.

(150) Png, R.-Q.; Chia, P.-J.; Tang, J.-C.; Liu, B.; Sivaramakrishnan, S.; Zhou, M.; Khong, S.-H.; Chan, H. S. O.; Burroughes, J. H.; Chua, L.-L.; Friend, R. H.; Ho, P. K. H. *Nat. Mater.* **2010**, *9*, 152.

(151) Mills, A.; Davies, R.; Worsley, D. *Chem. Soc. Rev.* **1993**, *22*, 417.

(152) Gaya, U. I.; Abdullah, A. H. *J. Photochem. Photobiol. C Photochem. Rev.* **2008**, *9*, 1.

(153) Tran, P. D.; Wong, L. H.; Barber, J.; Loo, J. S. C. *Energy Environ. Sci.* **2012**, *5*, 5902.

(154) Joshi, U. A.; Palasyuk, A.; Arney, D.; Maggard, P. A. *J. Phys. Chem. Lett.* **2010**, *1*, 2719.

(155) Izumi, Y. *Coord. Chem. Rev.* **2012**, *257*, 171.

(156) Cao, L.; Sahu, S.; Anilkumar, P.; Bunker, C. E.; Xu, J.; Fernando, K. A. S.; Wang, P.; Guliants, E. A; Tackett, K. N.; Sun, Y.-P. *J. Am. Chem. Soc.* **2011**, *133*, 4754.

(157) Zhang, S.; Arunachalam, P.; Abe, T.; Iyoda, T.; Nagai, K. *J. Photochem. Photobiol. A Chem.* **2012**, *244*, 18.

(158) Roncali, J. *Chem. Rev.* **1992**, *92*, 711.

(159) Zhao, G.; He, Y.; Li, Y. *Adv. Mater.* **2010**, *22*, 4355.

(160) El-Rashiedy, O. A.; Holdcroft, S. *J. Phys. Chem.* **1996**, *100*, 5481.

(161) Yang, S.; Fan, L. *J. Phys. Chem. B* **2004**, *108*, 4394.

(162) Yang, S.; Fan, L.; Yang, S. *Chem. Phys. Lett.* **2004**, *388*, 253.

(163) Abe, T.; Ichikawa, M.; Hikage, T.; Kakuta, S.; Nagai, K. *Chem. Phys. Lett.* **2012**, *549*, 77.

(164) Chen, T.; Wu, X.; Rieke, R. *J. Am. Chem. Soc.* **1995**, *117*, 233.

(165) Loewe, R. S.; Khersonsky, S. M.; McCullough, R. D. *Adv. Mater.* **1999**, *11*, 250.

(166) Loewe, R. S.; Ewbank, P. C.; Liu, J.; Zhai, L.; McCullough, R. D. *Macromolecules* **2001**, *34*, 4324.

(167) Mao, H.; Xu, B.; Holdcroft, S. *Macromolecules* **1993**, *26*, 1163.

(168) Veldman, D.; Meskers, S. C. J.; Janssen, R. a. J. *Adv. Funct. Mater.* **2009**, *19*, 1939.

(169) Liu, Y. R.; Lai, P. T.; Yao, R. H.; Deng, L. F. *IEEE Trans. Device Mater. Reliab.* **2011**, *11*, 60.

(170) Goh, C.; Kline, R. J.; McGehee, M. D.; Kadnikova, E. N.; Fréchet, J. M. J. *Appl. Phys. Lett.* **2005**, *86*, 122110.

(171) Girotto, E.; Gazotti, W.; De Paoli, M. *J. Phys. Chem. B* **2000**, *104*, 6124.

(172) Santos, M. J. L.; Girotto, E. M.; Nogueira, A. F. *Thin Solid Films* **2006**, *515*, 2644.

(173) Dang, X. D.; Intelmann, C. M.; Rammelt, U.; Plieth, W. *J. Solid State Electrochem.* **2004**, *8*, 727.

(174) Cook, S.; Furube, A.; Katoh, R. *J. Mater. Chem.* **2012**, *22*, 4282.

(175) Shaw, P. E.; Ruseckas, A.; Samuel, I. D. W. *Adv. Mater.* **2008**, *20*, 3516.

(176) Yang, S. *J. Phys. Chem. B* **2001**, *105*, 9406.

(177) Nalwa, K. S.; Carr, J. a.; Mahadevapuram, R. C.; Kodali, H. K.; Bose, S.; Chen, Y.; Petrich, J. W.; Ganapathysubramanian, B.; Chaudhary, S. *Energy Environ. Sci.* **2012**, *5*, 7042.

(178) Yim, K.-H.; Zheng, Z.; Liang, Z.; Friend, R. H.; Huck, W. T. S.; Kim, J.-S. *Adv. Funct. Mater.* **2008**, *18*, 1012.

(179) Zotti, G.; Schiavon, G.; Zecchin, S. *Synth. Met.* **1995**, *72*, 275.

(180) Mårdalen, J.; Samuelsen, E. J.; Gautun, O. R.; Carlsen, P. H. *Solid State Commun.* **1991**, *77*, 337.

(181) Yu, Y.; Gunic, E.; Miller, L. L. *Chem. Mater.* **1995**, *7*, 255.

(182) Trznadel, M.; Pron, A.; Zagorska, M.; Chrzaszcz, R.; Pielichowski, J. *Macromolecules* **1998**, *31*, 5051.

(183) Trznadel, M.; Zagórska, M.; Lapkowski, M.; Louarn, G.; Lefrant, S.; Pron, A. *J. Chem. Soc. Faraday Trans.* **1996**, *92*, 1387.

(184) Chen, S.-A.; Hua, M.-Y. *Macromolecules* **1993**, *26*, 7108.

(185) Ikenoue, Y.; Chiang, J.; Patil, A.; Wudl, F.; Heeger, A. J. *J. Am. Chem. Soc.* **1988**, *110*, 2983.

(186) Maeda, K.; Domen, K. *J. Phys. Chem. Lett.* **2010**, *1*, 2655.

(187) Osterloh, F. E. *Chem. Mater.* **2008**, *20*, 35.

(188) Chen, H. M.; Chen, C. K.; Liu, R.-S.; Zhang, L.; Zhang, J.; Wilkinson, D. P. *Chem. Soc. Rev.* **2012**, *41*, 5654.

(189) Lin, Y.; Yuan, G.; Liu, R.; Zhou, S.; Sheehan, S. W.; Wang, D. *Chem. Phys. Lett.* **2011**, *507*, 209.

(190) Abe, R. *J. Photochem. Photobiol. C Photochem. Rev.* **2010**, *11*, 179.

(191) Yang, T.; Wang, H.; Ou, X.-M.; Lee, C.-S.; Zhang, X.-H. *Adv. Mater.* **2012**, *24*, 6199.

(192) Reece, S. Y.; Hamel, J. A.; Sung, K.; Jarvi, T. D.; Esswein, A. J.; Pijpers, J. J. H.; Nocera, D. G. *Science* **2011**, *334*, 645.

(193) Mayer, M. T.; Du, C.; Wang, D. *J. Am. Chem. Soc.* **2012**, *134*, 12406.

(194) Rodenas, P.; Song, T.; Sudhagar, P.; Marzari, G.; Han, H.; Badia-Bou, L.; Gimenez, S.; Fabregat-Santiago, F.; Mora-Sero, I.; Bisquert, J.; Paik, U.; Kang, Y. S. *Adv. Energy Mater.* **2013**, *3*, 176.

(195) Wang, X.; Liu, G.; Chen, Z.-G.; Li, F.; Wang, L.; Lu, G. Q.; Cheng, H.-M. *Chem. Commun.* **2009**, 3452.

(196) Wang, H.; Deutsch, T.; Turner, J. A. *J. Electrochem. Soc.* **2008**, *155* , F91.

(197) Ding, C.; Qin, W.; Wang, N.; Liu, G.; Wang, Z.; Yan, P.; Shi, J.; Li, C. *Phys. Chem. Chem. Phys.* **2014**, *16*, 15608.

(198) Doscher, H.; Geisz, J. F.; Deutsch, T. G.; Turner, J. A. *Energy Environ. Sci.* **2014**, *7*, 2951.

(199) Yahyaie, I.; McEleney, K.; Walter, M.; Oliver, D. R.; Thomson, D. J.; Freund, M. S.; Lewis, N. S. *J. Phys. Chem. Lett.* **2011**, *2*, 675.

(200) Bettis, S. E.; Ryan, D. M.; Gish, M. K.; Alibabaei, L.; Meyer, T. J.; Waters, M. L.; Papanikolas, J. M. *J. Phys. Chem. C* **2014**, *118*, 6029.

(201) Weingarten, A. S.; Kazantsev, R. V; Palmer, L. C.; McClendon, M.; Koltonow, A. R.; Samuel, A. P. S.; Kiebala, D. J.; Wasielewski, M. R.; Stupp, S. I. *Nat. Chem.* **2014**, *6*, 964.

(202) Ji, Z.; He, M.; Huang, Z.; Ozkan, U.; Wu, Y. *J. Am. Chem. Soc.* **2013**, *135*, 11696.

(203) Scharber, M. C.; Muehlbacher, D.; Koppe, M.; Denk, P.; Waldauf, C.; Heeger, A. J.; Brabec, C. J. *Adv. Mater.* **2006**, *18*, 789.

(204) Kim, J. Y.; Lee, K.; Coates, N. E.; Moses, D.; Nguyen, T.-Q.; Dante, M.; Heeger, A. J. *Science* **2007**, *317*, 222.

(205) Yoshinob, K. *J. Chem. Soc. Chem. Commun.* **1985**, 474.

(206) McCullough, R. D.; Lowe, R. D. *J. Chem. Soc. Chem. Commun.* **1992**, 70.

(207) Suppes, G.; Ballard, E.; Holdcroft, S. *Polym. Chem.* **2013**, *4*, 5345.

(208) Suppes, G. M.; Fortin, P. J.; Holdcroft, S. *J. Electrochem. Soc.* **2015**, *162*, H551.

(209) Wang, Z.; Gao, G.; Zhu, H.; Sun, Z.; Liu, H.; Zhao, X. *Int. J. Hydrogen Energy* **2009**, *34*, 9334.

(210) Nagashree, K. L.; Ahmed, M. F. *Synth. Met.* **2008**, *158*, 610.

(211) Ferreira, V. C.; Melato, A. I.; Silva, A. F.; Abrantes, L. M. *Electrochim. Acta* **2011**, *56*, 3567.

(212) Shan, J.; Pickup, P. G. *Electrochim. Acta* **2000**, *46*, 119.

(213) Trueba, M.; Trasatti, S. P.; Trasatti, S. *Mater. Chem. Phys.* **2006**, *98*, 165.

(214) Grzeszczuk, M.; Poks, P. *Electrochim. Acta* **2000**, *45*, 4171.

(215) Tueken, T.; Cavusoglu, A. B.; Altunbas, E.; Erbil, M. *Prog. Org. Coatings* **2011**, *71*, 153.

(216) Huang, X.; Li, Y.; Chen, Y.; Wang, L. *Sensors Actuators, B Chem.* **2008**, *134*, 780.

(217) Shih, H.-H.; Williams, D.; Mack, N. H.; Wang, H.-L. *Macromolecules* **2009**, *42*, 14.

(218) Wang, H.-L.; Gao, J.; Sansinena, J.-M.; McCarthy, P. *Chem. Mater.* **2002**, *14*, 2546.

(219) Patra, S.; Munichandraiah, N. *Langmuir* **2009**, *25*, 1732.

(220) Mourato, A.; Viana, A. S.; Correia, J. P.; Siegenthaler, H.; Abrantes, L. M. *Electrochim. Acta* **2004**, *49*, 2249.

(221) Seok, J.; Shin, T. J.; Park, S.; Cho, C.; Lee, J.-Y.; Yeol Ryu, D.; Kim, M. H.; Kim, K. *Sci. Rep.* **2015**, *5*, 8373.

(222) Bard, A. J.; Faulkner, L. R. *Electrochemical Methods; Fundamentals and Applications*; 2nd ed.; John Wiley & Sons: New Jersey, 2001.

(223) Klahr, B.; Gimenez, S.; Fabregat-Santiago, F.; Hamann, T.; Bisquert, J. *J. Am. Chem. Soc.* **2012**, *134*, 4294.

(224) Klahr, B.; Gimenez, S.; Fabregat-Santiago, F.; Bisquert, J.; Hamann, T. W. *Energy Environ. Sci.* **2012**, *5*, 7626.

(225) Klahr, B.; Gimenez, S.; Fabregat-Santiago, F.; Bisquert, J.; Hamann, T. W. *J. Am. Chem. Soc.* **2012**, *134*, 16693.

(226) Zhong, D. K.; Choi, S.; Gamelin, D. R. *J. Am. Chem. Soc.* **2011**, *133*, 18370.

(227) Peter, L. M. *J. Solid State Electrochem.* **2013**, *17*, 315.

(228) Abdi, F. F.; van de Krol, R. *J. Phys. Chem. C* **2012**, *116*, 9398.

(229) Le Formal, F.; Sivula, K.; Grätzel, M. *J. Phys. Chem. C* **2012**, *116*, 26707.

(230) Morales-Guio, C. G.; Tilley, S. D.; Vrubel, H.; Grätzel, M.; Hu, X. *Nat. Commun.* **2014**, *5*, 4059/1.

(231) Dominey, R. N.; Lewis, N. S.; Bruce, J. A.; Bookbinder, D. C.; Wrighton, M. S. *J. Am. Chem. Soc.* **1982**, *104*, 467.

(232) Fekete, M.; Riedel, W.; Patti, A. F.; Spiccia, L. *Nanoscale* **2014**, *6*, 7585.

(233) Bellani, S.; Fazzi, D.; Bruno, P.; Giussani, E.; Canesi, E. V.; Lanzani, G.; Antognazza, M. R. *J. Phys. Chem. C* **2014**, *118*, 6291.

(234) Abdou, M. S. A.; Orfino, F. P.; Son, Y.; Holdcroft, S. *J. Am. Chem. Soc.* **1997**, *119*, 4518.

(235) Sperlich, A.; Kraus, H.; Deibel, C.; Blok, H.; Schmidt, J.; Dyakonov, V. *J. Phys. Chem. B* **2011**, *115*, 13513.

(236) Winther-Jensen, B.; Winther-Jensen, O.; Forsyth, M.; MacFarlane, D. R. *Science* **2008**, *321*, 671.

(237) Winther-Jensen, B.; Fraser, K.; Ong, C.; Forsyth, M.; MacFarlane, D. R. *Adv. Mater.* **2010**, *22*, 1727.

(238) Gu, C.; Norris, B. C.; Fan, F.-R. F.; Bielawski, C. W.; Bard, A. J. *ACS Catal.* **2012**, *2*, 746.

(239) Song, Y.-J.; Oh, J.-K.; Park, K.-W. *Nanotechnology* **2008**, *19*, 355602/1.

(240) Lee, K.; Kim, J. Y.; Park, S. H.; Kim, S. H.; Cho, S.; Heeger, A. J. *Adv. Mater.* **2007**, *19*, 2445.

(241) Cho, S.; Seo, J. H.; Park, S. H.; Beaupre, S.; Leclerc, M.; Heeger, A. J. *Adv. Mater.* **2010**, *22*, 1253.

(242) Fukuzumi, S.; Amasaki, I.; Ohkubo, K.; Gros, C. P.; Guilard, R.; Barbe, J.-M. *RSC Adv.* **2012**, *2*, 3741.

(243) Du, P.; Schneider, J.; Jarosz, P.; Eisenberg, R. *J. Am. Chem. Soc.* **2006**, *128*, 7726.

(244) Zhu, H.; Song, N.; Lv, H.; Hill, C. L.; Lian, T. *J. Am. Chem. Soc.* **2012**, *134*, 11701.

(245) Kiwi, J.; Grätzel, M. *J. Am. Chem. Soc.* **1979**, *101*, 7214.

(246) Bock, C. R.; Meyer, T. J.; Whitten, D. G. *J. Am. Chem. Soc.* **1974**, *96*, 4710.

(247) Young, R. C.; Meyer, T. J.; Whitten, D. G. *J. Am. Chem. Soc.* **1975**, *97*, 4781.

(248) Green, D. E.; Strickland, L. H. *Biochem. J.* **1934**, *28*, 898.

(249) Moradpour, A.; Amouyal, E.; Keller, P.; Kagan, H. *Nouv. J. Chim.* **1978**, *2*, 547.

(250) Bird, C. L.; Kuhn, A. T. *Chem. Soc. Rev.* **1981**, *10*, 49.

(251) Kalyanasundaram, K.; Kiwi, J.; Grätzel, M. *Helv. Chim. Acta* **1978**, *61*, 2720.

(252) Miller, D.; McLendon, G. *Inorg. Chem.* **1981**, *20*, 950.

(253) Keller, P.; Moradpour, A. *J. Am. Chem. Soc.* **1980**, *102*, 7193.

(254) Johansen, O.; Launikonis, A.; Loder, J. W.; Mau, A. W. H.; Sasse, W. H. F.; Swift, J. D.; Wells, D. *Aust. J. Chem.* **1981**, *34*, 981.

(255) Furlong, D. N.; Launikonis, A.; Sasse, W. H. F.; Sanders, J. V. *J. Chem. Soc. Faraday Trans. 1 Phys. Chem. Condens. Phases* **1984**, *80*, 571.

(256) Ershov, B. G. *Russ. Chem. Bull.* **2001**, *50*, 626.

(257) Devi, G. S.; Rao, V. J. *Bull. Mater. Sci.* **2000**, *23*, 467.

(258) Yang, H.; Glynos, E.; Huang, B.; Green, P. F. *J. Phys. Chem. C* **2013**, *117*, 9590.

(259) Hitchcock, A. H.; Stringer, J. *J. Phys. D Appl. Phys.* **1971**, *4*, 810.

(260) Miller, D. S.; McLendon, G. *J. Am. Chem. Soc.* **1981**, *103*, 6791.

(261) Miller, D. S.; Bard, A. J.; McLendon, G.; Ferguson, J. *J. Am. Chem. Soc.* **1981**, *103*, 5336.

(262) Dunn, W. W.; Aikawa, Y.; Bard, A. J. *J. Electrochem. Soc.* **1981**, *128*, 222.

(263) Ward, M. D.; Bard, A. J. *J. Phys. Chem.* **1982**, *86*, 3599.

(264) Ward, M. D.; White, J. R.; Bard, A. J. *J. Am. Chem. Soc.* **1983**, *105*, 27.

(265) Du, P.; Schneider, J.; Jarosz, P.; Zhang, J.; Brennessel, W. W.; Eisenberg, R. *J. Phys. Chem. B* **2007**, *111*, 6887.

(266) Close, T.; Tulsyan, G.; Diaz, C. A.; Weinstein, S. J.; Richter, C. *Nat. Nanotechnol.* **2015**, *10*, 418.

(267) Artero, V.; Chavarot-Kerlidou, M.; Fontecave, M. *Angew. Chem. Int. Ed. Engl.* **2011**, *50*, 7238.

(268) Lakadamyali, F.; Reisner, E. *Chem. Commun.* **2011**, *47*, 1695.

Appendix

Supporting Information

P3HT NMR

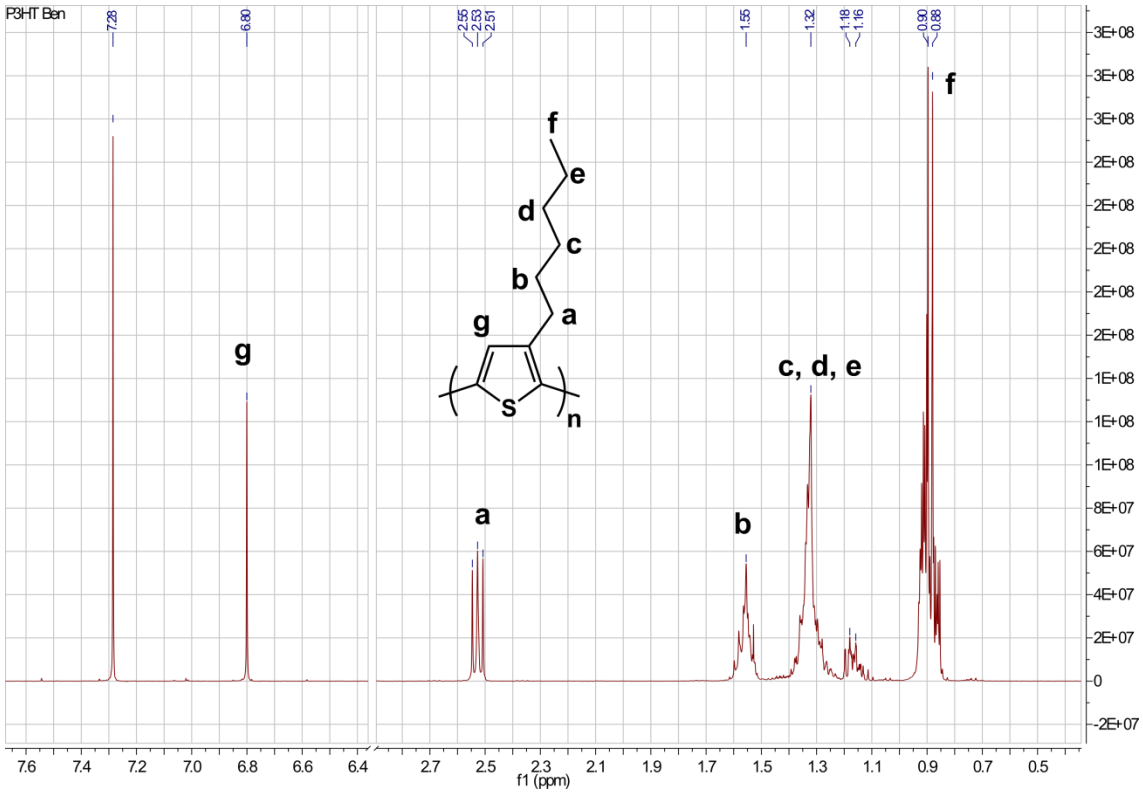

Figure A-1: H^1 NMR (400 MHz) of P3HT, δ/ppm ($CDCl_3$): 6.80 (s, 1H), 2.53 (t, 2H), 1.55 (m, 2H), 1.32 (m, 6H), 0.90 (t, 3H).

Platinum Colloid UV-Visible Absorbance

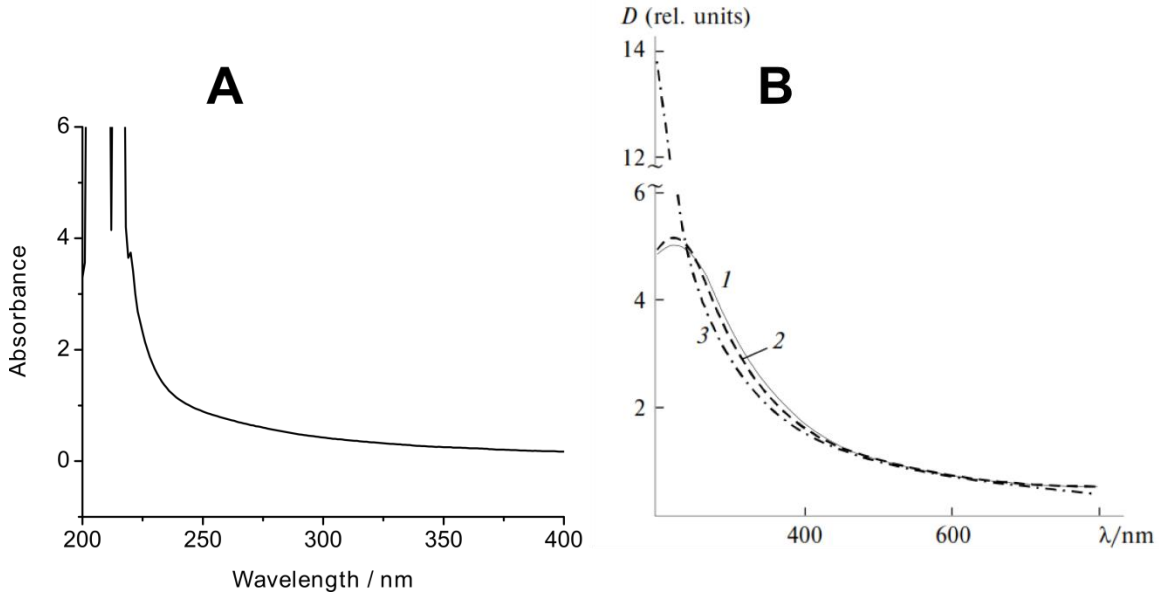

Figure A-2: UV-visible spectroscopy of a 0.31 mM Pt colloid solution (A) and comparison to a literature spectra (B) of Pt colloid solution (all 0.1 mM Pt^0) prepared using radiolysis (1), hydrogen gas (2) and sodium citrate (3).[256]

Energy dispersive x-ray

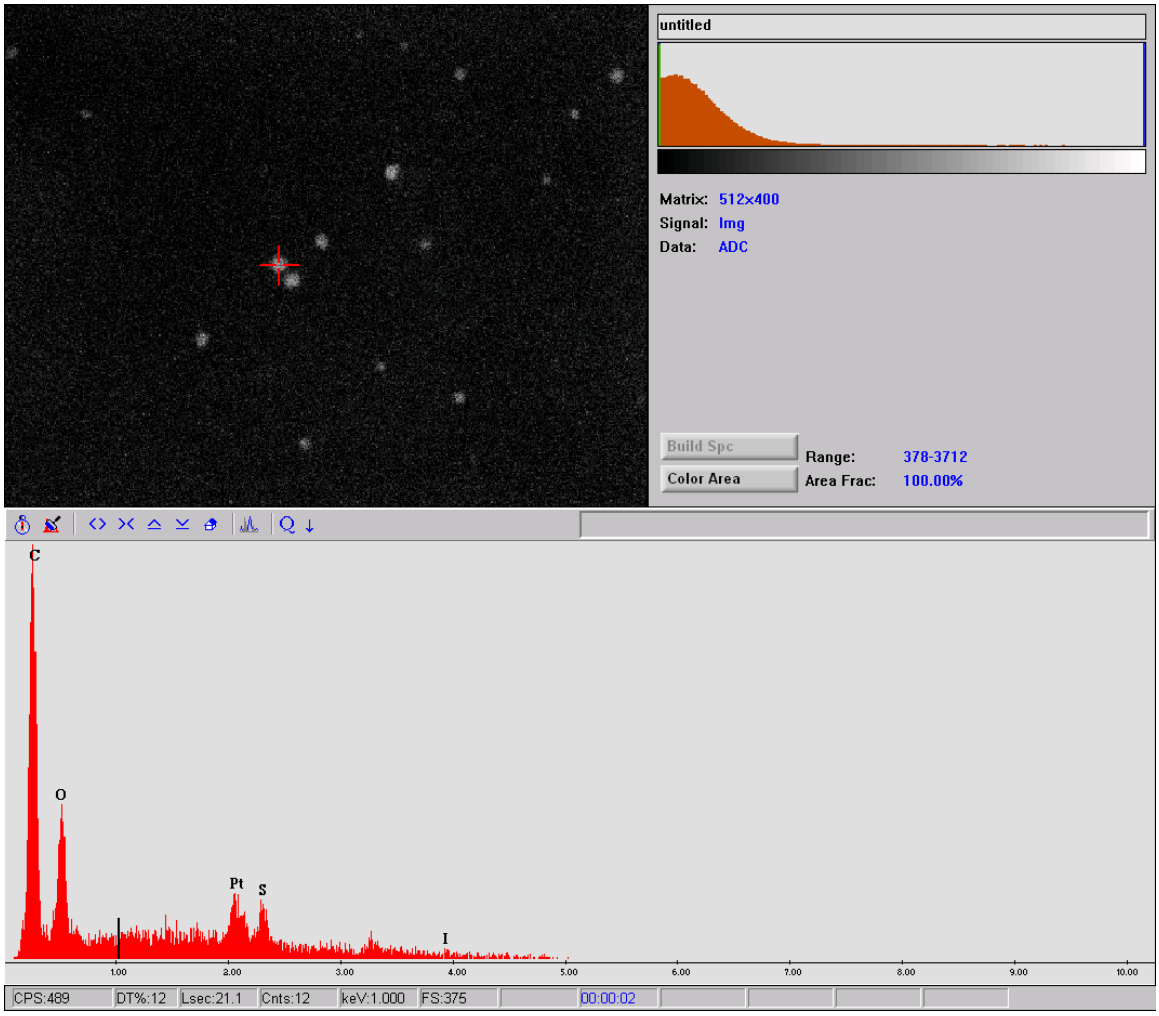

Figure A-3: Energy dispersive x-ray analysis of a P3HT-Pt NP film (0.23 µg cm^{-2}). The red crosshair indicates the position being analysed and the presence of platinum is observed.

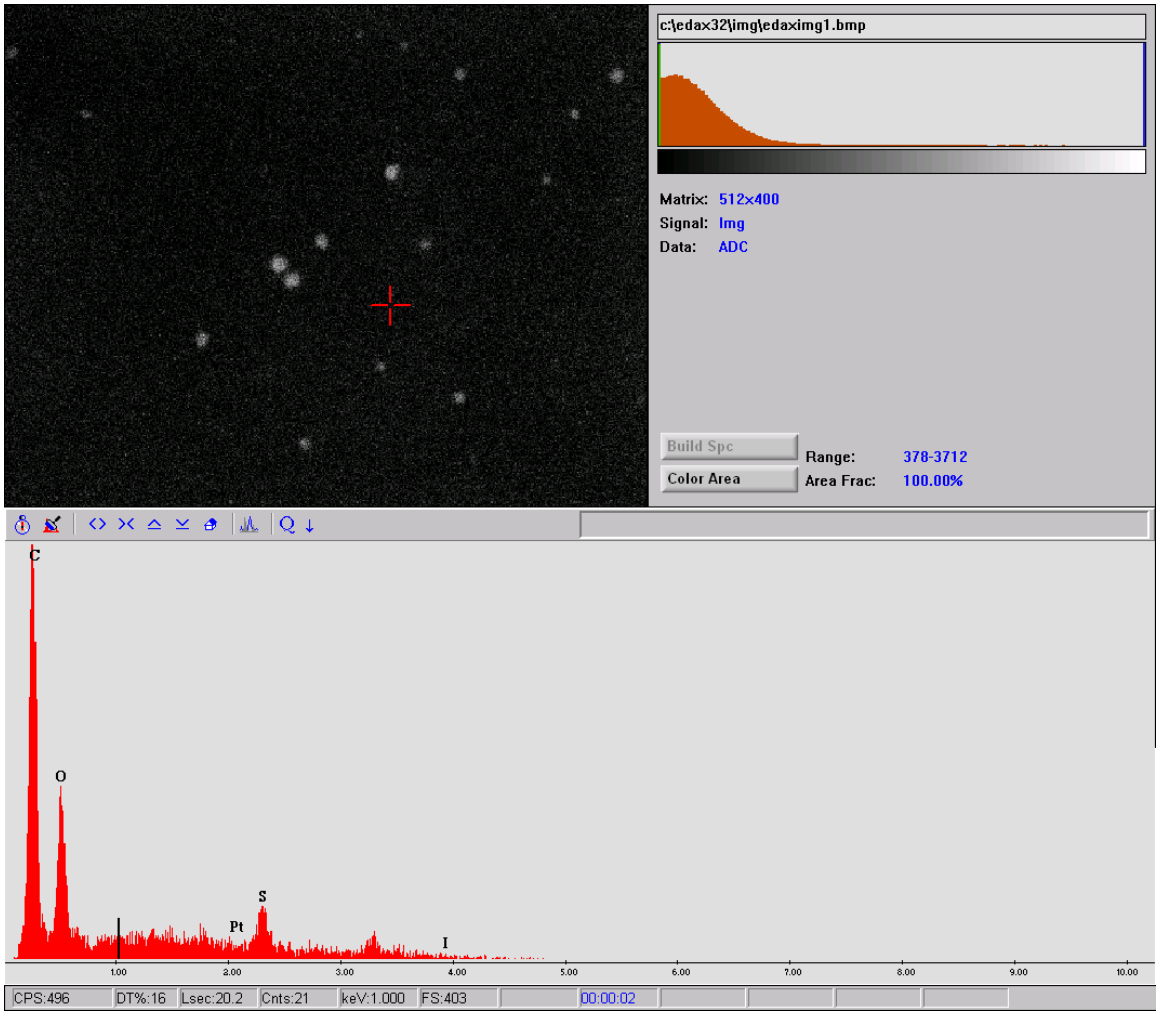

Figure A-4: Energy dispersive x-ray analysis of a P3HT-Pt NP film (0.23 µg cm^{-2}). The red crosshair indicates the position being analysed and no platinum is detected. Note: the expected position of platinum was labeled to confirm its absence.